INSTITUTO TECNOLÓGICO Y DE ESTUDIOS SUPERIORES DE MONTERREY

CAMPUS MONTERREY

GRADUATE PROGRAM IN ELECTRONICS AND INFORMATION TECHNOLOGIES

EXPERIMENTAL RESEARCH OF THE POLYAMIDOAMINE DENDRIMER AS A COATING LAYER FOR MICROFABRICATED SILICON BIOSENSORS

THESIS

PRESENTED AS PARTIAL REQUISITE TO OBTAIN THE ACADEMIC DEGREE OF:

MASTER OF SCIENCE IN ELECTRICAL ENGINEERING WITH FOCUS IN ELECTRONIC SYSTEMS

BY:

JOSÉ ALBERTO QUIROGA CONTRERAS

MONTERREY , N.L. AUGUST 2007

INSTITUTO TECNOLÓGICO Y DE ESTUDIOS SUPERIORES DE MONTERREY

DIVISON OF ELECTRONICS AND INFORMATION TECHNOLIGIES

GRADUATE PROGRAM IN ELECTRONICS AND INFORMATION TECHNOLOGIES

The members of this thesis committee recommend that the thesis presented by JOSE ALBERTO QUIROGA CONTRERAS be admitted as partial requisite to obtain the academic degree of MASTER OF SCIENCE IN ELECTRICAL ENGINEERING WITH FOCUS ON ELECTRONIC SYSTEMS.

Thesis Committee:

_____
Dr. Sergio Omar Martínez Chapa
Chair

_____
M.C. Jesús Ángel Valencia Gallegos
Advisor

_____
Dr. Alfonso Avila Ortega
Advisor

_____
Dr. Graciano Dieck Assad
Director of Graduate Programs in Electronics and Information Technologies

August 2007

Experimental Research of the Polyamidoamine Dendrimer as a Coating Layer for Microfabricated Silicon Biosensors

BY:

JOSE ALBERTO QUIROGA CONTRERAS

THESIS

Presented to the Graduate Program in
Electronics and Information Technologies

This work is a partial requisite to obtain the degree of Masters of Science in Electrical Engineering with focus in Electronic Systems

INSTITUTO TECNOLÓGICO Y DE ESTUDIOS
SUPERIORES DE MONTERREY

August 2007

DEDICATION

I dedicate this work to my family, without whom
none of this would be possible. Thank you for your support
and for always believing in me, even when I doubted myself.
You gave me the inspiration to carry on
and the strength to never give up.

ACKNOWLEDGEMENTS

Sergio O. Martinez; thank you for all the guidance, support and trust in making this project a reality, there is still a long way to go but I hope these first steps laid the groundwork for future projects.

Jesus Angel Valencia; thank you for all the supervision on the construction of the dendrimer structures as well as granting me access to the chemistry laboratory and materials.

Ruben Garcia Brahm, I'm very grateful for your accessibility in letting me use the FTIR microscope at the Universidad Autonoma de Coahuila in Saltillo. This equipment gave a huge added value to my investigation.

Victor Serdio and Alfonso Garcia; thank you for all the time you spent with me using the Atomic Force Microscope and for your interest in my project. The images obtained really enhanced the characterization of the silicon surface and improved my understanding of the surface coating technique.

Guillermo Colunga; thank you for your interest in this research project and for always being available and willing to learn new things using the infrared spectroscope from the Physics Department at Tec.

Jose Francisco (Chepo) Islas; thanks for all the ideas and contributions to this project. Thank you for helping me understand the chemical reactions involved in the experiments and for donating so much of your time to this investigation.

Liliana Urrea; thank you for being the source of my distractions as well as my inspirations, thanks for all your patience and understanding and for keeping me focused towards the end.

ABSTRACT

This investigation was conducted towards the development of a sensor that can interact in a biological environment to detect a specific biochemical component. The motivation of this research came upon by the need to reduce the periodical bone marrow biopsies that follow treatment on patients with Leukemia; as well reducing the costs associated with the monitoring phase and improving the quality of life of patients. This biosensor could serve as an early-detection device that monitors the concentration of the Angiotensin Converting Enzyme (ACE) inside bone marrow, to send a wireless signal outside the body, indicating a high probability that the patient is entering relapse.

In order to develop this type of biosensor, an active biolayer needs to be constructed on top of the sensing mechanism, to be able to "trap" the desired molecule to be detected. The proposed MicroElectroMechanical System (MEMS) to sense the ACE molecule is an array of microcantilevers connected to a microcircuit for data acquisition and analysis, along with radiofrequency transmission capabilities. This work focuses on creating a selective coating material that can interact with a biological medium and sense a specific molecule to measure its concentration.

This research started with an exhaustive literature review to target specific problems such as: selecting the MEMS platform, the coupling agent, the coating material, as well as identifying a possible leukemia relapse biochemical indicator. Once the design parameters were established, an experimental phase was conducted. The first step was to functionalize the silicon structure with γ-aminopropyltriethoxysilane (γ-APS). Next, a series of iterative reactions were performed, alternating between a Michael addition and an amidation reaction, using methyl acrylate and ethylenediemine respectively to construct the poly(amidoamine) (PAMAM) dendrimer to be used as the coating layer. At the end of each reaction a sample was taken for analysis with Fourier transform infrared (FTIR) spectroscopy and with an atomic force microscope (AFM). Results show that the PAMAM dendrimer was successfully grown on top of the silicon wafers, but the attachment was not evenly distributed along the surface. A suggested improvement is to perform an oxidizing reaction to the silicon wafer prior to the γ-APS functionalization, in order increase the –OH groups and obtain a uniform attachment of the PAMAM dendrimer on the surface.

This thesis concludes with a "future work" section that lays the groundwork to take the next steps in verifying the validity of the model. Among the suggested experiments, the use of ACE antibodies with fluorescent markers is highly recommended to quantify the amount of ACE molecules that are trapped by the PAMAM biolayer with an ACE inhibitor (Captopril) as the molecular sensor.

TABLE OF CONTENTS

LIST OF TABLES

LIST OF FIGURES

LIST OF ABBREVIATIONS

ACE	Angiotensin conveting enzyme
CBC	Complete blood count
MRD	Minimum residual disease
ALL	Acute Lymphoblastic Leukemia
CLL	Chronic Lymphoblastic Leukemia
AML	Acute Myeloid Leukemia
CML	Chronic Myeloid Leukemia
RAS	Rennin-Angiotensin System
ACE	Angiotensin Converting Enzyme
ADH	Anti-Diuretic Hormone
MEMS	MicroElectroMechancal Systems
SAMS	Self-Assembled Mono-Layers
PMAA	Poly(methacrylic acid)
PAMAM	Poly(amidoamine)
AFM	Atomic Force Microscope
FTIR	Fourier Transform Infrared
γ-APS	gamma-aminopropyltriethoxysilane
THF	Tetrahydrofuran

I. INTRODUCTION

1. PURPOSE STATEMENT AND MOTIVATION

The aim of this research is to propose a potential surface coating technique that can be used in silicon-based microfabricated biosensors for *in-situ* enzymatic detection. This study was conducted towards the development of a biosensor that can serve as an early-detection device for leukemia relapse. This thesis is the culmination of a two year study as part of a long-term joint effort between the department of electrical engineering and the school of medicine at Tecnológico de Monterrey to create a fully functional biosensor to monitor leukemia patients after treatment.

The motivation of this study came upon by the need to reduce the cost, discomfort and periodic biopsies that leukemic patients experience associated with the monitoring phase that follows treatment. A low-cost, painless alternative method for monitoring the progress of treatment would be beneficial for improving the life quality of patients. This type of device would detect changes in concentration of a specific biological indicator, and send a signal to the physician with information that there is a high risk that the patient is entering relapse. This early detection device would in turn, allow more time to take preventive measures. A Microfabricated biosensor can be designed to make *in-situ* measurements of a certain biomolecule that is associated with the disease at hand, processing the data and transmitting it wirelessly outside the body.

For a biosensor of this nature to work, it has to be coated with an active bio-layer that can interact with the molecule to be sensed. This work focuses on the challenge of incorporating a coating technique to grow an organic structure on top of a silicon substrate. This organic layer will serve as a support to immobilize an enzyme, inhibitor or receptor that can trap a desired molecule on top of the biosensor to detect its concentration or presence in a biological medium.

2. BACKGROUND

The coating technique researched on this work has been focused towards the development of a biosensor that can improve the quality of life of leukemia patients after treatment. This is an arduous process during which doctors have to evaluate the effectiveness of the treatment to determine if a patient has complete remission or the possibility of a relapse.

Physicians use the five-year relative survival rate as an indicator that shows how many patients survive cancer, five years after treatment. During this period of time, numerous tests are performed to evaluate if a patient has entered in relapse. These tests are performed periodically after treatment and consist of bone marrow biopsies and a complete

blood count (CBC). A common measure that indicates how much of the original disease is left in the body after treatment is the minimum residual disease (MMR). If results from the CBC show that the MMR is 5% or more, it is said that a patient has entered in relapse, or in other words, that the disease has returned. This means that 5% of the total number of cells examined are at an immature state of differentiation. These immature cells are called blasts and their elevated quantities in the blood and abnormal proliferation rates give rise to a type of blood cancer that is commonly known as Leukemia.

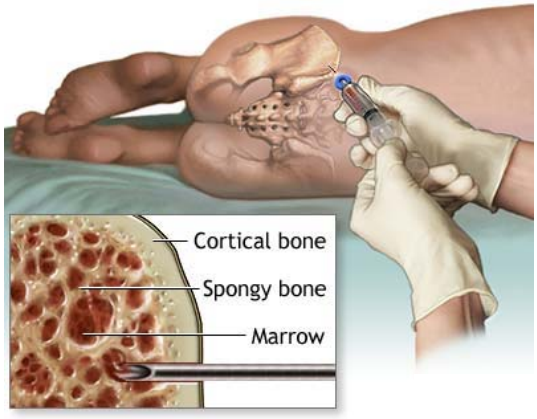

Figure 1: Bone marrow biopsy

2.1 LEUKEMIA

Leukemia is a cancer of the blood that emerges as a result of the rapid proliferation of immature white blood cells called blasts. These blasts do not have the proper functionality or are completely inactive due to the undeveloped state at which its differentiation stopped. The following sections will give a brief outline of the disease to introduce the non-medical reader to Leukemia, its detection methods and treatments.

2.1.1 PHYSIOLOGY

Bone marrow is the soft tissue found in the hollow interior of bones and is where the body's hematopoetic stem cells are located. These hematopoetic stem cells are the precursors to every cell found in the circulatory system, and they have the ability to differentiate into myeloid and lymphoid lineages. The differentiation of stem cells into myeloid or lymphoid cells can be altered by a cancer of the progenitor cells which causes defects in their development, stopping their differentiation process at an immature state.

Differentiation errors occurring in these two main blood cell lineages, give rise to the two main types of leukemia (myeloid and lymphocytic). Also, leukemia is further characterized as acute or chronic, which depends on the level of immaturity of the blast.

Acute leukemia is characterized by the rapid proliferation of blasts inside the bone marrow, which hinders the growth of healthy blood cells, and eventually leaking into the blood stream. Chronic leukemia is defined as the accumulation of relatively mature cells, but still abnormal.

There are few symptoms that a patient will experience during the early stages of the disease, often making a prompt diagnosis a challenge. Among the most common symptoms are: easy bruising, frequent infections, excessive bleeding, weakness, loss of appetite, swollen or bleeding gums, among others.

2.1.2 TYPES OF LEUKEMIA

As previously mentioned, there are two main types of leukemia, which further subdivide into acute or chronic. These classifications result in the four main types of leukemia which are briefly described below.

Acute Lymphoblastic Leukemia (ALL): This is the most common type of leukemia among children, and accounts for 3,930 new cases of leukemia in the United States each year, representing an 11% of leukemias. ALL is distinguished by the increased number of lymphoid (white blood cells) blasts in the peripheral blood and bone marrow, accounting for more than 30% of the total number of cells[1].

Acute Myeloid Leukemia (AML): AML is most common among adults, and accounts for 11,930 new cases each year, representing 34% of leukemias. AML is characterized by the rapid growth and accumulation of blasts of the myeloid cell line inside the bone marrow. This accumulation interferes with the reproduction and migration of healthy cells from the bone marrow to the peripheral blood stream[1].

Chronic Lymphoblastic Leukemia (CLL): CLL is the most common type of leukemia among adults, affecting men twice as much as women. There are more than 10,020 new CLL cases diagnosed each year in the United States, representing 29% of leukemias. CLL is distinguished by the excessive proliferation of lymphoid cells which may look mature, but are still dysfunctional[1].

Chronic Myeloid Leukemia (CML): CML accounts for 4,500 new cases each year, representing 13% of leukemias. CML is distinguished by the increased and unregulated production of myeloid blasts in bone marrow[1].

2.1.3 DETECTION METHODS

There are several detection methods which consist in the analysis of the cell's morphological, chemical, molecular and genetic properties. Most tests will start with a simple blood extraction and a complete blood count. A drastic increase in white blood cells (WBC) in the peripheral blood is a positive indicator of leukemia. While in a normal healthy subject, there could be between 4,000 and 10,000 cells/mL, in a person with leukemia, this concentration can be as high as 100,000 cells/mL.

This drastic increase in WBC in the peripheral blood is a strong indicator of leukemia, but requires a bone marrow biopsy or lumbar puncture for a proper prognosis. This is a relatively quick and simple procedure in which a hollow needle is used to perforate the pelvic bone and extract a sample of bone marrow and sometimes a piece of bone. When there is suspicion that leukemia has invaded the central nervous system, a lumbar puncture is required to extract a sample of cerebrospinal fluid. Some of the following analyses are performed to detect leukemia:

Cell count: a complete count of the different types of cells in a bone marrow sample to determine the number of immature white blood cells.

Morphological classification: a visual classification of the cell's characteristics under a microscope. This categorization of the cells can sometimes lead to the type of leukemia present or give some insight on the level of blast immaturity.

Immunologic properties: in some cases, the blast will seem normal to the naked eye, but will display irregular immunologic properties. A study of their surface antigens and receptors will determine their proper or improper functionality.

Cytogenetic properties: This technique refers to the study of chromosomes of the white blood cells obtained by a short term culture and collection during the metaphase stage. Specific dyes and markers are used to reveal genetic abnormalities.

2.1.4 TREATMENT AND FOLLOW-UP

Leukemia, as most of all other cancers, does not have a cure but there are several treatment options that can help control the disease. Some of the most common treatments are described below.

Chemotherapy: Chemotherapy refers to a treatment in which cytotoxic drugs are used to hinder the reproduction of cell with high proliferation rates. These drugs are usually delivered intravenously but there are also some chemotherapy drugs that can be administered orally. Since cancer cells reproduce at an uncontrolled high rate, these drugs affect their cell divisions and prevent their multiplication. Unfortunately, these drugs are

not specific for cancer and also attack other fast dividing cells in the body such as the ones responsible for hair growth and intestinal epithelium, resulting in massive hair loss and diarrheas among other potentially fatal side effects.

Radiotherapy: Radiotherapy is a treatment in which ionizing radiation is used to damage the DNA of cells and affect their reproduction. This radiation is directed to the diseased organ with a beam of photons, electrons or protons that ionize the atoms that make up the DNA chain. Because cancer cells are at an undifferentiated or immature state, they lack the ability to repair the damaged DNA and are killed, while healthy cells posses the ability to self-repair damaged DNA and survive.

Bone marrow transplant: This treatment involves the replacement of leukemic bone marrow cells with healthy hematopoetic stem cells. There are two types of bone marrow transplants, autologous and allogenic. The autologous transplant consists in the extraction and storage of hematopoetic stem cells from a patient that will undergo chemotherapy for their later re-implantation after treatment. Allogenic transplant refers to the transferring of hematopoetic stem cells from a donor to another patient which must have matching tissue types. For allogenic transplants, the recipient has to take immunosuppressive medications to decrease the possibility of rejection.

Any of the previous treatments mentioned above require an arduous follow-up phase in which several tests have to be made in order to assess the effectiveness of the treatment. Among the types of tests that are required, bone marrow examinations are the most useful to determine if a patient responded positively to the treatment and to evaluate the possibility of a relapse. Bone marrow biopsies are performed periodically which represent a very expensive and painful experience for patients. Therefore, an alternative monitoring method that can determine the possibility of a relapse by means of an indicator, other than bone marrow biopsies, would improve the quality of life of post-treatment patients. A solution to this challenge can be the detection of an enzyme or another biological substance whose concentration increases or becomes more prominent under a state of leukemic hematopoiesis. The following section describes the rennin-angiotensin system and some findings about its relationship with leukemic hematopoiesis.

2.2 RENIN-ANGIOTENSIN SYSTEM

For many years, the Renin-Angiotensin System (RAS) has been defined as a neurohormonal system found only in peripheral blood plasma, which main purpose is the regulation of blood pressure and electrolyte homeostasis. It is now known that different components of the RAS are locally active in specific organs and have a direct impact on their function.

2.2.1 RAS ACTIVATION

The RAS (Figure 2) is initiated by Renin (step 1), which is a circulating enzyme produce by the juxtaglomerular cells located in the kidneys in response to low blood volume/pressure or low electrolyte blood content. When Renin is released into the circulatory system, it cleaves to an oligopeptide (molecule formed by a chain of aminoacids) produced in the liver called Angiotensinogen (step 2). The cleavage of Renin and Angiotensinogen produce Angiotensin I (step 3), which has no biological activity and only serves as the precursor for Angiotensin II. The conversion of Angiotensin I to Angiotensin II is done by the removal of two terminal residues, catalyzed by the Angiotensin Converting Enzyme (ACE) (step 4). When elevated levels of Angiotensin II are present in the blood plasma, the outer section of the adrenal cortex releases the steroid hormone Aldosterone (step 5), which in turn stimulates the kidneys to retain salts, hence regulating the electrolyte concentration in the blood.

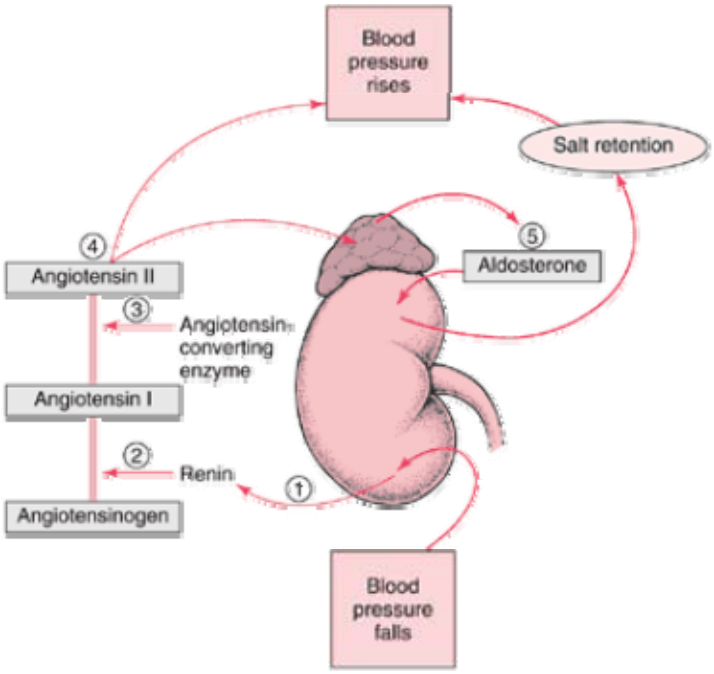

Figure 2: Rennin-Angiotensin System

2.2.2 RAS EFFECTS

The RAS has the primary function of regulating blood pressure and sodium concentration in the body. This system employs vasoconstriction and vasodilatation mechanisms activated by Angiotensin II to modify the diameter of blood vessels in order to regulate blood pressure. Also, to regulate electrolyte homeostasis, Angiotensin II stimulates the pituitary gland for the secretion of Anti Diuretic Hormone (ADH) that causes the re-

absorption of water in the kidneys and stimulates the subfornical organ in the brain, triggering the signals that increases thirst sensation and desire for salt.

Recent findings have confirmed the active presence of some components of the RAS in different organs in the body. Some of the mayor organs with active components of the RAS are: heart, lungs, blood vessel walls, kidneys, adrenal gland, brain, pituitary gland, among others. Additionally to these organs, studies have shown the presence of several components of the RAS in bone marrow, which might ultimately be linked to cellular proliferation and differentiation in physiological or pathological states.

2.2.3 CLINICAL SIGNIFICANCE

The Renin Angiotensin System has been studied to understand the impact it has on the body, in order to create treatments that target components of the RAS to inhibit or promote their effects. One of the first treatments that were suggested were the ACE inhibitors, which block the ACE molecule; hence, obstructing the conversion of Angiotensin I to Angiotensin II. These ACE inhibitor drugs are used to treat hypertension and congestive heart failure.

As previously stated, components of the RAS have been found to have other noncardiovascular effects in different organs in the body. These organ-based RAS exert diverse physiological effects at the cellular level, influencing cell growth, cell differentiation and data has shown that it may play an important role as mediators of apoptosis (programmed cell death). The following section describes some of the work related to the local bone marrow RAS and its possible use as an indicator for leukemic hematopoiesis.

2.2.4 CORRELATIONS WITH LEUKEMIC HEMATOPOIESIS

The first publication mentioning a local RAS in the bone marrow[2] was published by Haznedaroğlu et al. in 1996. After this publication, increasing investigations have been made to understand its effects on physiological and pathological hematopoiesis. Among the different components of the RAS, Renin, ACE, AcSDKP, Angiotensin II and AT1 receptors have been proven to be actively present inside the cellular elements and/or microenvironment of the hematopoetic bone marrow in health and disease.

A study conducted by Hüseyin et al., 2002 demonstrated a statistical increase in the local concentrations of ACE in bone marrow when leukemic samples were compared with healthy bone marrow samples[3]. Other studies by Rodgers et al. 2000 showed that Angiotensin II induces the proliferation of hematopoetic progenitor cells[4]. These findings further supports the theory that increased amounts of ACE have a direct impact in the

irregular proliferation of blasts by means of an increased conversion of Angiotensin I to Angiotensin II. Gomez et al. 2002 reported the presence of Renin in myeloid blasts while normal bone marrow cells do not display this expression[5].

Based on these findings, it was decided to work towards the design of a biosensor that can monitor a specific component of the RAS to determine the possibility of a leukemia relapse. This study focuses on the hypothesis that altered concentrations of the Angiotensin Converting Enzyme can be used as an early detection mechanism to predict a relapse after a leukemic patient has been treated with chemotherapy, radiotherapy or bone marrow transplant.

3. SCOPE OF RESEARCH

The information provided in the introduction section, sets up the framework and context of this research. The scope of this study centers on the first steps toward the development of a biosensor that can detect variations in the concentration of an enzyme whose fluctuations are correlated with leukemic hematopoiesis. This study focuses in the development of an organic layer that can cover a silicon-based microcantilever biosensor used for the concentration measurement of the angiotensin converting enzyme as an early detection mechanism for leukemia relapse.

This research encompasses the chemical reaction mechanisms necessary to construct this organic layer, reports the experimental lab work performed on silicon wafers to build the dendrimeric support and presents the data that supports these findings.

II. LITERATURE REVIEW

4. MEMS AS BIOLOGICAL SENSORS

Since their evolution from the integrated circuit (IC) industry, Micro-electromechanical systems (MEMS) have permeated into several fields with numerous applications as sensors and actuators. A major discipline with great potential for innovative applications for MEMS is the biomedical field, which introduced a new area of research unto itself called bio-MEMS. Bio-MEMS are sensors and/or actuators that can detect biological components in an organic medium with the purpose of monitoring a specific physical, biological or chemical function.

Different MEMS designs can be implemented to act as biosensors such as microcantilevers, microdiaphragms, and microchannels. The simplest types of bioMEMS are the microcantilevers, which acts as a platform that undergoes some kind of physical deformation or a change in its fundamental resonating frequency, due to molecular adsorption unto its surface. This sensing mechanism can be made very specific to a certain type of molecule by using receptor/ligand binding, enzyme/enzyme inhibitor reactions, or enzyme immobilization techniques over the biosensor's surface.

The following sections give a comprehensive review of the state-of-the-art research being done to develop bioMEMS: the materials and fabrication methods used, microcantilevers and their function as biosensors, and the surface coating techniques to sense biological molecules.

4.1 MICROCANTILEVER-BASED BIOSENSORS

Microcantilever sensors operate by detecting changes in resonance response or deflections caused by mass loading, surface stress variations, or changes in damping conditions. Four resonance response parameters (resonance frequency, amplitude, Q-factor and deflection) can be detected with microcantilevers to be used as sensing parameters for numerous applications. Surface stress produced as molecules adsorb on a cantilever can be observed as changes in deflections using chemically specific coatings.

The resonance frequency f of a microcantilever can be expressed as:

$$f = \frac{1}{2\pi}\sqrt{\frac{K}{m*}} \tag{4.2.1}$$

Where K is the spring constant of the lever and m^* is the effective mass of the microcantilever. The effective mass can be related to the mass of the beam, m_b through the relation $m^* = n(m_b)$, where n is a geometric parameter. From equation (1), it is clear that the resonating frequency can change due to changes in the effective mass as well as changes in spring constant. Therefore, the changes in frequency can be represented as:

$$df(m^*,K) = \left(\frac{\partial f}{\partial m^*}\right)dm^* + \left(\frac{\partial f}{\partial K}\right)dK = \frac{f}{2}\left(\frac{dK}{K} - \frac{dm^*}{m^*}\right) \tag{4.2.2}$$

By carefully designing microcantilevers with localized adsorption areas at the terminal end of the lever, the contribution of the dK/K term in equation (4.2.2) can be ignored and the entire change in frequency can be attributed to mass loading[6]. For rectangular cantilevers, the spring constant for vertical deflections is given by:

$$K = \frac{Ewt^3}{4L^3} \tag{4.2.3}$$

Where E is the modulus of elasticity for the composing material and w, t and L are the width, thickness and length of the beam respectively. Assuming that contributions from changes in spring constant are insignificantly small, equation (4.2.1) can be rewritten as:

$$f = \frac{1}{2\pi}\sqrt{\frac{Ewt^3}{4L^3(m_d + 0.24\rho wtL)}} \tag{4.2.4}$$

Where ρ is the density of the cantilever material and m_d is a discrete mass from $m_{eff} = m^* + m_d$ and m_{eff} is the effective mass of the cantilever-adsorbate system.

Another alternative method for measuring cantilever response is based on bending. This phenomenon only works when the adsorption is confined to one side of the cantilever. Bending under these circumstances is due to differential stress on the microstructure induced by molecular adsorption. Using Stoney's formula, the radius of curvature of the element undergoing bending can be expressed as:

$$\frac{1}{R} = \frac{6(1-\upsilon)}{Et^2}\delta s \tag{4.2.5}$$

Where R is the radius of curvature of the cantilever, υ and E are the Poisson's ratio and Young's modulus for the substrate, respectively; t is the thickness of the cantilever and δs is the film stress. The radius of curvature R is related to the deflection in the vertical direction z and the length of the cantilever L by the following equation:

$$z = \frac{3L^2(1-\upsilon)}{Et^2}\delta s \tag{4.2.6}$$

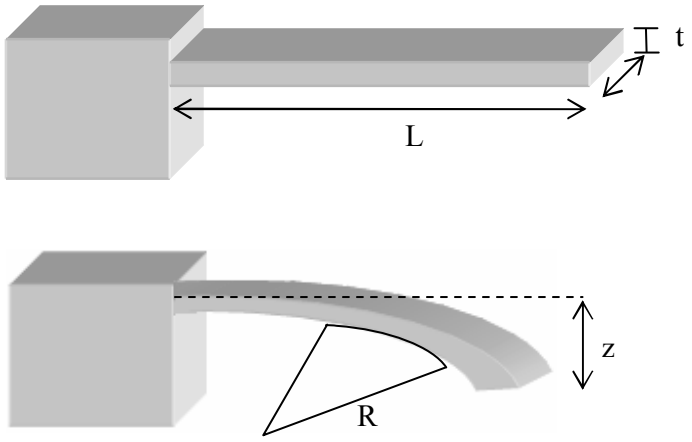

Figure 3: Representation of a microcantilever undergoing bending

Another important parameter to consider when using microcantilevers as biosensors is the damping effect. Damping of the medium can affect the resonance response of a cantilever. This phenomenon can be mathematically represented as a one-dimensional damped harmonic oscillator with a spring constant K and an effective mass m^*. Due to the viscosity of the medium, a portion of its mass will be carried along with the lever through its oscillation cycle.

5. BIOSENSOR SURFACE COATING

In the past few years, much research has been done to make chemically selective sensors by coating their surface with different layers that provide specificity to a desired chemical compound or molecule. These surface coating techniques allow interactions between organic and inorganic materials. With the purpose of evaluating the best coating method for this design, the following paragraphs will explain the different types of materials currently being explored to serve as chemically selective coating surfaces for biosensors.

5.1 SELF ASSEMBLED MONOLAYERS

Self-assembled monolayers (SAMs) can be made out of many types of molecules to adhere to almost any kind of substrate. SAMs are long alkane chains that are designed with a terminal side that has a strong affinity to the substrate material. This coating technique consists in the preparation of the solution containing the alkane chains and submerging the substrate in the solution. When the engineered molecules come in contact with the substrate they were designed to adhere to, they self-arrange and distribute evenly on top of the surface, forming a single thin layer (Figure 4). These layers are as thick as the length of a single alkane chain, which allow the creation of nanometric coatings.

Some examples of suggested and implemented applications for SAMs are: molecular recognition, SAMs as model substrates and biomembrane mimetics in studies of biomolecules at surfaces, selective binding of enzymes to surfaces, chemical force microscopy, metallization of organic materials, corrosion protection, molecular crystal growth, alignment of liquid crystals, pH-sensing devices, patterned surfaces on the µm scale, electrically conducting molecular wires and photoresists.

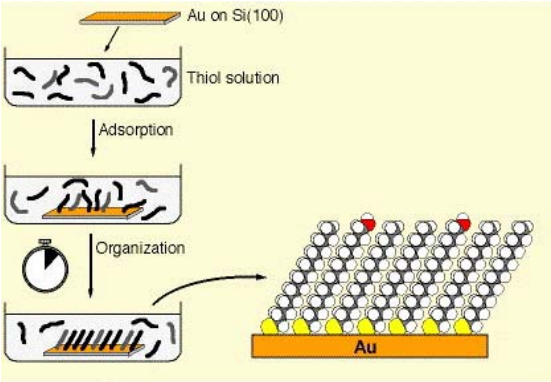

Figure 4: Schematic of self-assembled monolayers

SAMs were discovered in 1983 by a group of researchers experimenting with disulfides[7] and later with alkyl thiols[8] on gold plated surfaces. Sulfur and alkanes with a thiol head group have a particular affinity for gold, adhering with a binding energy[3] of 85-145 kJ/mol. For alkyl thiols on gold, the extended alkyl chains typically orient with an angle of ~30 degrees from the perpendicular of the substrate, and are assumed to be in a fully extended linear arrangement[3]. Since then, numerous investigation projects have been conducted to find other structures that self-assemble onto different substrates; some examples include: Alkyl silane molecules that adhere to silicon oxide surfaces[9], and alkyl carboxylates that self-assemble onto aluminum and mica.

5.2 HYDROGELS

Hydrogels are another viable source for coating biosensors to be used for *in-situ* detection. Hydrogels are mainly hydrophilic polymer networks that swell to a high degree due to an extremely high affinity for water, yet are insoluble because of the incorporation of chemical or physical cross-links. Among their numerous applications, one of the most promising implementations for hydrogels is their use as a protective coating for implantable biomedical devices since their water content is very similar to living tissue, are permeable to metabolites, are inert to biological processes, resist degradation, are not absorbed by the body, and can be prepared in various shapes and forms.

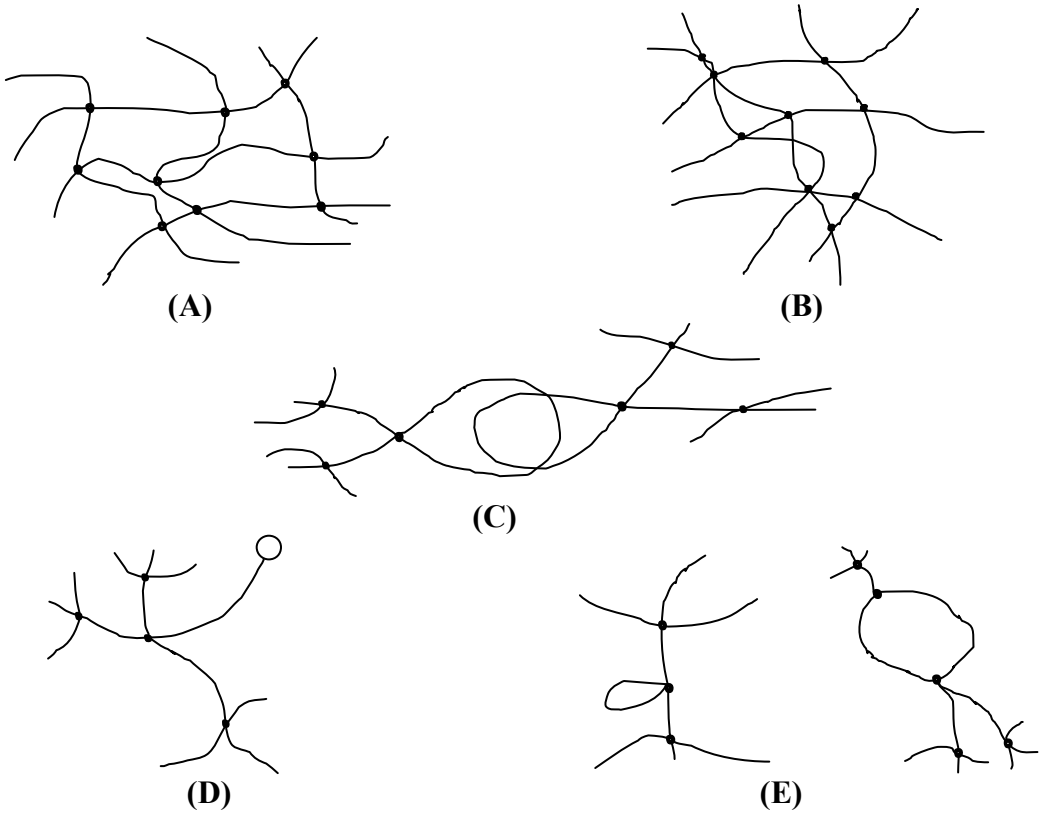

Figure 5: Macromolecular network of hydrogels

Figure 5 shows the ideal macromolecular network of a hydrogel (A), forming tetrafunctional cross-links (junctions). These ideal structures are rarely encountered and in reality, there are multifunctional junctions (B) and physical entanglements (C). Also, molecular defects are present such as unreactive functionalities with partial entanglements (D) and chain loops (E). Neither of these effects contributes to the physical and mechanical properties of hydrogels[10].

Hydrogels may be classified in several ways, depending on their method of preparation, ionic charge or physical structure features. Based on their preparation,

hydrogels may be (1) homopolymer (2) copolymer (3) multipolymer and (4) interpenetrating polymeric. Based on their ionic charges, hydrogels may be classified as (1) neutral (2) anionic (3) cationic and (4) ampholytic. Based on physical structural features of the system, they can be classified as (1) amorphous hydrogels, (2) semicrystalline hydrogels and (3) hydrogen bonded structures.

Some of the most recent work on hydrogels as surface coatings for biosensors has shown that by carefully selecting the functional groups along the polymer chains, hydrogels can be made sensitive to the environment and react to temperature, pH, electric field, ionic strength and specific analytes[11]. Figure 6 shows a pH-responsive microcantilever based biosensor coated with poly(methacrylic acid) PMAA and patterned onto SOI wafers with photolithography. The hydrogel micropatterns were prepared by spin coating the polymer and exposing it to UV light. The micropatterns were aligned on top of the microcantilever structures and adhered using the organosilane coupling agent, γ-methacryloxypropyl trimetoxysilane (γ-MPS). Results showed an ultra-sensitivity response of 5 x 10^{-5} ΔpH for every nanometer bending. This pH microcantilever sensor works due to the bending inflicted by the hydrogel when swelling by coming in contact with different pH solutions[12].

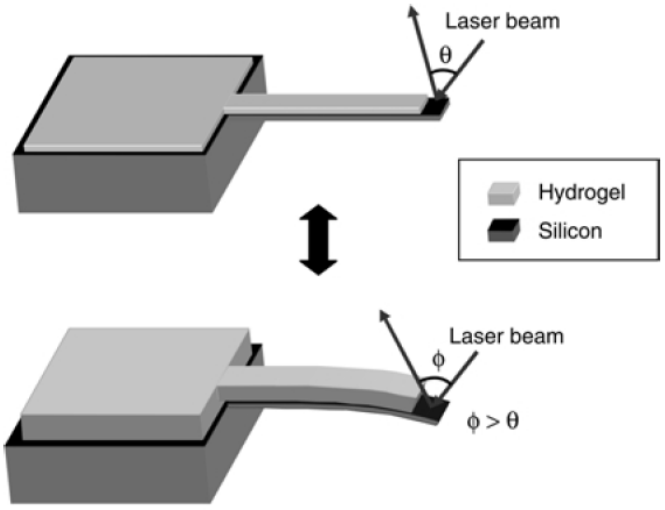

Figure 6: Microcantilever coated with a hydrogel

5.3 DENDRIMERS

Another major coating structure currently being explored to create biologically sensitive microstructures are dendrimer-based monolayers. Dendrimers are highly ordered, fully synthetic, tree-like structures, comprised of perfectly-branched repeated units. Figure 7 shows the structure of one of the most studied dendrimers: the polyamidoamine (PAMAM) dendrimer. Dendrimer chemistry is a novel research area with numerous applications in the fields of biomedicine and nanotechnology[13]. Unlike polymers, dendrimers have a high degree of molecular uniformity, narrow molecular weight distribution, specific size and shape characteristics, and a highly functionalized terminal surface.

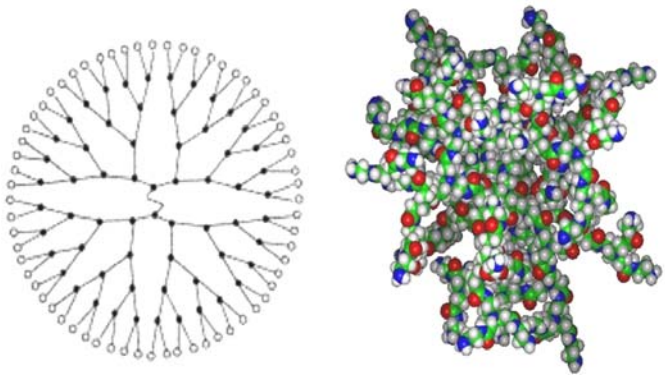

Figure 7: PAMAM Dendrimer

Dendrimers can be chemically engineered to have affinity to almost any compound and their manufacturing consists of repetitive chemical reactions, starting with a central initiator core. Each branch represents a new generation, and the iterative reactions can be repeated for as long as it is required to obtain a desired molecular diameter. Some of the applications in medicine and bioengineering with great potential for dendrimers are described below.

Drug delivery applications where dendrimers are used as encapsulation structures to either protect the drugs from the harsh environment in the stomach, or to provide a controlled release of the drug over a longer period of time. Also, these encapsulation structures can be made chemically selective to deliver drugs to a specific target. This application has an enormous potential for anticancer drugs, which have high systemic toxicity and affect other normal cells, by making them more selective in terms of which cells they are going to attack. Drugs can be inserted into a nanocapsule made of dendrimers, which could have the ability to penetrate the cell membrane and deliver drugs, genetic material or cell markers directly inside the cell.

Dendrimers can also be used as resists for scanning probe lithography. This technique makes use of the nanometric coating that can be grown on a semiconductor substrate and an atomic force microscope (AFM) to pattern the dendrimer surface to obtain

nanometric feature sizes in microelectronic circuitry components. The ultra thin dendrimer films formed on top of semiconductor materials are much smaller than the ones obtained by spin-coating ordinary polymers. A group from the University of California Berkley reported a successful nanometric patterning of silicon using poly(benzylether) dendrimer monolayers and an AFM operating in contact mode. The AFM tip was connected to a voltage source while lithography software controlled the path of the tip over the thin monolayer to pattern the surface. AFM Images in contact mode were collected right after the patterns were written. Results showed feature sizes of 2nm in height and 60nm in width on average. It was determined that feature sizes can be reduced by regulating the geometry of the electric field produced by the AFM tip, and that in optimal lithography conditions, single molecular resolution could be achieved[14].

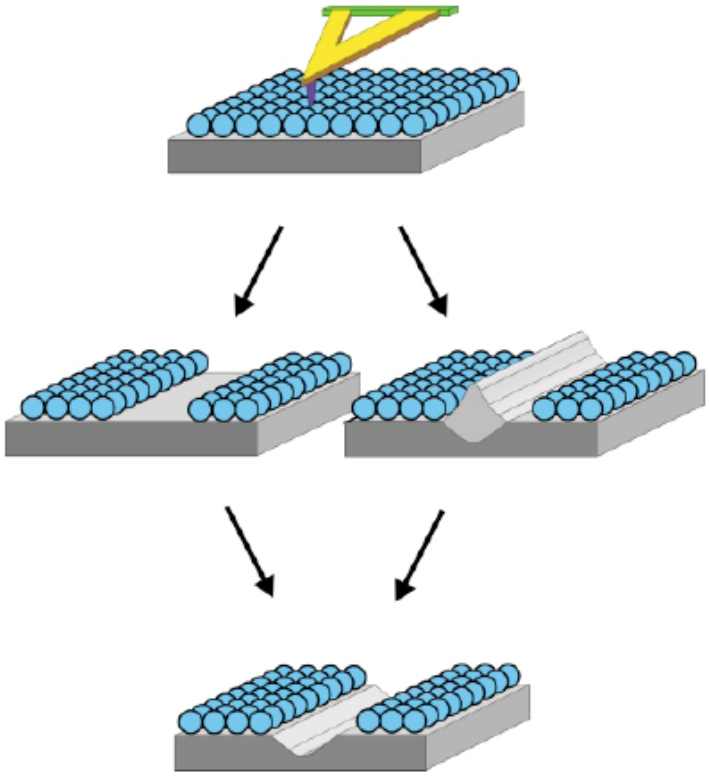

Figure 8: Schematic of scanning probe lithography

Figure 8**:** Schematic representation of field enhanced oxidation: dendrimer self-assembled monolayer (top); oxidative degradation of dendrimer monolayer at low field intensity (center left); oxidation of silicon substrate at high field intensity (center right); aqueous HF transfers pattern into positive tone image in silicon wafer (bottom).

6. SILANES AS COUPLING AGENTS

In order to successfully coat a silicon microcantilever with an organic layer, it is necessary to use a bonding substance that has affinity on one side to the inorganic substrate and on the other side, to the organic material. These types of coupling agents are known as silanes. These hybrid chemicals possess both organic and inorganic properties and have the ability to form strong covalent bonds across the interface[15]. Silanes have the following general structure shown in Figure 9:

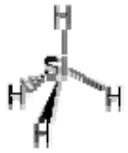

Figure 9: Silane general structure

Several industrial and medical applications exist for silanes. For instance, silanes are used as coupling agents to adhere glass fibers to a polymer matrix, stabilizing the composite material. They can also be used to couple a bio-inert layer on a titanium implant. Other applications include water repellants, masonry protection, control of graffiti, applying polycrystalline silicon layers on silicon wafers when manufacturing semiconductors, and as sealants.

Silica (SiO_2) is hygroscopic ie. it absorbs water onto its surface where the water breaks down into hydoxyl (-OH) groups. It is impossible to avoid the water especially as the surface modifier or 'size' is applied in a water based solvent. The coupling agent takes the form of a silane ($R\text{-}SiX_3$) where R is an organic radical that is compatible with the polymer matrix and X is a hydrolisable organic group such as an alcohol. The most common silane couplant is tri-ethoxy-silane. Heat will force the elimination of water between the -OH pairs at the hydrated silica surface and the silane as well as between the adjacent silane moecules

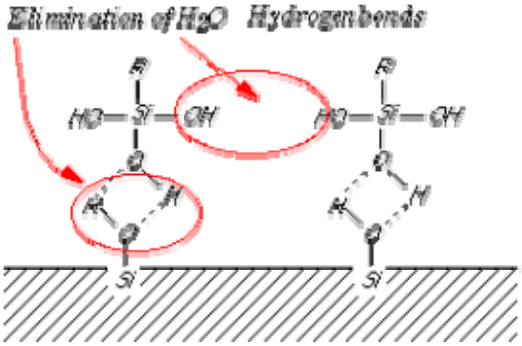

Figure 10: Formation of silane covalent bonds

In the presence of water, coupling agents produce highly reactive silanols. Subsequently, these silanols begin to condense, forming oligomeric structures while also

forming weak hydrogen bonds to the surface of inorganic materials. Finally, drying the inorganic materials leads to further condensation and dehydration between the coupling agent and the surface. This process yields multiple strong, stable, covalent bonds to the surface.

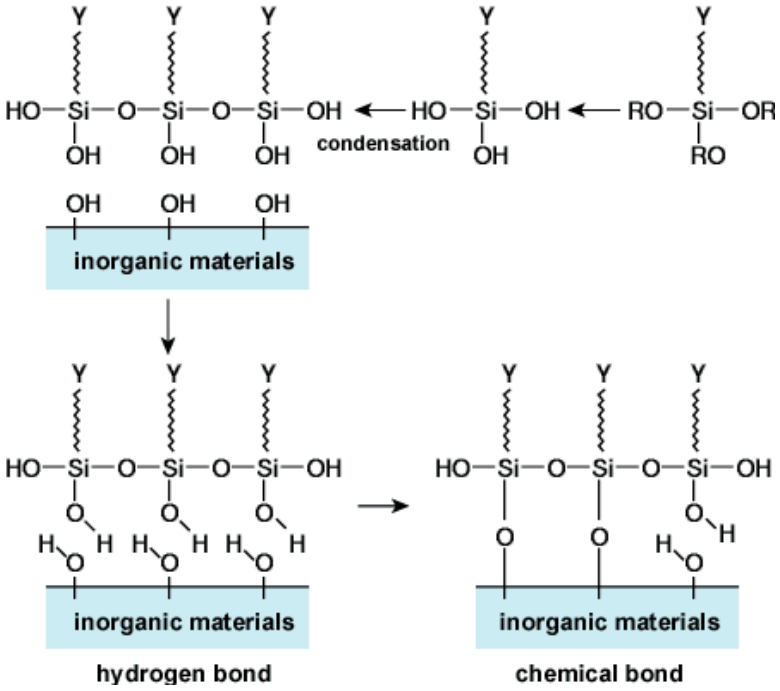

Figure 11: Silane adhesion mechanism

The silane used for this work is the γ-aminopropyltriethoxysilane (γ-APS), which has the following structure:

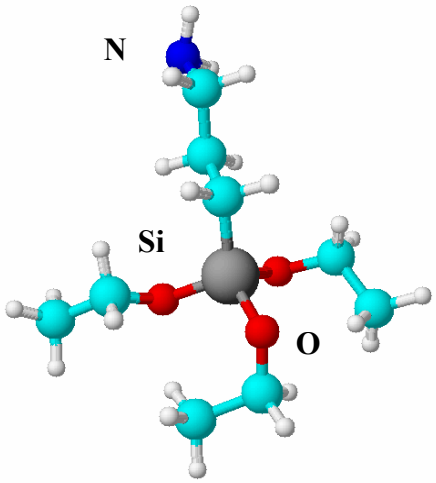

Figure 12: γ-aminopropyltriethoxysilane

7. DENDRIMER CHEMISTRY

The following pages will describe the chemical characteristics, structure and synthesis of dendrimers, which serve as a justification for their use in this work as a coating surface for silicon microfabricated biosensors. As briefly mentioned in section 5.3 as part of the biosensor surface coating chapter, dendrimers constitute a unique class of polymers that have a perfectly branched and monodisperse architecture. These man-made molecules can be easily controlled by synthetic methods to have a specific size, molecular weight and chemical functionality.

It is important to note that although most previous work on dendrimers depict their structure as a globular architecture, dendrimers can also be grown as layers when built on a flat solid substrate. This investigation tries to demonstrate their use as active layers to sense molecules in biological environments.

7.1 SYNTHESIS

The two main synthetic methods of preparing dendrimers are divergent and convergent approaches, both of which add a branch to the next generation in an iterative process, leading to a well defined macromolecule. When prepared in solution, dendrimers adopt a three-dimensional globular structure to minimize their free energy, having a direct impact on their physical properties. Also, by selecting the terminal ends of the dendrimer, their chemical composition can be manipulated to affect its properties such as: solubility, viscosity, hydrophobicity / hydrophilicity, and affinity to different compounds.

7.1.1 DIVERGENT APPROACH

First reported by Tomalia, Vögtle and Newkome during the mid 1980´s [16,17, 18], the divergent approach initiates growth from a central core, and expands outward in a series of repetition of coupling and activation steps. The coupling step consists of a reaction of the peripheral functionalities of the initiator core with a complementary reactive group. This step adds a new latent branch point at each coupling site, producing an increased number of peripheral functionalities (Figure 13).

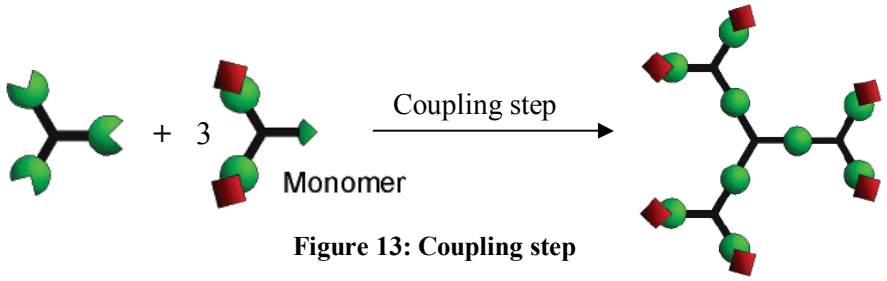

Figure 13: Coupling step

The peripheral functionalities (red squares) on each monomer are carefully selected to be unreactive with the third functionality of the monomer, in order to prevent uncontrolled hyperbranched polymerization. Once the first coupling takes place, the functional groups in the new branches can be removed to give place to a new branch point; this is known as the activation step (Figure 14).

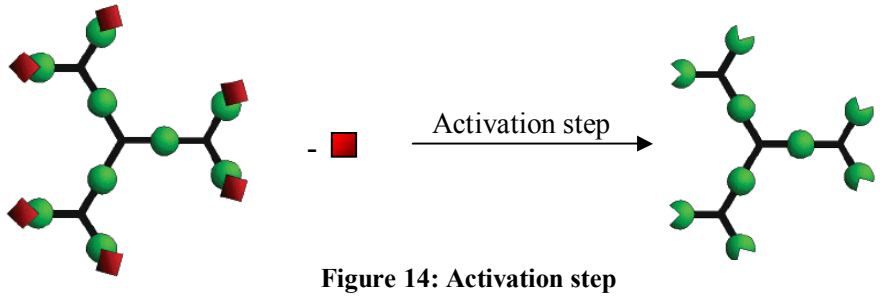

Figure 14: Activation step

The repetition of coupling and activation steps exponentially increases the number of functional sites, therefore requiring a large excess of reagents to drive the reactions to completion.

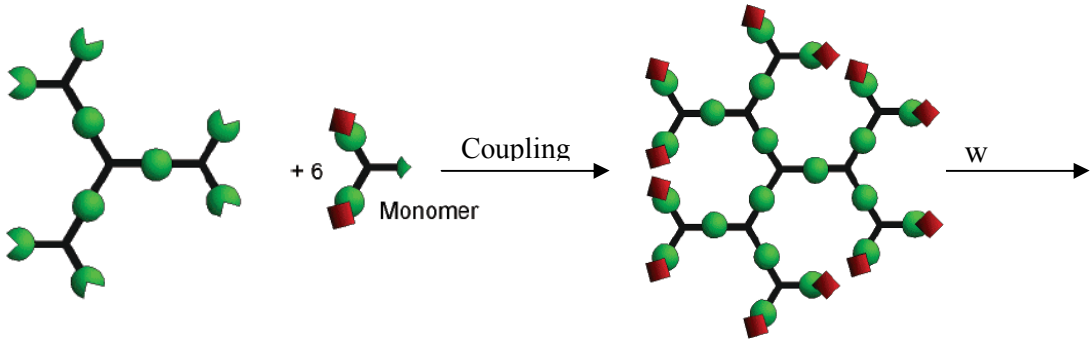

Figure 15: Repetition steps

7.1.2 CONVERGENT APPROACH

The convergent synthesis method was first reported in the early 1990´s by Hawker and Fréchet[19,20,21]. This method starts from what eventually will become the exterior of the molecule, growing inward by a series of coupling and activation steps. The main difference between the two synthetic approaches is that in the convergent method requires only a small number of reactions per molecule. As a result, the reactions can be driven to completion with only a slight excess of reagent, in contrast to the massive excess of reagent required for the divergent synthesis of high generation dendrimers. The work presented in this thesis is focused on the divergent approach, since the starter core of the dendrimer will be the surface of a silicon wafer.

7.2 DENDRIMER CHARACTERIZATION

Previous work on dendrimer characterization has reported several methods to analyze their structure, size and chemical composition. Among the most common methods used to date are: gel electrophoresis, atomic force microscopy (AFM), spectroscopic techniques, small angle neutron scattering (SANS), small angle x-ray scattering (SAXS), and transmission electron microscopy (TEM). The following sections will briefly describe the first three forementioned characterization techniques and their use.

7.2.1 GEL ELECTROPHORESIS

Gel electrophoresis has been widely used to separate biopolymers such as proteins or nucleic acids, but little has been done to separate synthetic polymers, such as dendrimers, due to their water insolubility. Also, since dendrimers are designed using a very controlled structure synthesis, their molecular weight distribution becomes too narrow and difficult to separate using this technique, although there have been reports of successful separation using gel electrophoresis[22,23], primordially on water-soluble dendrimers such as the poly(amidoamine) PAMAM[24]. Gel electrophoresis is based in the principle that charged particles move in the direction of an applied electric field towards the opposite electrode, through a medium that exerts a frictional resistance that the particles must overcome in order to migrate. This principle obeys Stokes´ Law:

$$f = 6\pi r v \eta \tag{7.2.1}$$

Where f is the frictional resistance, r is the radius of the particle, v is the particle's velocity and η is the viscosity of the medium. The electrophoretic driving force for a particle, depending on the electric field strength (E) and the net charge on the particle (z), is balanced by the frictional resistance (v):

$$f = E \times z \tag{7.2.2}$$

A particle's mobility (m) is defined as its migration distance (d) in time (t) under the influence of unit electric field strength (E):

$$m = \frac{d}{E \times t} = \frac{v}{E} \tag{7.2.3}$$

When combining equations 7.2.1, 7.2.2 and 7.2.3, one can see that when E·t is kept constant, the mobility of a particle depends on its net charge, size and nature of the medium. This technique has been proven useful to assess dendrimer purity, molecular weight and probe the binding between dendrimers and DNA[25].

7.2.2 SPECTROSCOPIC TECHNIQUES

A powerful qualitative tool used to characterize dendrimers is by the use of light in several ranges of the electromagnetic spectrum. There have been many dendrimer characterization studies using indirect spectroscopic methods implementing photophysical and photochemical probes by ultraviolet spectroscopy on the visible range (UV-Vis) and fluorescence spectroscopy, as well as spin probes by electron paramagnetic resonance (EPR) spectroscopy.

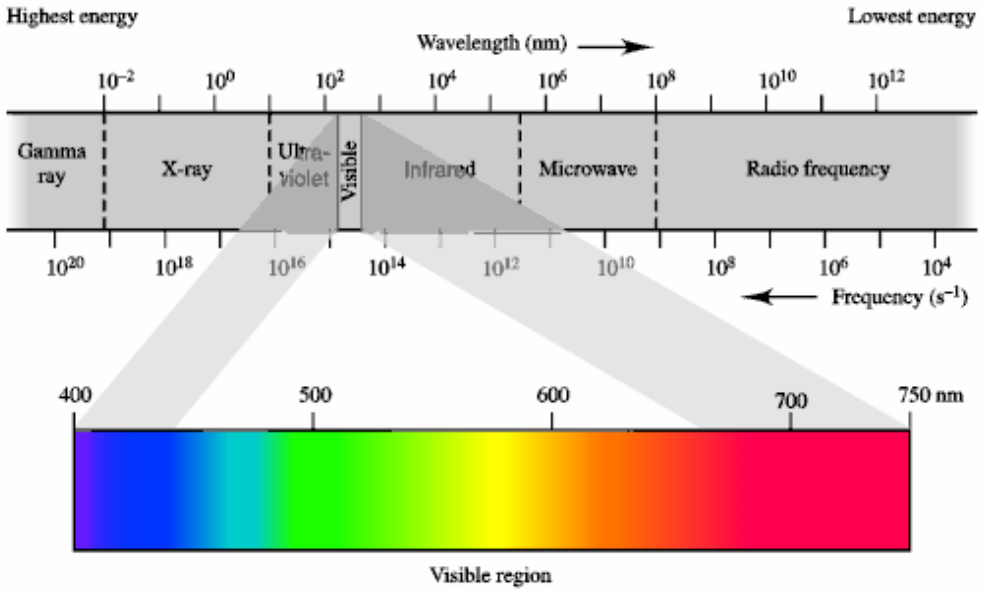

Figure 16: Electromagnetic spectrum

Another method mentioned in literature is the Fourier transfer infrared (FTIR) spectroscopy technique. This characterization method consists in the use of infrared light to analyze the vibration of molecules. Each functional group in a chemical structure vibrates at a unique frequency that allows for its detection in a sample. The sum of all the vibrations generates a "fingerprint" for the sample, determining which functional groups are present, thus allowing for its characterization. This method implements Fourier's mathematical operations to translate a complex curve into its component curves. In an FTIR instrument, the sum of the constructive and destructive interferences generated by the overlap of light waves is called an interferogram. This complex curve is then broken down to its component curves using Fourier's transform to generate the infrared spectrum of a sample. This spectrum is displayed as a graph of percent transmittance (%T) vs. light frequency (cm^{-1}). The following paragraphs will give a brief introduction to FTIR spectroscopy and the principles of its operation.

FTIR Basic Principles

The infrared region of the electromagnetic spectrum is bound by the high-frequency red end of the visible range and by the low frequency microwaves (Figure 16), ranging in wave lengths (λ) from 0.78 to 1000 μm. Every atom in a molecule is in constant vibration with respect to one another; when a molecule is hit by an IR frequency that equals its vibrational frequency, the molecule absorbs this radiation. This absorption is interpreted by the instrument and is given a value between zero and infinity. To interpret the results as a percentage, the absorbance is converted to a ratio of radiant power transmitted by the sample (I) to the radiant power incident on the sample (I0), or percent transmittance (%T). As shown on equation 7.2.2, absorbance is a logarithm base 10 of the reciprocal of the transmittance.

$$A = \log_{10}\left(\frac{1}{T}\right) = -\log_{10}(T) = -\log_{10}\left(\frac{I}{I_0}\right) \tag{7.2.2}$$

Each atom has 3 degrees of freedom which corresponds to motion in any of the 3 Cartesian coordinates. The principal molecular movements are: bending and stretching, which can happen symmetrically or anti-symmetrically, in the same plane or out-of-plane (Figure 17).

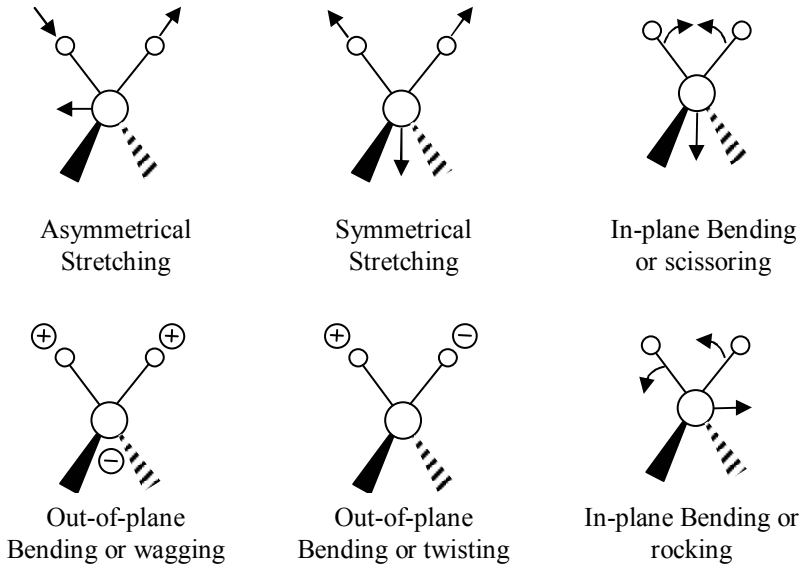

Figure 17: Molecular vibrations

The Fourier transform infrared (FTIR) spectrometer does a complete frequency sweep through the sample and analyzes all the absorbency frequencies simultaneously. The IR source releases a ray of light which passes through a beam splitter, dividing it in two halves, one half goes to a fixed mirror and the other half to a movable mirror. Due to changes in the relative position of the moveable mirror with respect to the fixed mirror, an

interference pattern is produced. Both halves are recombined at the splitter and pass through the sample and into the detector (see Figure 18).

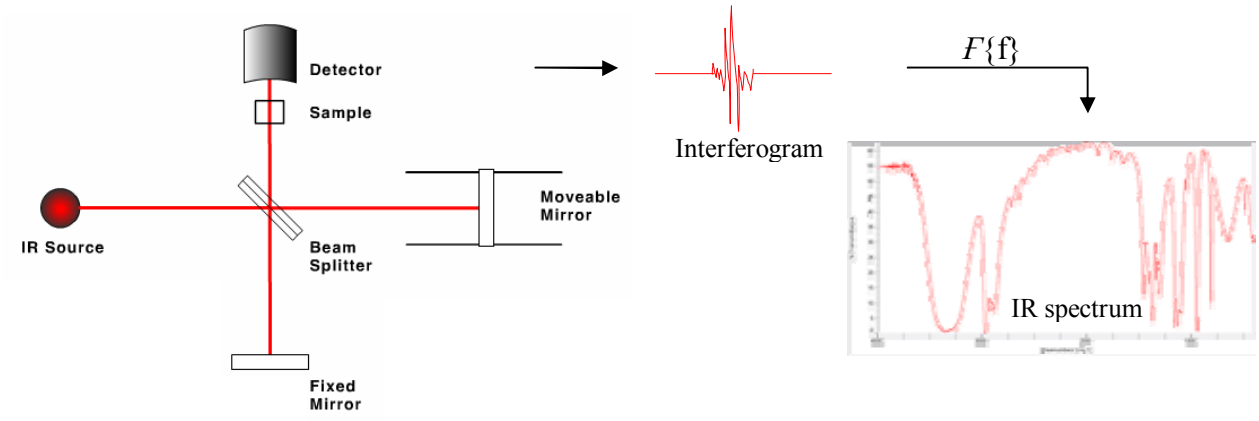

Figure 18: Schematic of a FTIR spectrometer

When the mirror is moved at a constant velocity, the intensity of radiation reaching the detector varies in a sinusoidal manner to produce the interferogram output, which is the record of the interference signal. It is actually a time domain spectrum and records the detector response changes versus time within the mirror scan. If the sample happens to absorb at this frequency, the amplitude of the sinusoidal wave is reduced by an amount proportional to the amount of sample in the beam.

7.2.3 ATOMIC FORCE MIRCOSCOPY

Atomic force microscopy (AFM) has been proven to be a very useful tool for analyzing dendrimer surface topography as well as measuring other molecular level and nanoscale structure properties using high-resolution imaging. AFM, in contrast to traditional microscopy, does not implement the use of lenses, but rather utilizes a cantilever beam in contact with the sample. This extremely sensitive and sharp probe is only tens of nanometers wide and it is placed at the end of a cantilever arm as shown in Figure 19. As the probe scans the surface of the sample in contact mode, a laser bounces off the end of the cantilever onto a position sensitive photodetector. This signal is processed by a computer to generate three-dimensional images with aspect features in the order of 10pm[26].

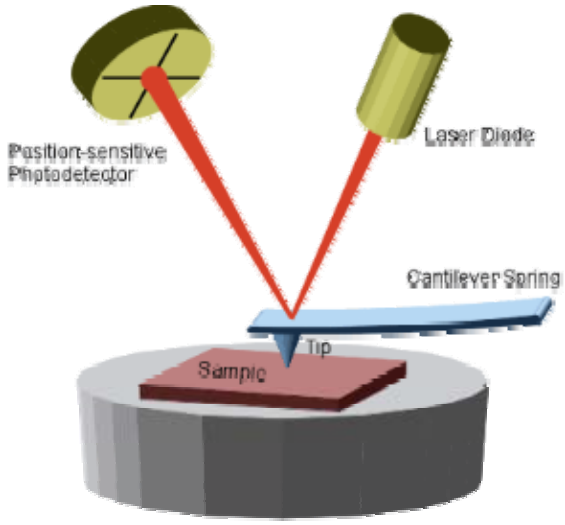

Figure 19: AFM schematic

AFM is one of the preferred characterization technique currently used to analyze the surface interactions of dendritic films on solid surfaces. A study conducted by Piehler, Baker and Tomalia[27] reported AFM images of PAMAM dendrimers on mica surfaces, which clearly showed monodispersed, dome-shaped individual molecules. These images led to the conclusion that amine terminated dendrimers tend to form uniform densely packed films in order to maintain lower surface tension at low concentrations. Also, results showed that the film uniformity is mostly determined by dendrimer solution concentration, regardless of the generation.

Figure 20a shows how the PAMAM dendrimers aggregate on mica forming globular structures at a concentration of 0.1% w/w, while Figure 20b shows a more uniform and flat adhesion on mica with a dendrimer concentration of 0.01% w/w.

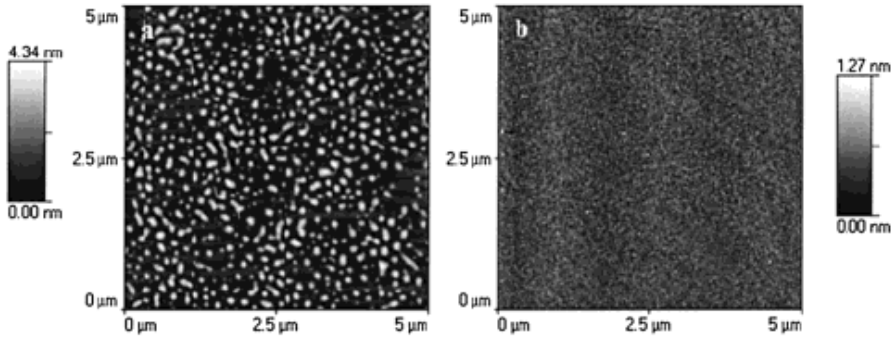

(a) (b)

Figure 20: PAMAM dendrimers at different concentrations

The specifications of the AFM used in this work can be found in Appendix B of this report.

8. DENDRIMERS AS ACTIVE BIOLAYERS

As previously stated, due to their well defined and unique macromolecular structure, dendrimers can provide an ideal matrix to serve as a support for biological molecules such as enzymes. Their globular representation in most articles can be misleading since dendrimers can also be grown as layers on top of a flat substrate such as a silicon wafer. This vertical growth allows dendrimers to be used as bio-active layers for microfabricated biosensors.

The earliest known study of dendrimers grown on a solid surface was conducted by Regen and Watanabe[28] in 1994. They first demonstrated the concept by constructing a PAMAM multilayer film on top of an oxidized silicon surface with a primary amine termination. After this work, numerous studies have been conducted to improve and suggest new surface coating techniques to give solid substrates a specific functionality.

Varahramyan and Lvov report a successful layer-by-layer dendrimer assembly on a silicon substrate in combination with traditional lithography to fabricate an ultrathin microcantilever[29]. In this work, hundreds of dendrimer coated microcantilevers were fabricated on a silicon wafer with the goal of developing chemical/biosensor arrays for massive data gathering.

PAMAM dendrimers have also recently been used as polyfunctional templates for the immobilization of biological molecules on inorganic surfaces. Anzai et al. demonstrated the sequential deposition of a dendrimer-protein miltilayer film on gold or quartz surfaces[30]. This study proposes an interesting approach to build dendrimers combined with biological molecules to be used as coating thin-film materials for biological sensors.

The table shown below (Table 1) shows the calculated properties of the amines surface PAMAM dendrimer by generation.

Generation	Molecular Weight	Measured Diameter (Å)	Surface Groups
0	517	15	4
1	1,430	22	8
2	3,256	29	16
3	6,909	36	32
4	14,215	45	64
5	28,826	54	128
6	58,048	67	256
7	116,493	81	512
8	233,383	97	1024
9	467,162	114	2048
10	934,720	135	4096

Table 1: PAMAM properties by generation

9. CHOICES FOR DESIGN

After a careful analysis of the different options presented in the preceding sections and following a diligent evaluation of the facilities and equipment available, the next choices for design were made:

1. A microcantilever based biosensor in static mode is the proposed mechanism to detect enzymatic concentrations.

2. For the biosensor surface coating, a PAMAM dendrimer structure has been selected as the ideal organic support for a molecular receptor (i.e. ligand, inhibitor, antibody, etc) due to its simple synthesis, biocompatibility and structural integrity.

3. The ideal coupling agent between organic and inorganic materials has been identified as the γ-aminopropyltriethoxysilane (γ-APS) for its simple structure and high affinity to silicon with an organic functional end-group (primary amine).

4. The PAMAM synthetic method that will be followed for the construction of the dendrimeric support will be the divergent approach, parting form the primary amine that becomes available after silicon functionalization with the γ-APS.

5. The chemical characterization will be made with a Fourier transform infrared spectrometer and the physical characterization with an atomic force microscope.

In the next chapter, a detailed description is given of the experimental procedures that were carried, out implementing the aforementioned design choices. This investigation was performed in order to evaluate the use the PAMAM dendrimer as a coating layer grown on a silicon substrate, which can serve as a support structure for a molecular receptor in microfabricated biosensors.

III. EXPERIMENTAL PROCEDURES

10. SILICON WAFER FUNCTIONALIZATION

As mentioned in section 6 of this thesis, the first step to form an active organic layer on top of an inorganic substrate, is to implement the use of a silane as a coupling agent. The following procedure describes the materials and methods used to functionalize a silicon wafer with the gamma-aminopropyltriethoxysilane (γ-APS) shown in Figure 12.

Materials:

A set of 25 p-type (Boron doped), 1-side polished, 2-inch diameter, 300µm thick, Si(100) wafers were purchased from Wafer World Inc. (see specifications on Appendix A). Also, 500mL of γ-APS from the United Carbide Corporation were donated by the Department of Chemistry at Tecnológico de Monterrey – Campus Monterrey (see specifications on appendix A).

Methods:

A silicon wafer was carefully cut into ~5mm square pieces with a glass cutter as shown in figure 18. The silicon pieces were washed with acetone and dried in an oven for 5 minutes at a temperature of 50°C. The samples were transferred to a 125 mL Erlenmeyer flask and submerged in 25 mL of the γ-APS for an hour. The flask was shaken constantly to stir the samples in the silane solution.

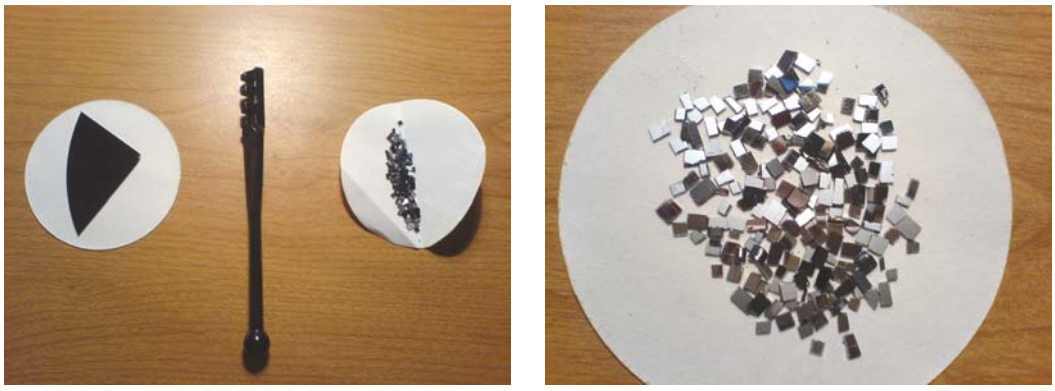

Figure 21: Silicon pieces

The γ-APS adhesion to the silicon substrate follows the mechanism described in section 6 of this thesis. As illustrated in Figure 22, the silane forms a covalent bond with the silicon wafer, which becomes functionalized with a primary amine group.

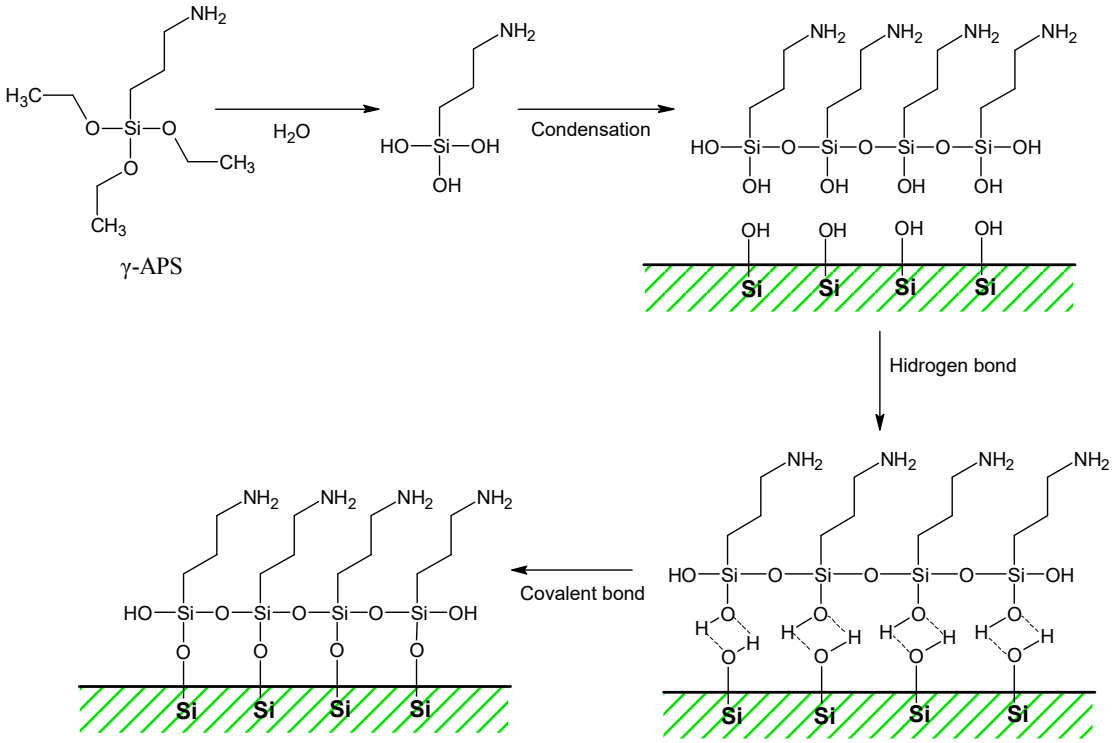

Figure 22: Mechanism of silane adhesion to silicon

After an hour, the silicon pieces were removed from the silane solution and washed with ethanol. 2 samples were removed from the original batch and were set aside in 1.5 mL vials to characterize with the atomic force microscope and a Fourier Transform Infrared (FTIR) spectroscope with the Attenuated Total Reflectance (ATR) accessory. The rest of the silicon pieces were rinsed thoroughly with ethanol and set to dry on a filter paper.

Once the surface of the silicon samples were completely aminated, the dendrimer can start its growth by a series of iterative reactions that will start with the alkylation of the amino functional groups. The subsequent section describes the procedure followed for the dendrimer growth, using the divergent synthesis approach described in section 7.1.1 of this report.

11. ITERATIVE REACTIONS

As previously mentioned, the construction of the PAMAM dendrimer, parting from an aminated silicon surface, follows the divergent synthesis approach proposed by Tomalia[9] et al. and described in section 7.1.1 of this report. This synthesis starts with a Michael addition and an exhaustive alkylation at the amino group with two molecules of methyl acrylate. The second reaction in the sequence of iterations is the exhaustive amidation of the ester functional groups using a large excess of ethylenediamine. This process continues by repeating a Michael addition followed by an amidation reaction to reach a specific dendrimer size, or in this case, a specific layer thickness. Each new addition represents a new generation of the dendrimer, which branches out in a fractal fashion. The steps described below were followed in order to construct a 4 generation (G4) PAMAM dendrimer using the aminated silicon surface from the previous section.

Reactants:

Ethylenediamine Methyl Acrylate Tetrahydrofuran (THF) Ethanol

Step 1: Michael addition

Half of the functionalized silicon wafer pieces from the previous step were placed in a 250 mL Erlenmeyer flask with excess (~30mL) methyl acrylate in the presence of 10mL of the polar aprotic solvent: tetrahydrofuran (THF). The reaction was left at room temperature for a period of 24 hours. The other half of the silicon pieces were set on a different flask and were left in solution for a period of 48 hours. This strategy was implemented in order to test the effect of time in the reactions. The following mechanism describes the Michael addition reaction that occurred in step 1:

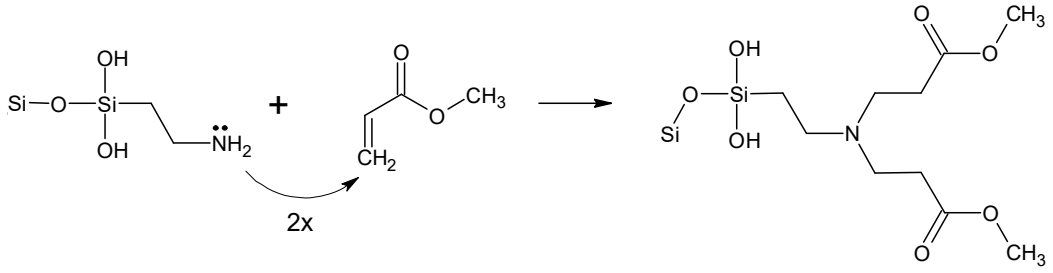

Figure 23: Michael addition

After the silicon samples were removed from the solution, they were filtered and rinsed first with THF and then with ethanol. The samples were dried in an oven at 60°C for one hour. When the pieces were removed from the oven, 2 samples were set aside for their future analysis and characterization with the FTIR and the AFM. The rest of the silicon pieces were transferred to a new flask for the amidation reaction that is described below. This constitutes the first generation (G1).

Step 2: Amidation reaction

When the dried silicon pieces were transferred to a clean flask, they were submerged in excess (30 mL) ethylenediamine with 10 mL of THF as a solvent and left to react at room temperature, one batch for 24 hours and the other for 48 hours. This reaction consists in the amidation of the terminal esters from the previous step. This process adds once more the amine functional group, extending the first generation by 2 carbons. The mechanism below describes the amidation reaction.

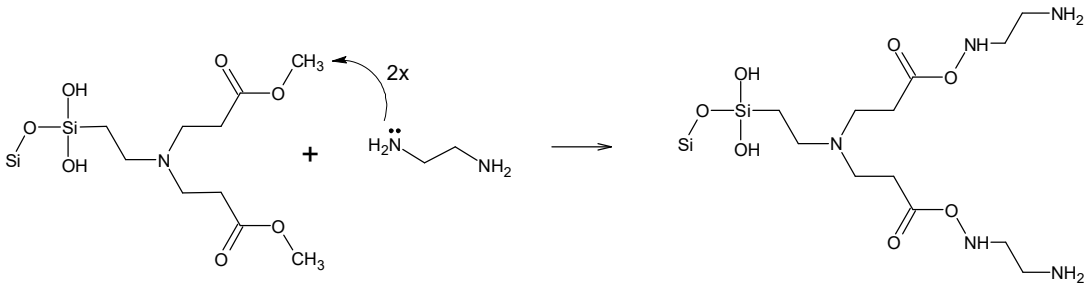

Figure 24: Amidation reaction

Once the amidation reaction was completed, the silicon pieces were filtered and rinsed first with THF then with ethanol. Afterward, the pieces were set to dry in an oven at 60°C for a period of 5 minutes. When the silicon pieces were dry, 2 samples were set aside for their future analysis and characterization with the FTIR and AFM. The rest of the batch was transferred to a clean flask to repeat step 1.

Steps 3-10: Alternating Michael addition and amidation steps

To generate a G4 dendrimer, or in this case, to coat the silicon pieces with a layer 4-generations-thick, iterative growth is continued by alternating between Michael addition and amidation reactions. At the end of each drying stage, 2 samples were removed from the batch for their analysis with the FTIR and the AFM. At the end of step 8, the fourth generation is completed and all remaining samples are stored. Table 1 summarizes the reaction steps.

Day	Generation	Reaction	Reaction time		Reagents
1	G 0	Silicon functionalization	1 Hr	1 Hr	Silane
	G 1.0	Michael addition	24 Hr	48Hr	Methyl acrylate + THF
2	G 1.5	Amidation	24 Hr	48Hr	Ethylenediamine + THF
3	G 2.0	Michael addition	24 Hr	48Hr	Methyl acrylate + THF
4	G 2.5	Amidation	24 Hr	48Hr	Ethylenediamine + THF
5	G 3.0	Michael addition	24 Hr	-	Methyl acrylate + THF
6	G 3.5	Amidation	24 Hr	-	Ethylenediamine + THF
7	G 4.0	Michael addition	24 Hr	-	Methyl acrylate + THF
8	G 4.5	Amidation	24 Hr	-	Ethylenediamine + THF

Table 2: Iterative reactions

Figure 25 summarizes the iterative steps followed to coat the silicon samples with a 4-generation-thick layer.

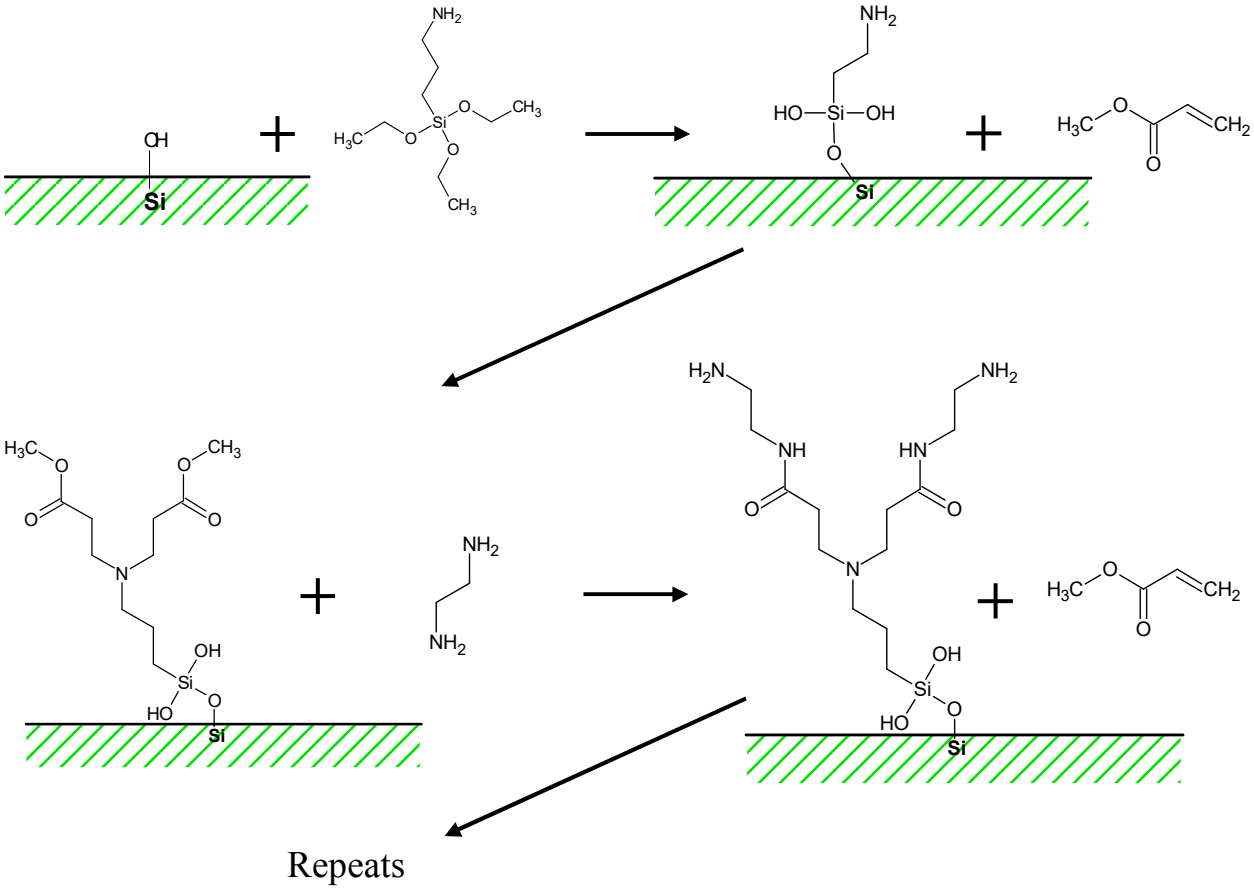

Figure 25: Iterative reactions

Figure 26-B shows a single G4 “tree” of the many dendrimers that branched out at each amine group in the functionalized silicon samples (represented in Figure 26-A).

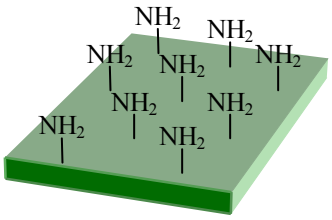

(A)

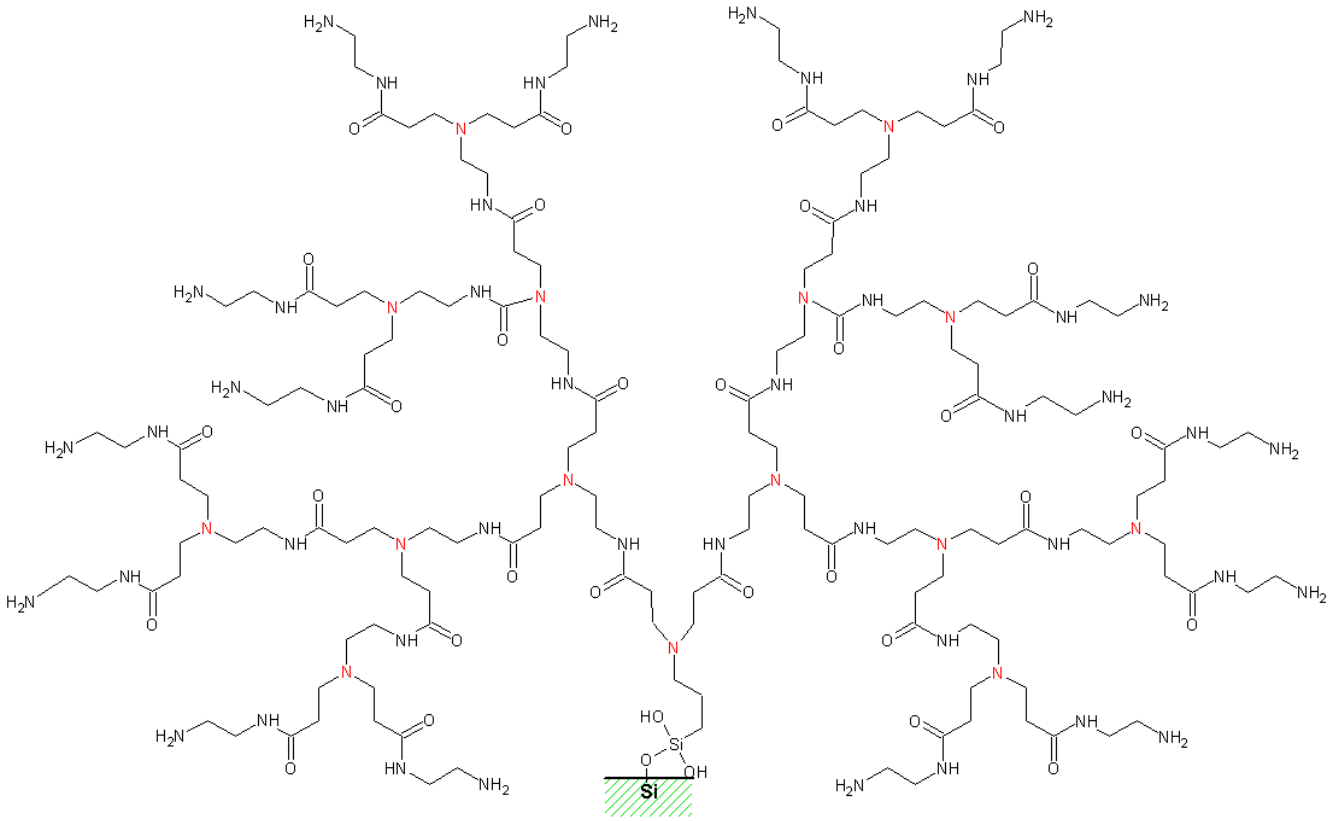

(B)

Figure 26: G4 PAMAM

12. FTIR CHARACTERIZATION

At the end of the experimental procedure, there were 2 sets of samples obtained at different stages of the overall reaction. The table below summarizes the samples obtained and the nomenclature used to identify them. "MA" stands for Michael addition reaction and "A" stands for amidation reaction:

	Pure Si	Silane	MA	A	MA	A	MA	A	MA	A
24 Hr	Si	G0	G1.0	G1.5	G2.0	G2.5	G3.0	G3.5	G4.0	G4.5
48 Hr		g0	g1.0	g1.5	g2.0	g2.5	-	-	-	-

Table 3: Samples obtained

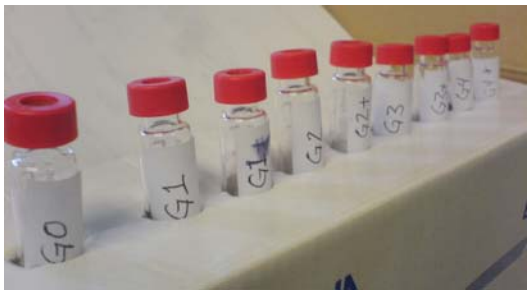

When all the samples were obtained, a Perkin-Elmer AutoIMAGE FT-IR Microscope, coupled to a Spectrum GX was used in reflectance mode to acquire a chemical map of each of the samples. The equipment used in this investigation was borrowed from the Department of Polymers at the Universidad Autonoma de Coahuila in Saltillo. Specifications for this instrument can be found in appendix B of this thesis. The Spectrum GX FTIR was set to a resolution and J-stop resolution of 4.00 cm^{-1}, an optical-path-difference (OPD) velocity of 2cm/s, and a gain of 1. Also, the line scans were swept in the mid-IR region, at a frequency range of 650cm^{-1} to 4000cm^{-1}. Each line scan consisted of eleven samples with 32 scans per sample, having an overall scanning time of about 4 minutes.

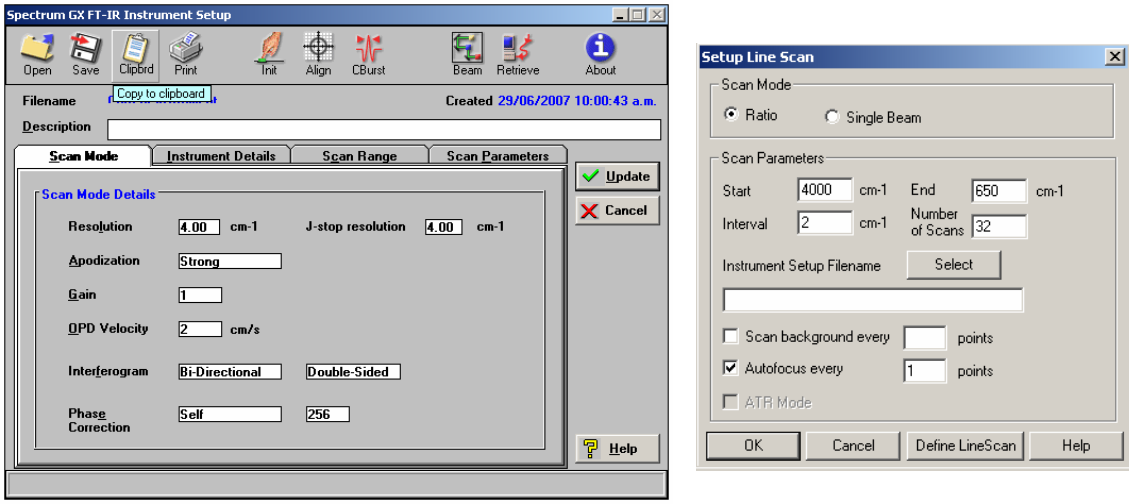

Figure 27: FTIR scan mode and setup

The image shown below displays the background acquired as part of the calibration of the FTIR microscope. The sharp pronounced peak at 2400 cm^{-1} is characteristic of the concentration of CO_2 of the surrounding environment.

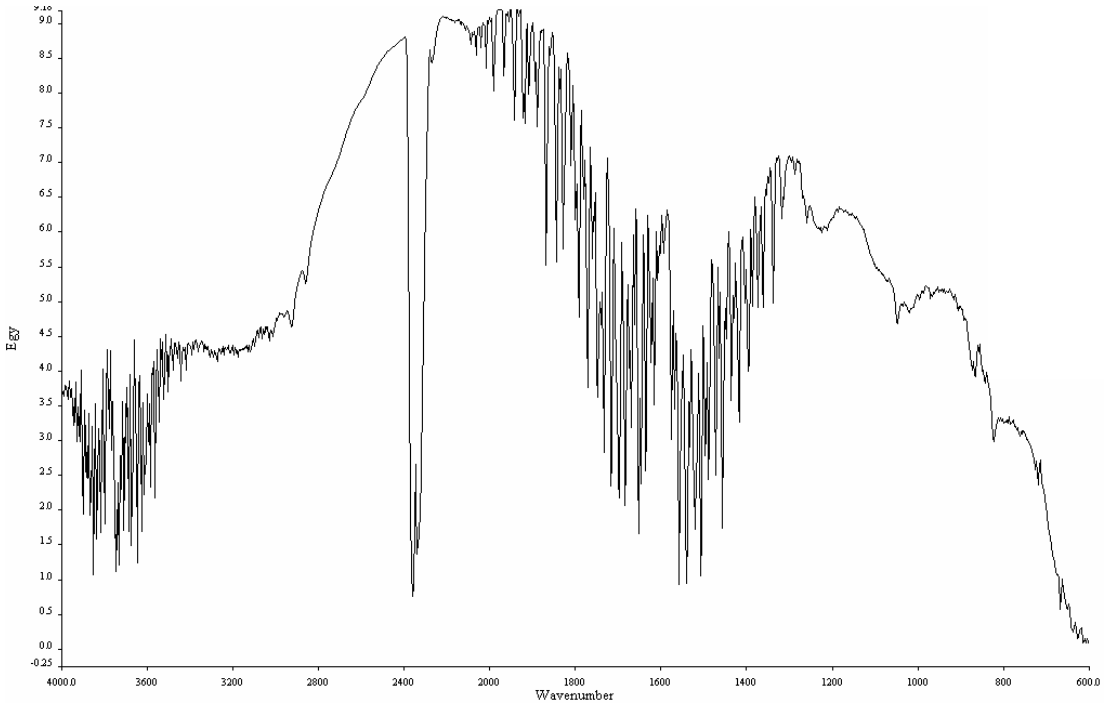

The following pages show the results of each of the scanned samples, shown in Table 3. Each sample has (1) a picture of the studied region with an 11-point line scan, (2) two overlapped infrared spectrums, (3) a 3D image and (4) a false-color map of the sample.

Pure Silicon

For comparison purposes, a clean silicon wafer was scanned using the same setup. It can be shown from the false-color map and from the 3D image, that the surface is chemically uniform, since the map shows a single shade of green throughout the sample. Also, at a frequency of about 1200 cm^{-1}, the silicon absorbs the least amount of energy, and the peaks observed at around 2350 cm^{-1} correspond to the amount of carbon dioxide (CO_2) present in the air at the time the sample was measured. The wireframe image shows the infrared spectrum at each of the eleven scanned points in the line scan.

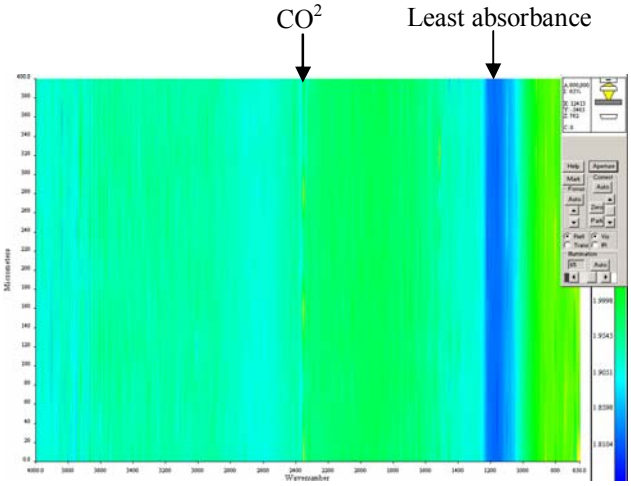

Si false-color map

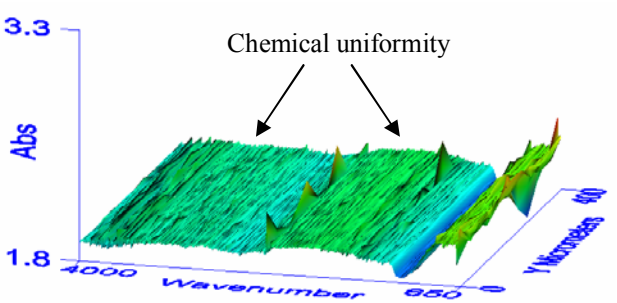

Si 3D image

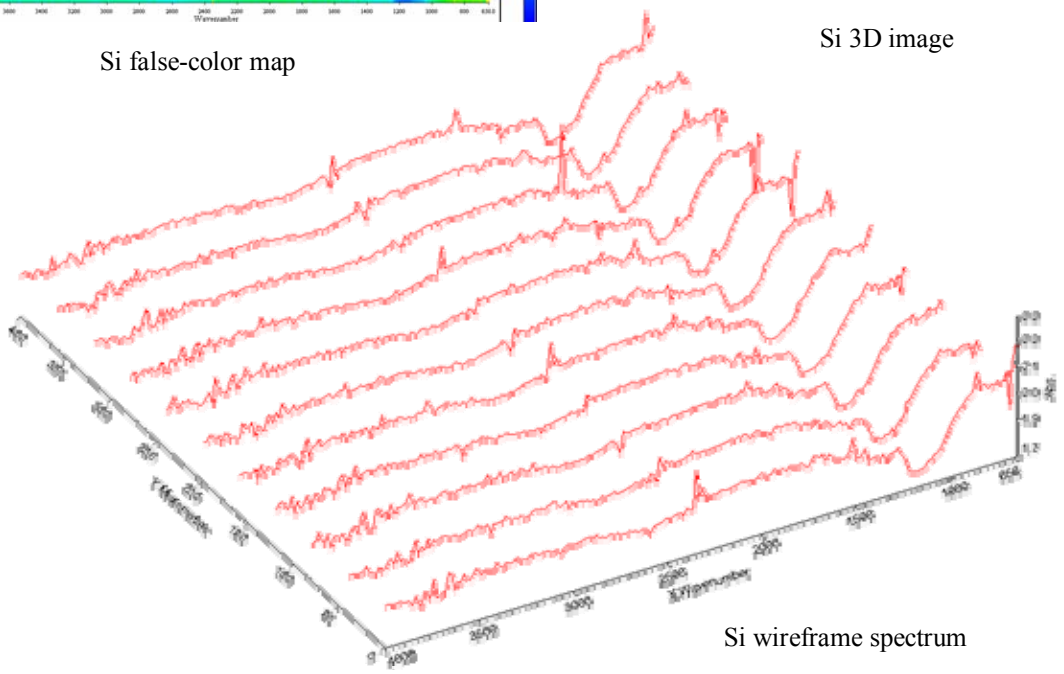

Si wireframe spectrum

Sample G0

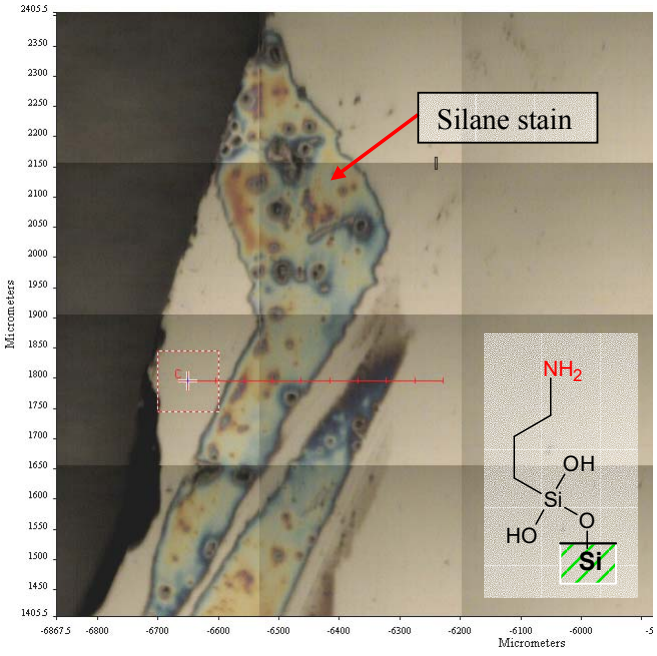

Referring back to section 9 and to Table 3 of this thesis, the sample taken at this stage is the silicon wafer functionalized with the γ- aminopropyltriethoxysilane.

The molecule shown depicts the type of chemical structure assumed to be present in the sample. The microscope picture of the sampled region shows a red line with the 11-point scans taken. This particular segment was chosen for analysis with the purpose of characterizing a region with an apparent high concentration of silane (shown as a stain) vs. other points with varying observable accumulation.

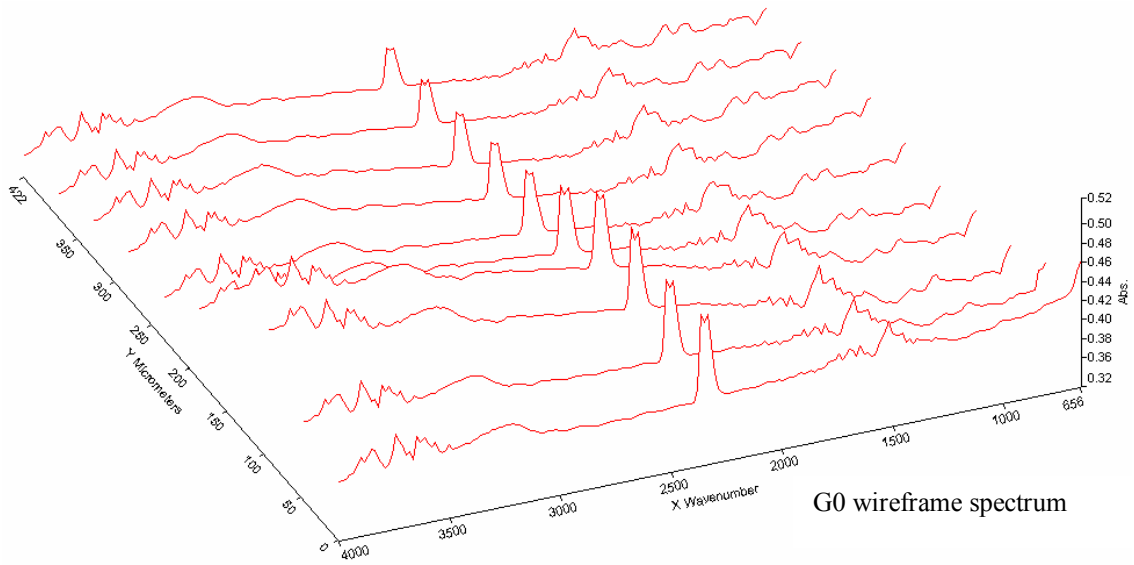

G0 wireframe spectrum

Comparing the G0 wireframe spectrum with the one obtained from the pure silicon wafer, it is evident that the ditch observed at 1200cm^{-1} decreased and a pronounced peak at 1500 cm^{-1} appears. This vibrational frequency corresponds to a primary amine, which verifies the presence of the silane. Also, it can be clearly observed that the amount of the amine group is constant throughout the scanned line, regardless of the visible accumulation in the stain.

In this side view of the wireframe spectrum, the vibration frequencies can be clearly interpreted. It can also be observed that the amount of CO_2 incremented from the pure silicon measurement, showing a pronounced peak at 2350 cm^{-1}. Also, a broad peak is now observed between 3200-3400 cm^{-1}, these stretching vibrations corresponds to a polymeric association of O – H bonds.

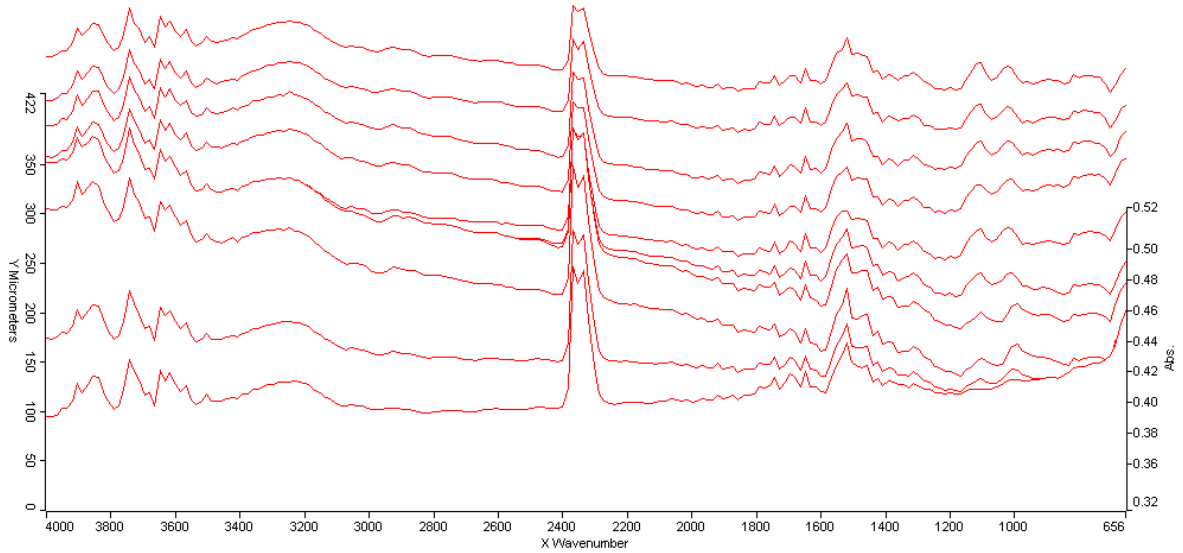

G0 wireframe spectrum – side view

The following table shows the expected theoretical values and compares them to the observed frequency vibrations.

Expected frequency vibrations (cm^{-1})	Description	Observed frequency vibrations (cm^{-1})
3400-3300	1° amine: two bands	3600
1650-1580	N–H bend (primary amines)	1550-1450
1250–1020	C–N stretch	1200-100
2300	CO_2	2350
3400-3200	Polymeric association O–H	3400-3000

Table 4: Frequency vibrations for sample G0

The following images display a 3D rendering and a false-color map of the 11-point line scan performed. In the following figures, the effect of the stain shown in the G0 microscope image can be clearly observed. It can be concluded that the stain is nothing more than a region of high concentration of the silane, but the chemical composition is maintained constant. The images provide a good indication that the silane has attached evenly to the silicon wafer, with some exceptions where a drop of silane dried up and formed a high-concentration region. .

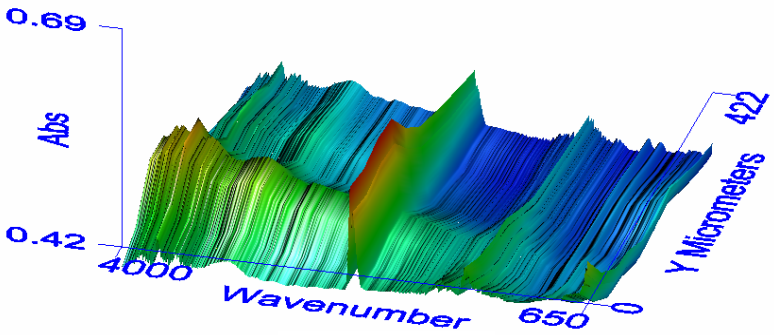

G0 3-D image

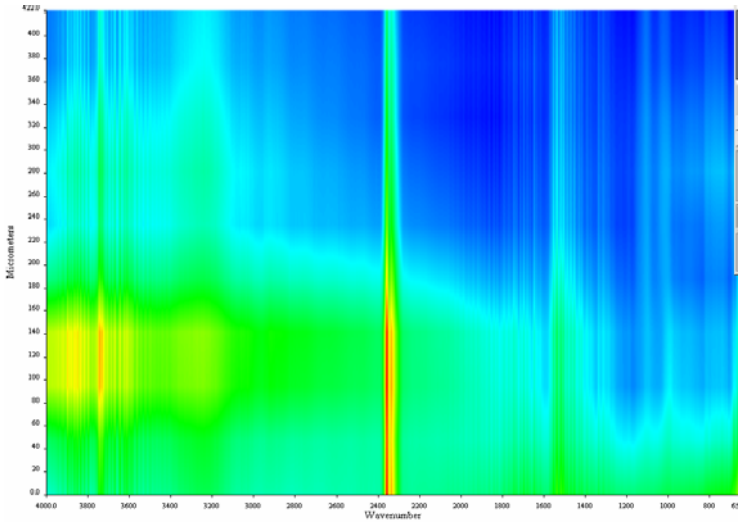

G0 false-color map

Sample G1.0

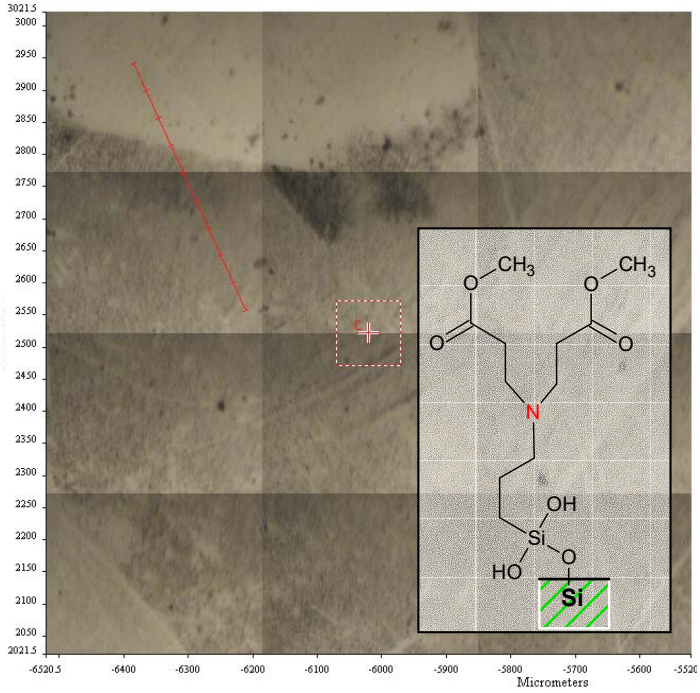

G1 microscope image

The G1 microscope image shown here, displays the segment of 11-point line scan performed on this sample. The molecule shown is the expected structure to be present at this stage of the iterative reactions. Again, this particular segment was chosen to analyze a region with an apparent higher concentration vs. a region of visibly low abundance of the chemical compound.

The wireframe spectrum of the 11-point scan shows a significant reduction in the CO_2 peak, since the researcher walk away from the spectrometer while the scanning was in progress. It can be seen how the CO_2 peak decreases as the line scan progresses. Also some other interesting peaks appear, but overall, the sample shows good chemical uniformity throughout.

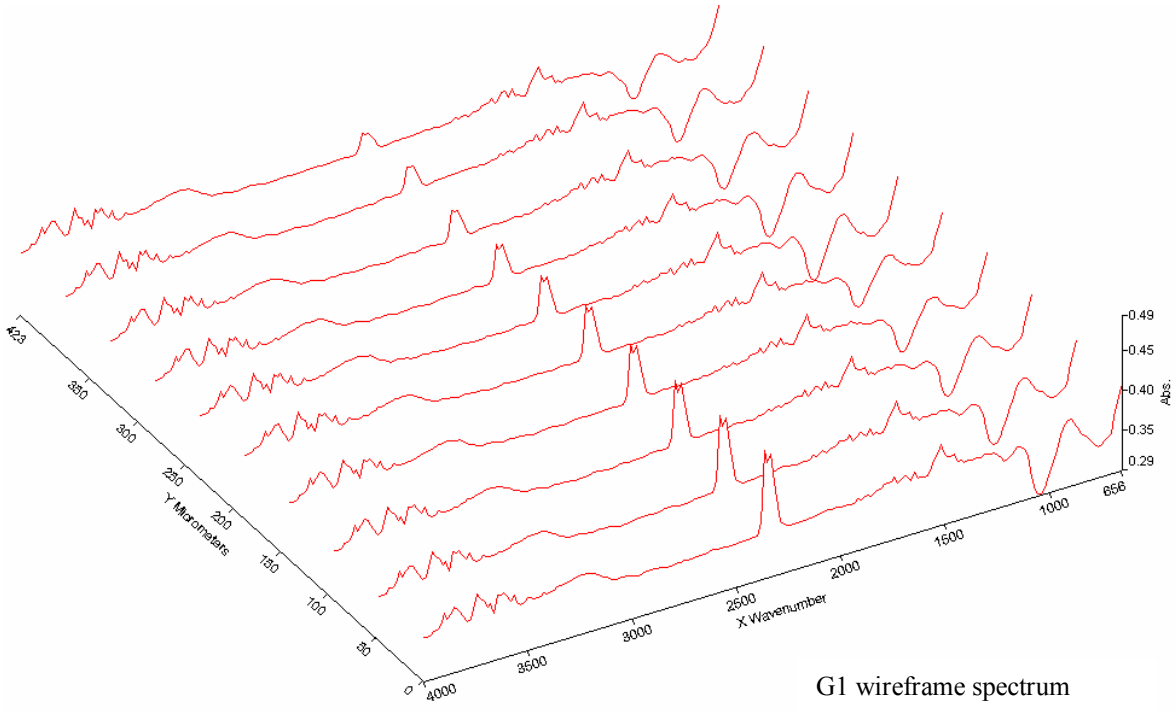

G1 wireframe spectrum

From the side view of the wireframe spectrum, the peaks can be clearly interpreted at the exact vibrational frequency. Comparing this wireframe spectrum with the one obtained for the G0 sample, a strong observation can be made regarding the peaks that appear on the right region of the spectrum. These peaks are very characteristic of the acrylate functional groups. Recalling from section 10 of this report, this sample has been taken out of the original batch after the Michael addition, using methyl acrylate to build the first generation of the dendrimer.

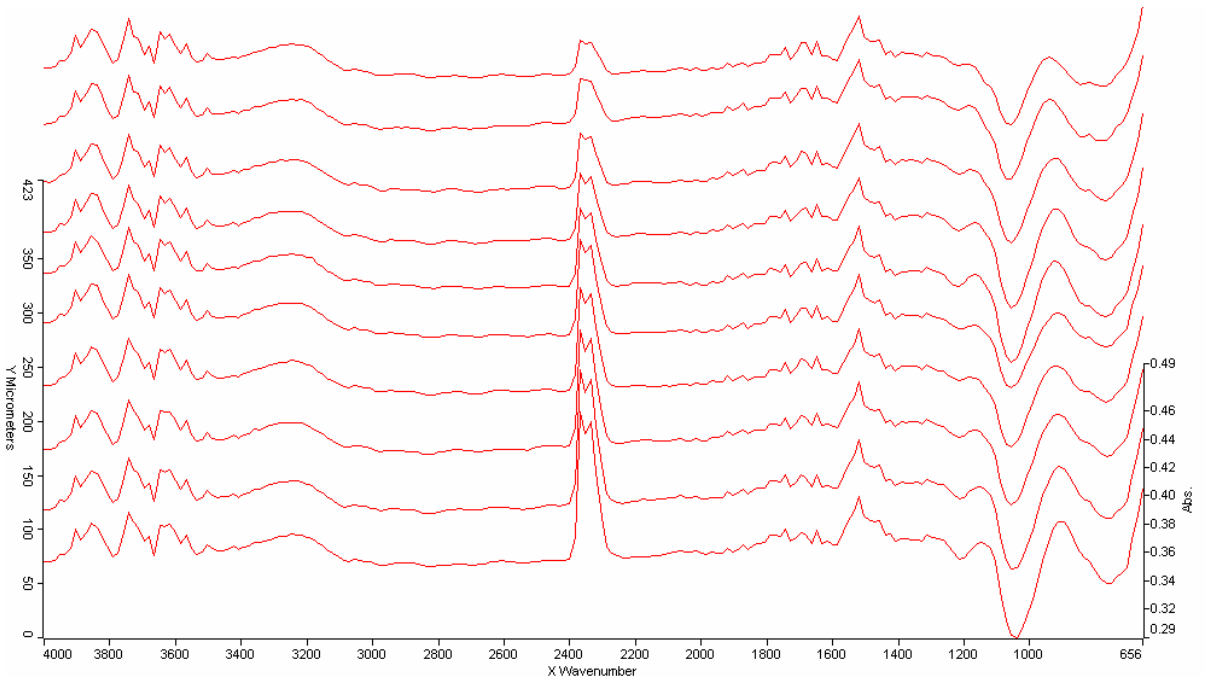

G1 wireframe spectrum –side view

All other peaks obtained from the G0 sample are still present on the G1 sample, with the new appearance of the peaks corresponding to the acrylates. The following table shows the expected theoretical peaks vs. the experimental peaks obtained.

Expected frequency vibrations (cm^{-1})	Description	Observed frequency vibrations (cm^{-1})
3400-3300	1° amine: two bands	3600
1650-1580	N–H bend (primary amines)	1550-1450
1250–1020	C–N stretch	1200-100
2300	CO_2	2350
3400-3200	Polymeric association O–H	3400-3000
1260-1000	Esters - acrylates	1200-800

Table 5: Frequency vibrations for sample G1

The 3D image and the false color map shown below, depict an even distribution of the chemical composition of the sample. The effect of walking away from the spectrometer while scanning the sample can also be clearly observed by a gradual decrease of the CO_2 band. A single shade of a specific color shows an area of chemical equality.

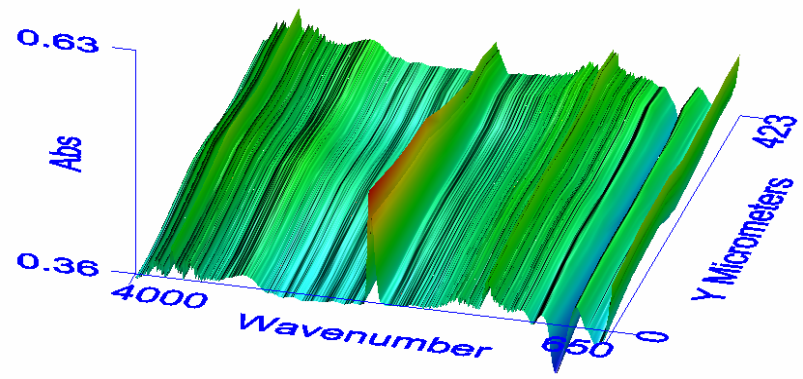

G1 3-D image

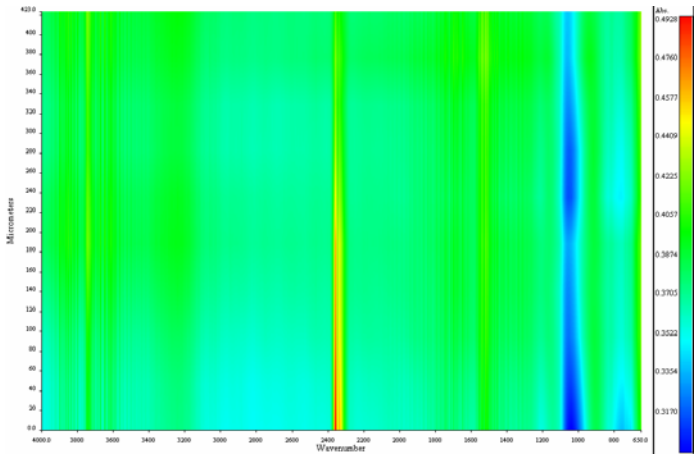

G1 false color map

Sample G1.5

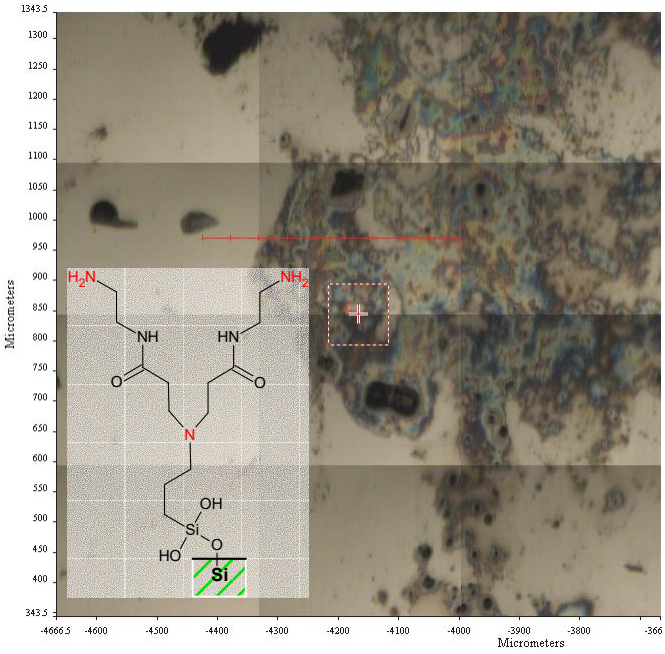

G1.5 microscope image

The next step in the iterative reactions is the exhaustive amidation of the ester functional groups. Hence, the expected chemical composition of the surface is depicted by the molecule shown on top of the image. This image shows the segment selected for scanning with a red line containing the eleven sample points.

The wireframe spectrum is very similar to the one obtained in the previous step, since all the components were already present. This stage only adds more amine terminal groups to the molecule.

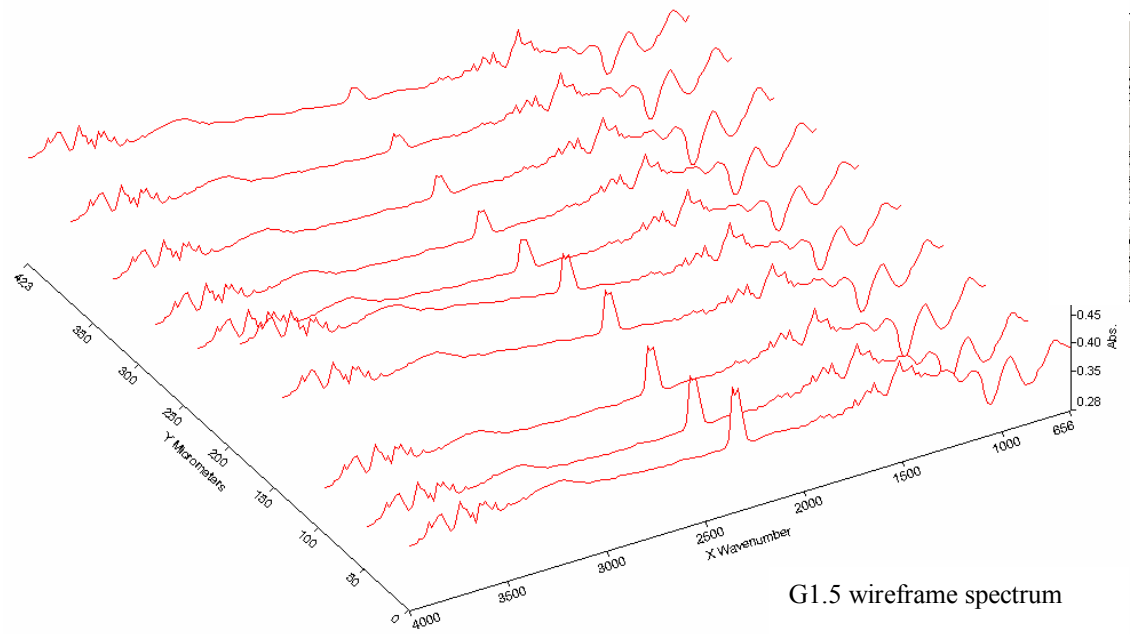

G1.5 wireframe spectrum

The side view of the wireframe spectrum shows the peaks at their bending and stretching frequency.

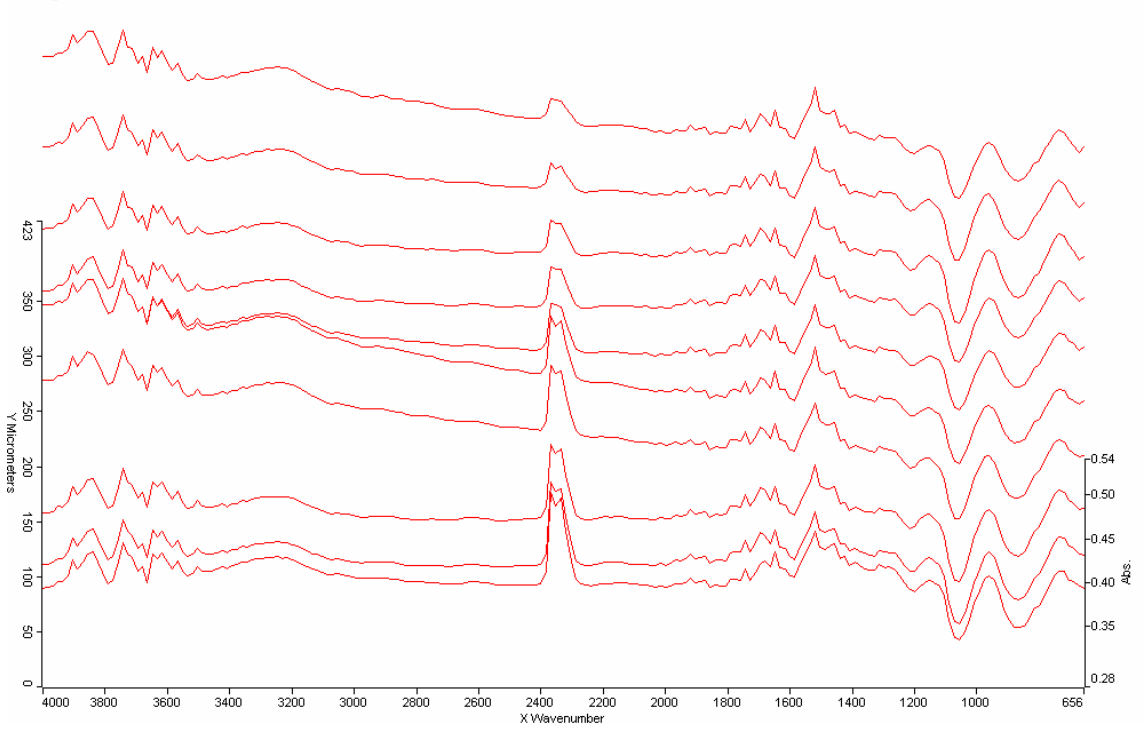

G1.5 wireframe spectrum – side view

From the 3D figure and the false color map, the stain shown in the microscope image can clearly be observed, showing more concentration of the chemical species on top of the satin.

G1.5 3D image

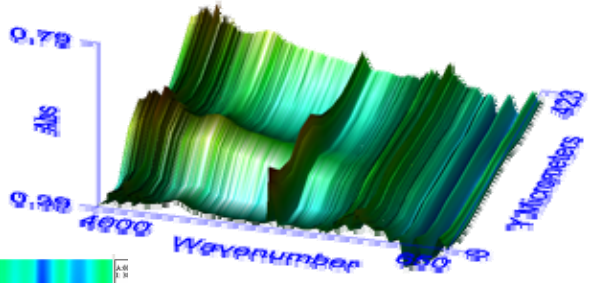

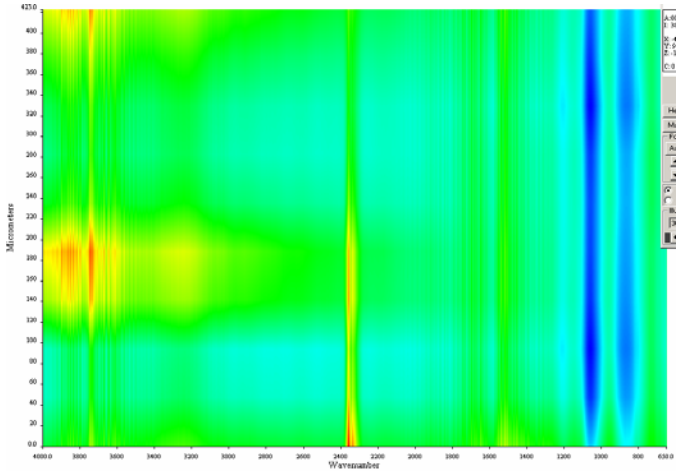

G1.5 false-color map

Sample G2.5

Figures shown: 11-point line scan segment, molecule of G2.5 layer, IR wireframe spectrum, 3D image and false color map of the sample.

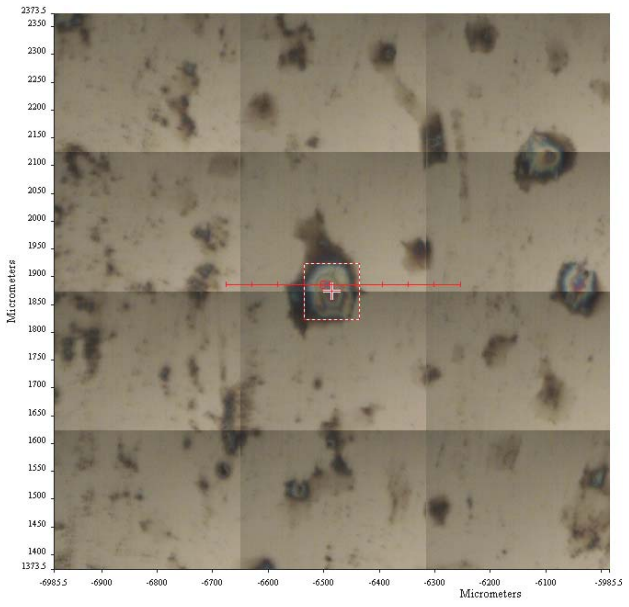

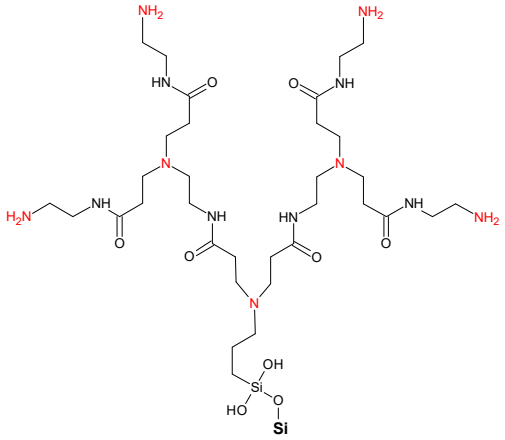

NOTE: The spectrometer was re-calibrated and a new blank was taken. Therefore the CO_2 peaks started appearing downwards

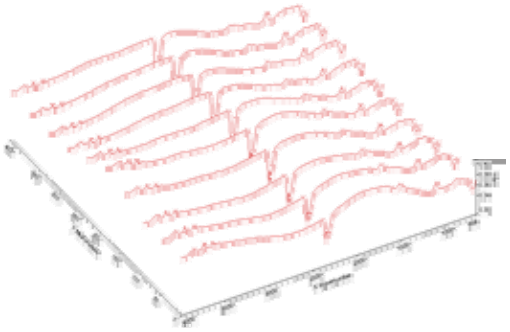

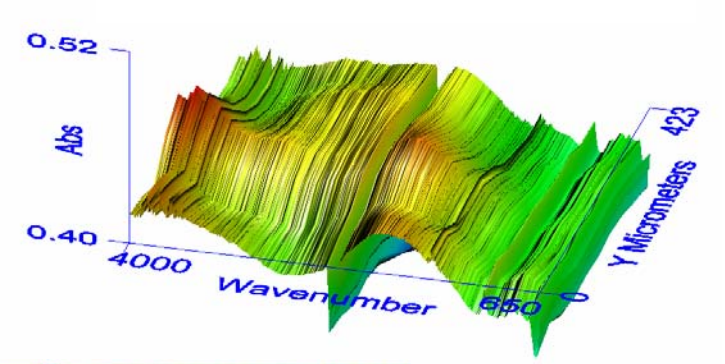

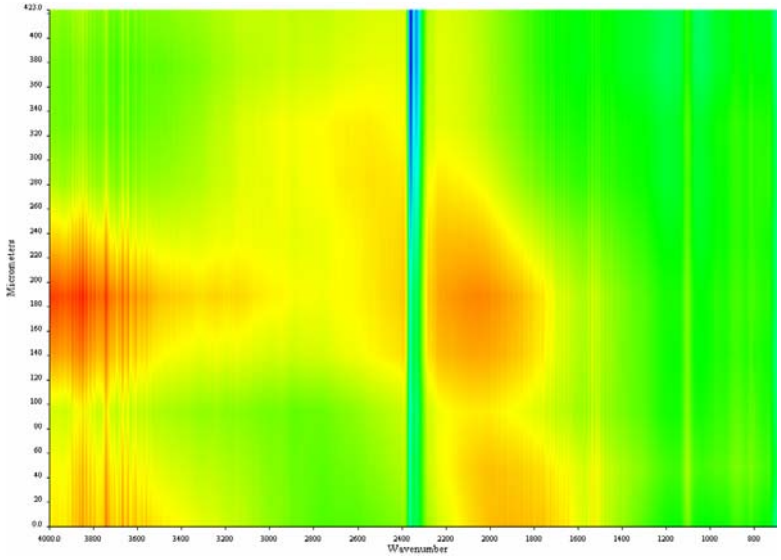

Sample G3.0

Figures shown: 11-point line scan segment, molecule of G3.0 layer, IR wireframe spectrum, 3D image and false color map of the sample.

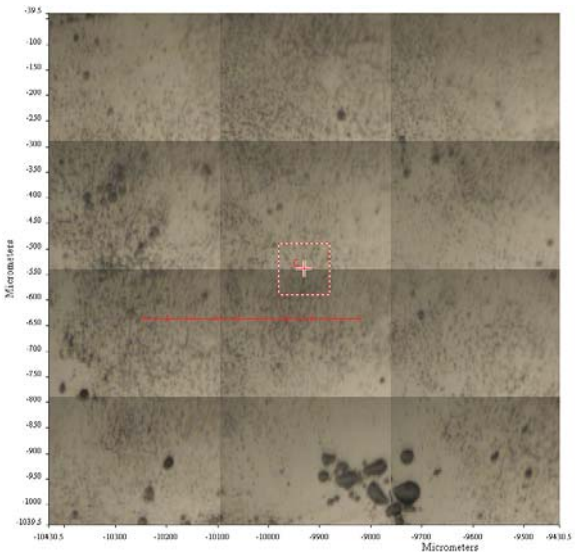

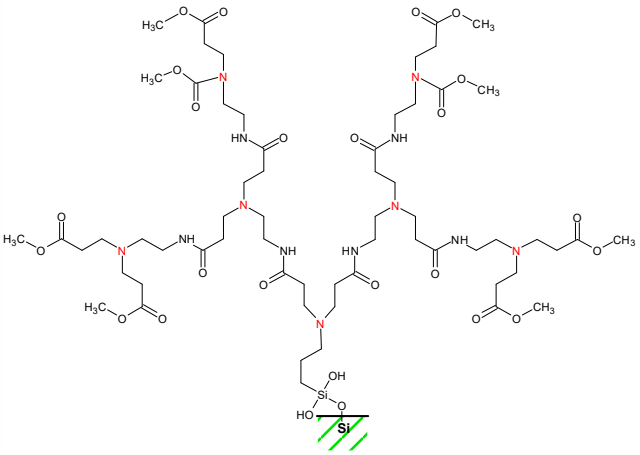

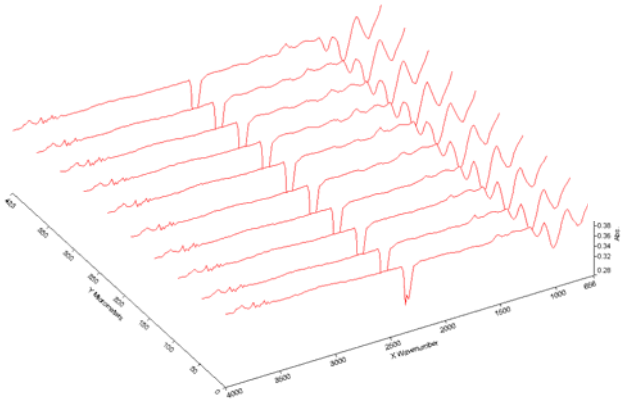

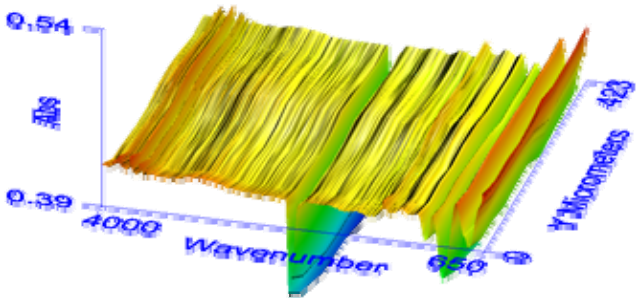

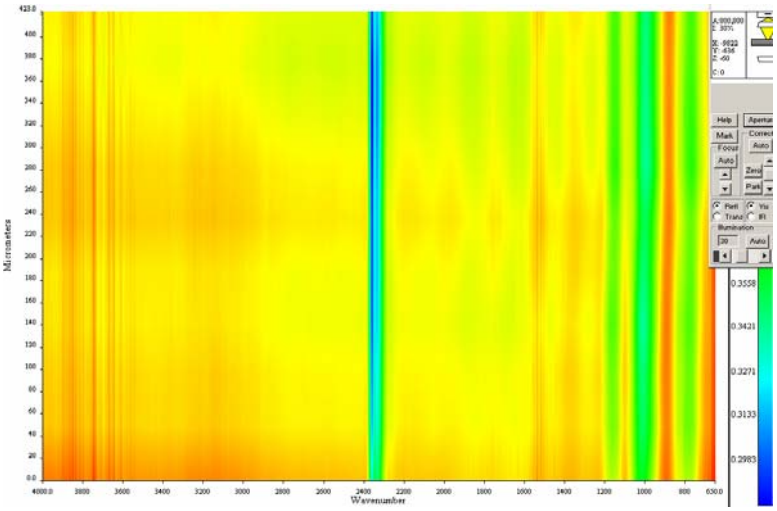

Sample G3.5 – Linear scan

At the moment the samples were analyzed, the highest generation of the dendrimer was the G3.5; therefore, this sample was studied more thoroughly than the rest. The figures displayed below, show a microscope image of the segment chsen for the 11-point line scan, an image of the molecule expected to be present on the substrate, and a wireframe spectrum of the line scan.

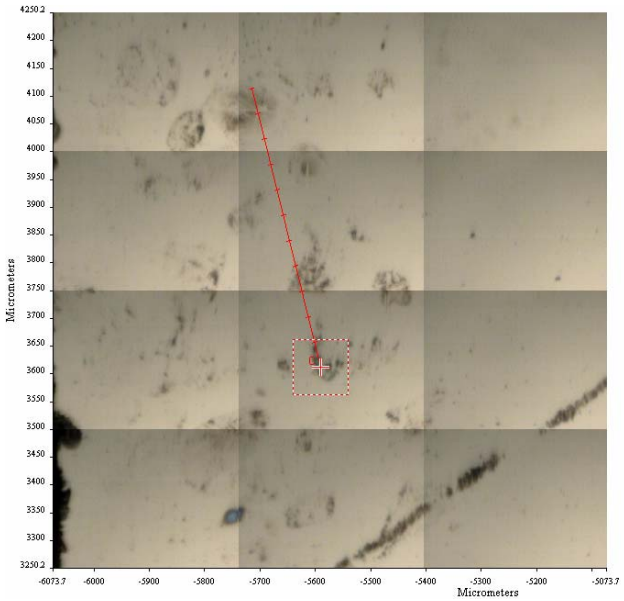

G3.5 microscope image

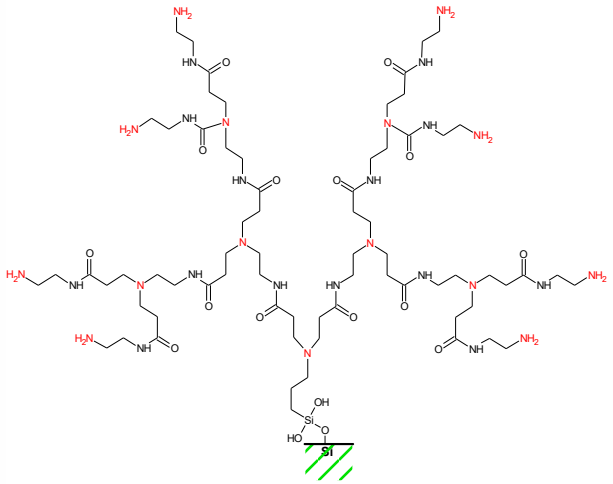

G3.5 molecule

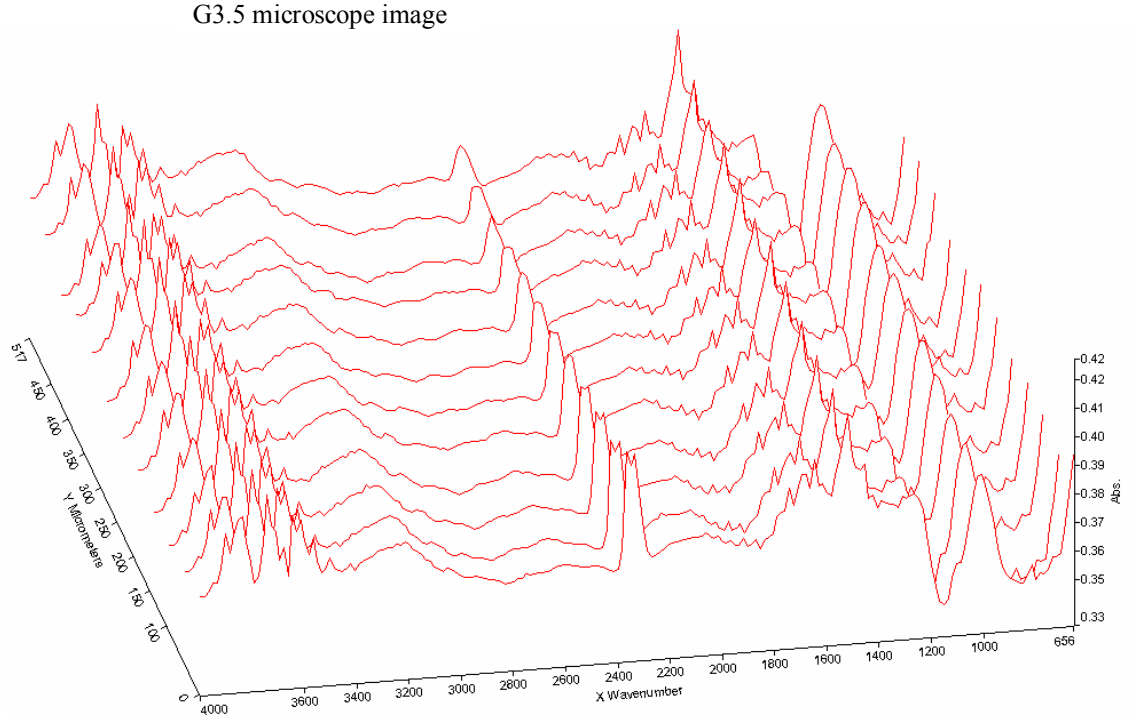

G3.5 wireframe spectrum

The side view of the wireframe spectrum shown below clearly depicts a chemically even surface topology, maintaining the same functional groups throughout the sample. The strong peaks that appear around 1500 cm^{-1} are quite characteristic of the primary amine group (NH_2) in-plane bending or scissoring. The wide peak that appears at around 1000cm^{-1} is characteristic of the siloxanes ($Si–CH_3$).

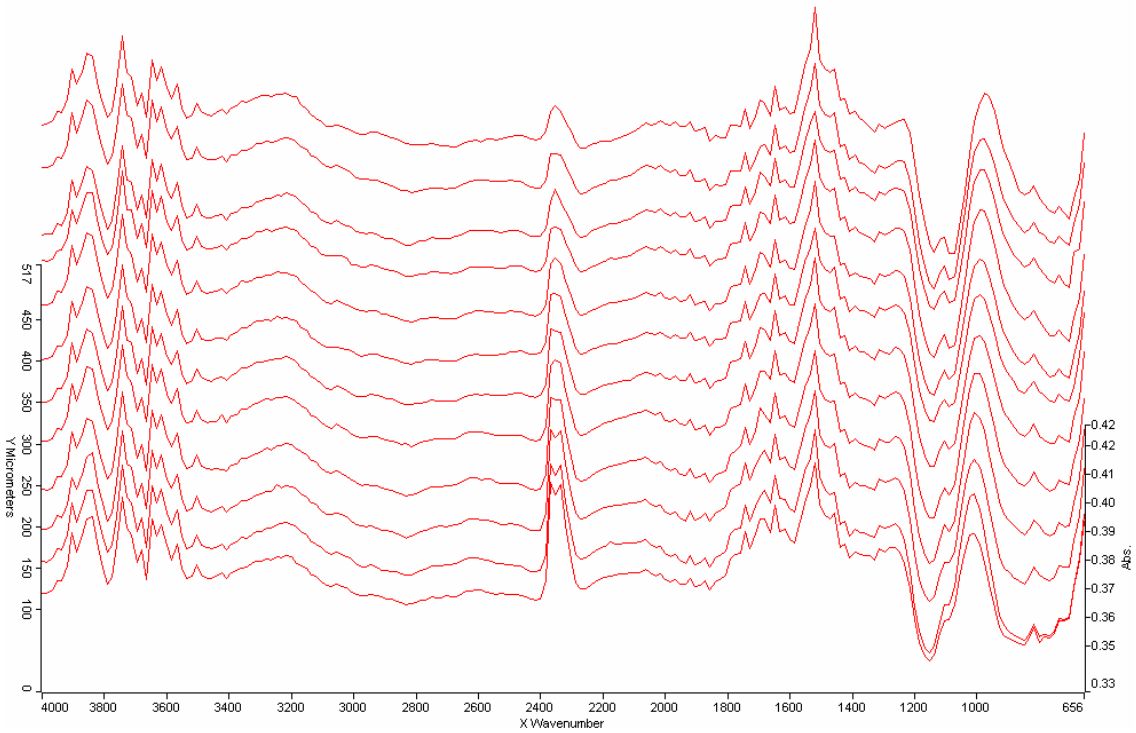

G3.5 wireframe spectrum – side view

The table below summarizes the peaks that are observed at the 3.5 generation of the PAMAM dendrimer grown as a layer on top of a p-type monocrystalline silicon (100) wafer.

Expected frequency vibrations (cm^{-1})	Description	Observed frequency vibrations (cm^{-1})
3400-3300	1° amine: two bands	3600
1650-1580	N–H bend (primary amines)	1550-1450
1250–1020	C–N stretch	1200-100
2300	CO_2	2350
3400-3200	Polymeric association O–H	3400-3000
1260-1000	Esters - acrylates	1200-800

Table 6: Frequency vibrations for sample G3.5

Sample G3.5 – Surface scan

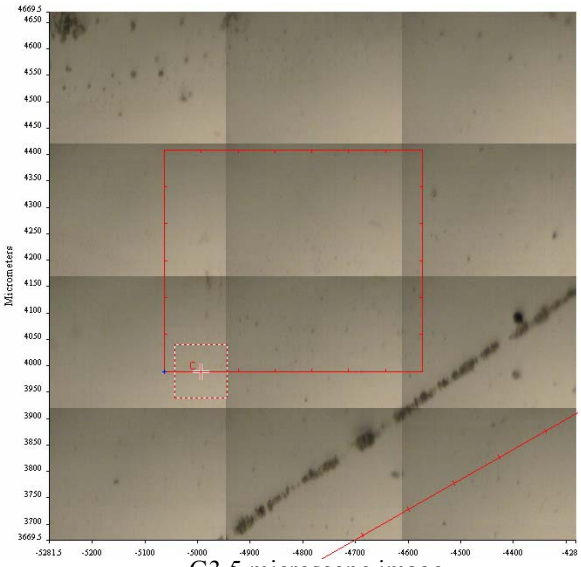

G3.5 microscope image

As previously mentioned, the generation 3.5 of the coating dendrimer was analyzed in more detail than the rest of the samples, given the fact that at this point, the layer was at its thickest. The microscope image shown here, displays the area selected to be analyzed using a surface scan, instead of a linear scan. The red square delineates the area with a 56 (7 x 8) point scan. Referring back to the original setup each point was to be scanned 32 times, giving a total of 1792 scans over the selected area. This procedure took approximately 30 minutes to complete.

The FTIR microscope generated the following chemical map of the selected area. It is important to note that this image is not a false color map generated with the line scans as the ones shown in the previous samples, this represents a two-dimensional scan. The colors displayed in the image are given as a function of absorbency of the surface: red represents high absorbency and blue represents low absorbency. From the chemical map shown, it can be concluded that almost the entire surface is constant in terms of functional groups, depicted with the same shade of green throughout the sample. The 3D image of this chemical map displays "hills" and "valleys" to represent high and low absorbency, respectively.

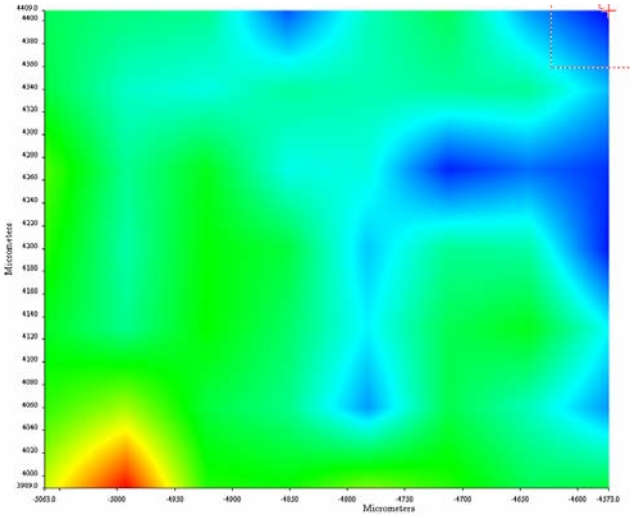

G3.5 chemical map

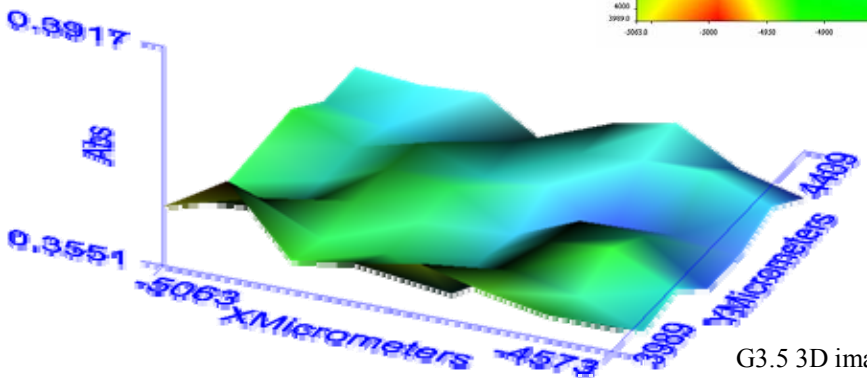

G3.5 3D image

48 hour reactions – Sample g1.0

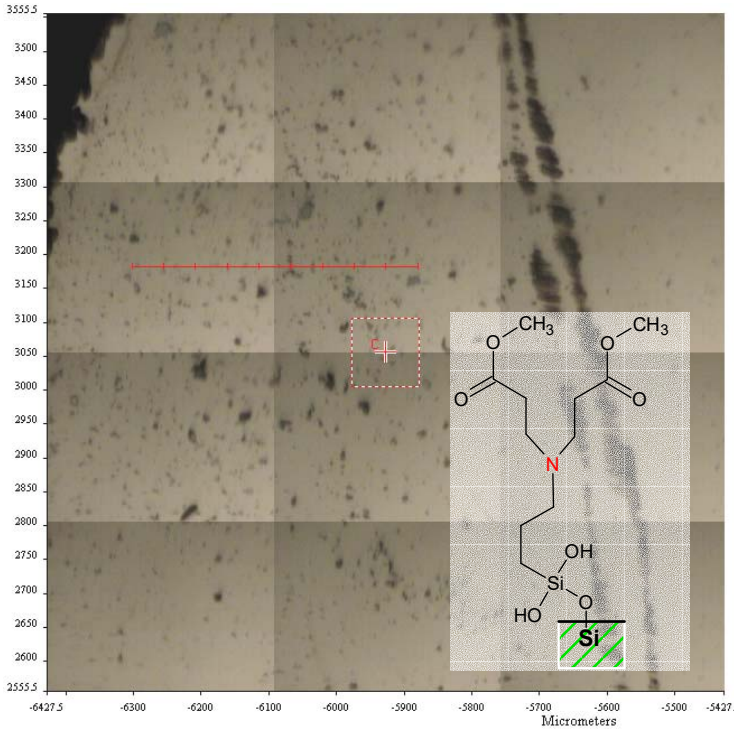

g1.0 microscope image

Recalling from Table 3, there is another batch of samples, on which the iterative reactions occurred every 48 hours; twice as long as the previous batch. This was performed in order to study the effect of time on the reactions. The figure shown to the left has the 11-point line scan and the image of the molecule at this point in the reaction.

The wireframe spectrum shown below was the result of the 11-point linear scan. It is important to note that the spectrometer was recalibrated and the CO_2 levels are now shown as peaks deflecting downwards at 2350 cm^{-1}. The wireframe spectrum shows a perfectly even surface in terms of functional groups.

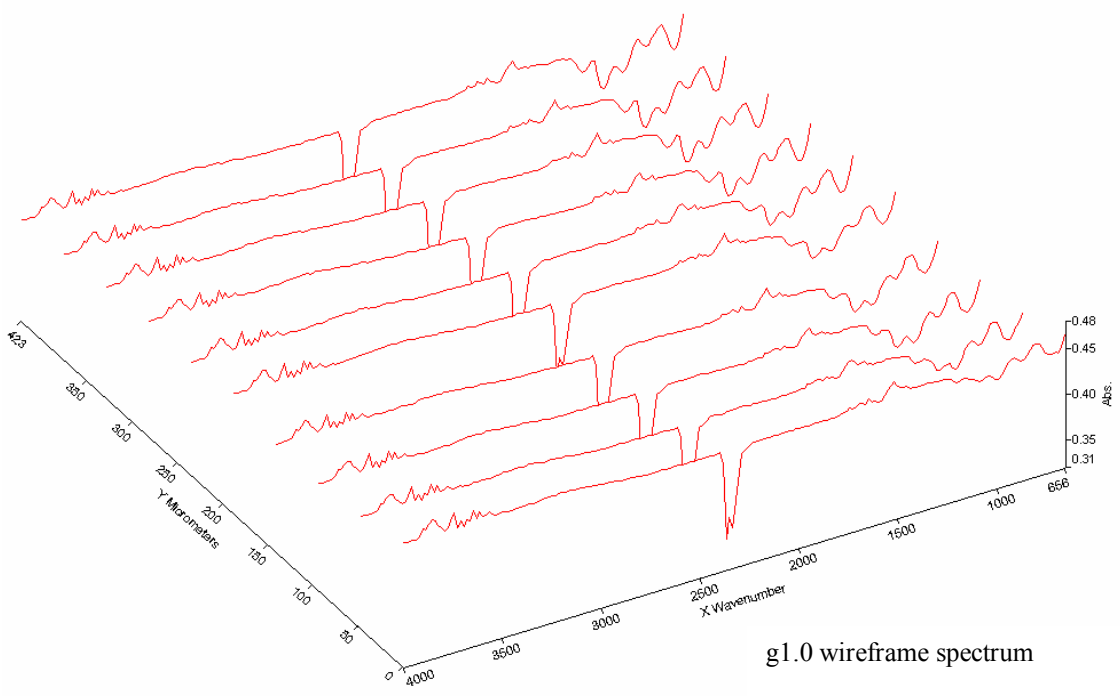

g1.0 wireframe spectrum

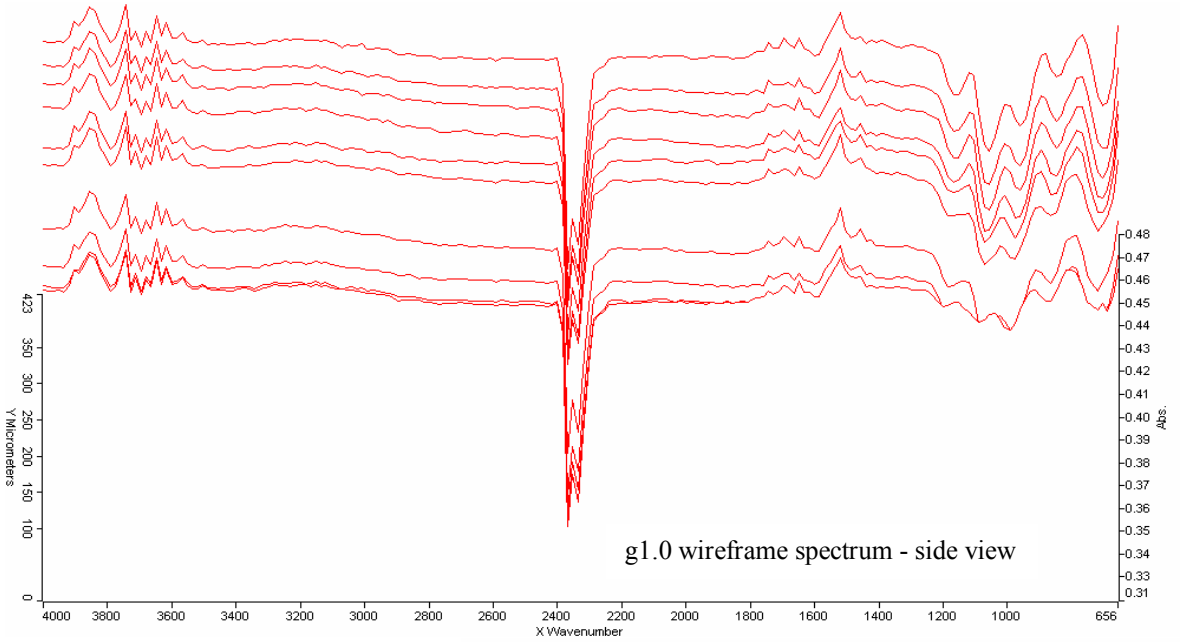

g1.0 wireframe spectrum - side view

The 3D image and the false color map of the sample display an even surface with the characteristic peaks of the primary amine functional groups, as well as the carboxylate groups.

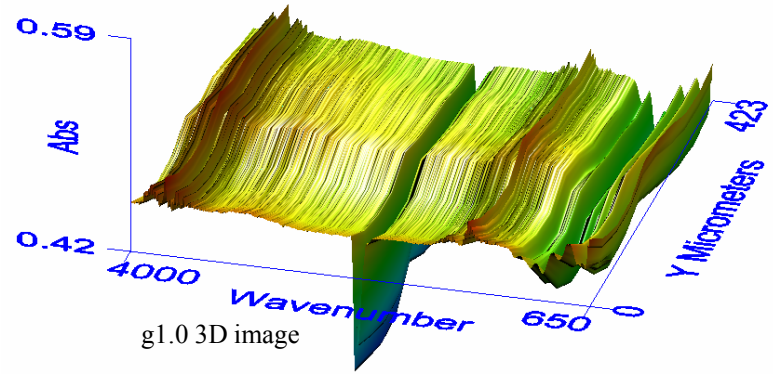

g1.0 3D image

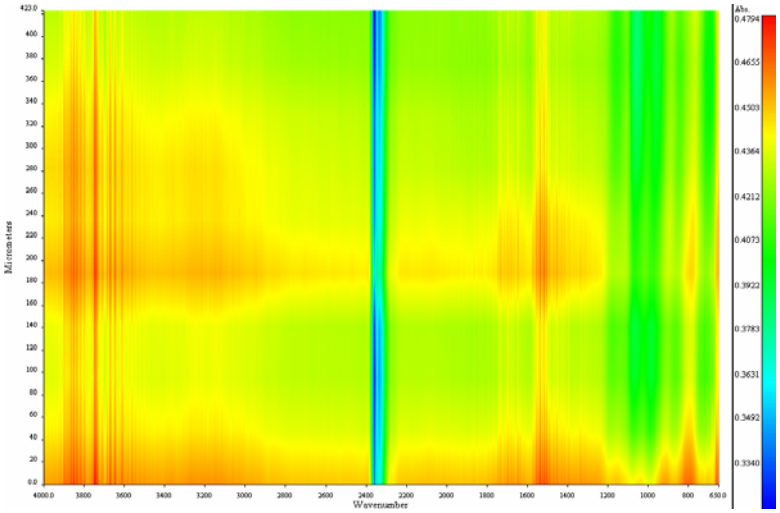

g1.0 false-color map

48 hour reactions – Sample g1.5: with stain

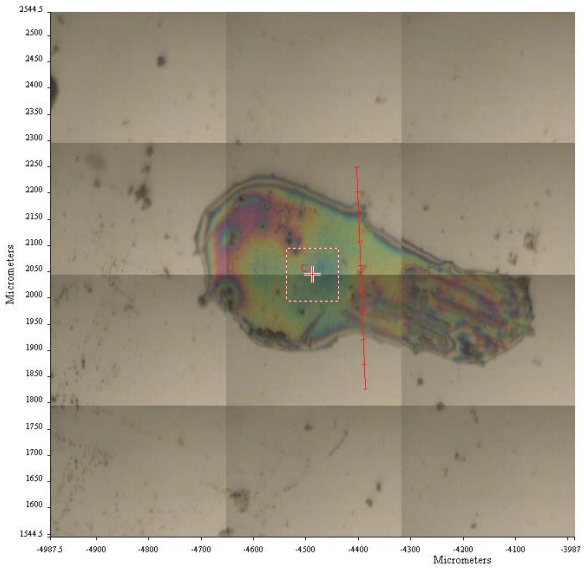

48Hr g1.5 microscope image

The image shown on the left is the area chosen for the 11-point linear scan. This area was chosen due to its interesting shape, and to study the chemical composition of the bubble that appears on the screen.

The wireframe spectrum displayed below shows a very chemically even composition of the surface, regardless of the bubble, which can be clearly observed with regions of higher absorbency. This increase in the absorbency is the effect of the bubble's height with respect to the substrate.

Observing the 11 scans, one can conclude that the same functional groups are present throughout the sampled region, only with higher absorbency values due to the elevation caused by the bubble.

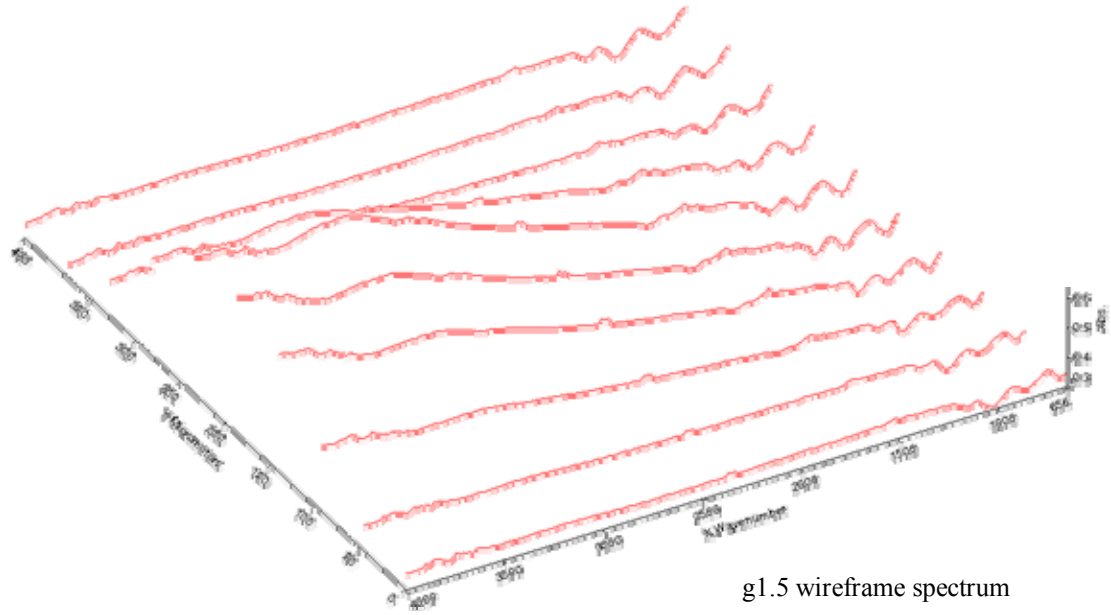

g1.5 wireframe spectrum

The next images show a 3D image of this linear scan and a false color map generated in function of the absorbency. These images clearly show the effects of the bubble but still confirm a chemically uniform surface with the same functional groups throughout the sample.

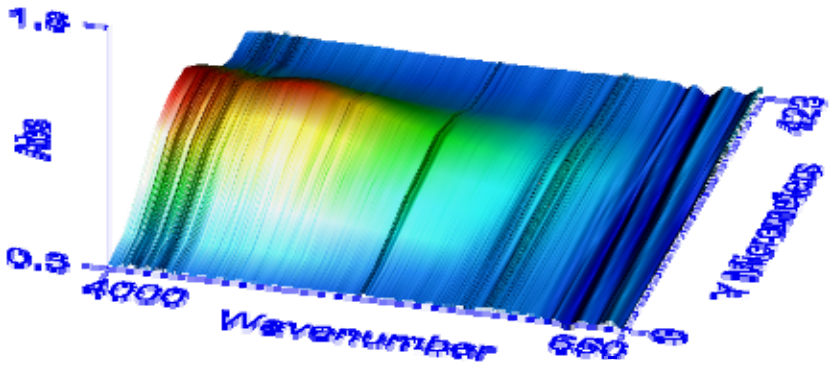

g1.5 3D image

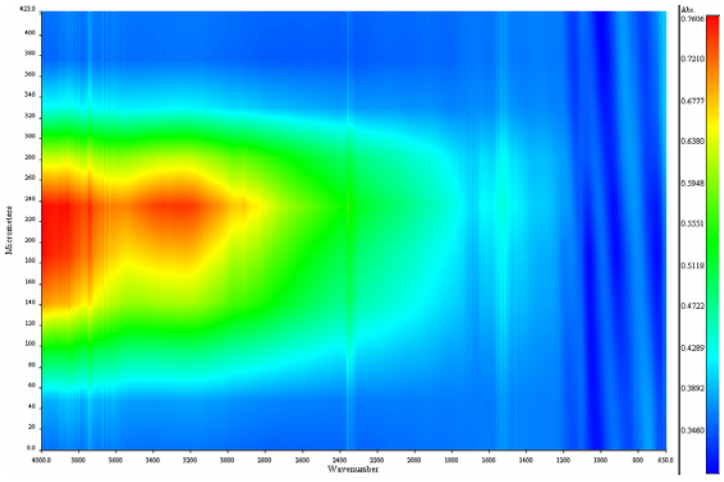

g1.5 false color map

48 hour reactions – Sample g1.5: no stain

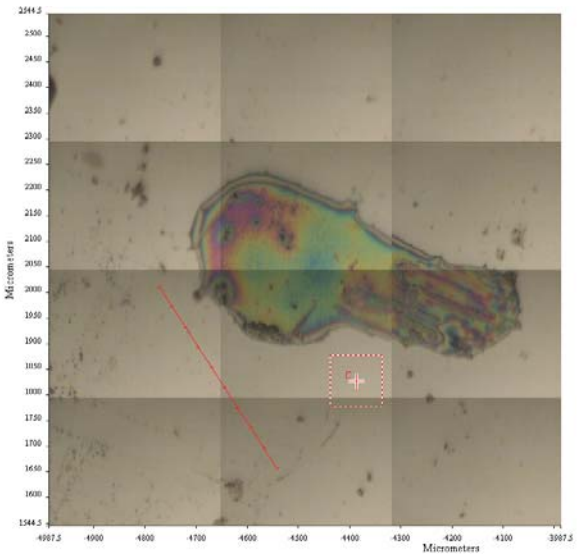

g1.5 microscope image

To verify the results obtained from the previous analysis, the same sample was scanned on a different area that apparently had no deposition of organic material. The red line shows the area chosen to be scanned.

The wireframe spectrum below confirms the conclusion that the whole surface is chemically the same, regardless of visual confirmation at this magnification. The peaks characteristic of the primary amine and siloxanes functional groups are evidently present in the spectrum.

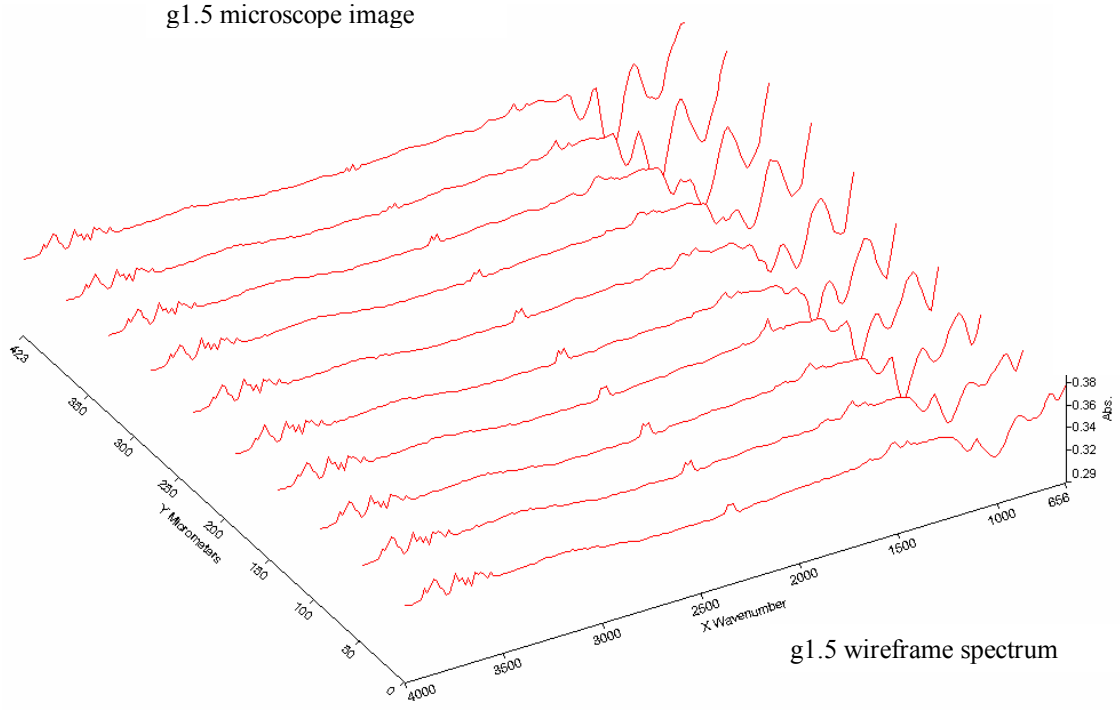

g1.5 wireframe spectrum

Comparing the wireframes from generation 1.5 which ran every 24 hours with generation 1.5 at 48 hrs, it can be concluded that time has no apparent effect on the chemical uniformity of the surface.

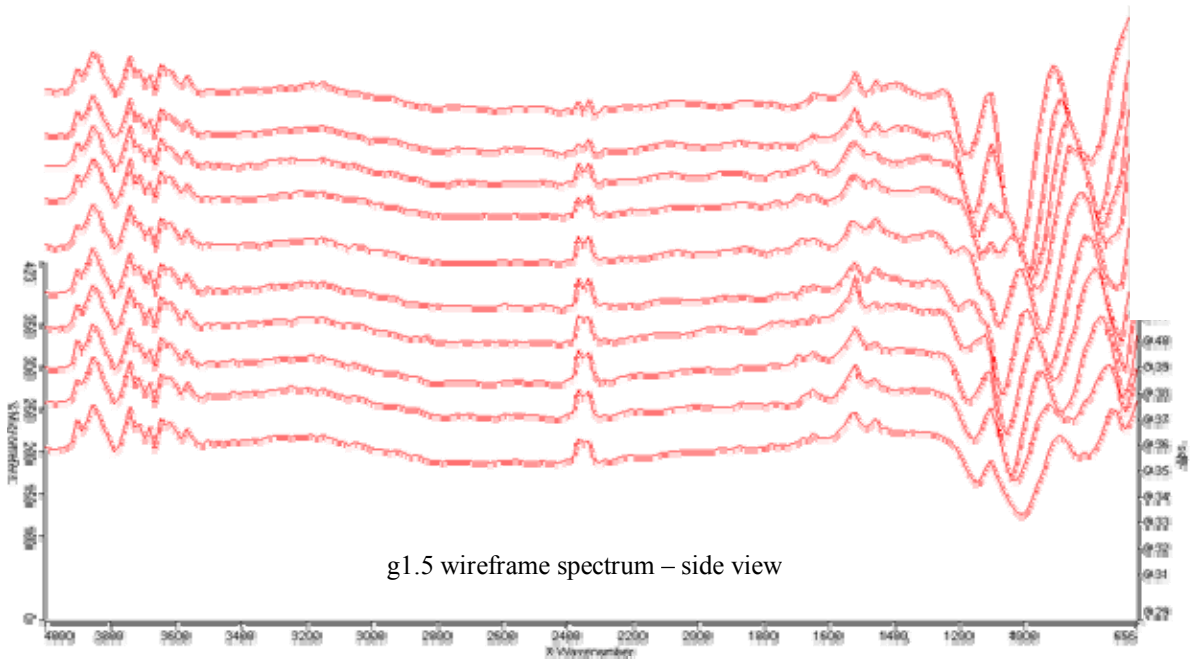

g1.5 wireframe spectrum – side view

The 3D image and the false color map shown on the next page show a very smooth and chemically even surface displayed as an equal shade of green. This confirms that there is the same infrared absorbency at most points in the sample.

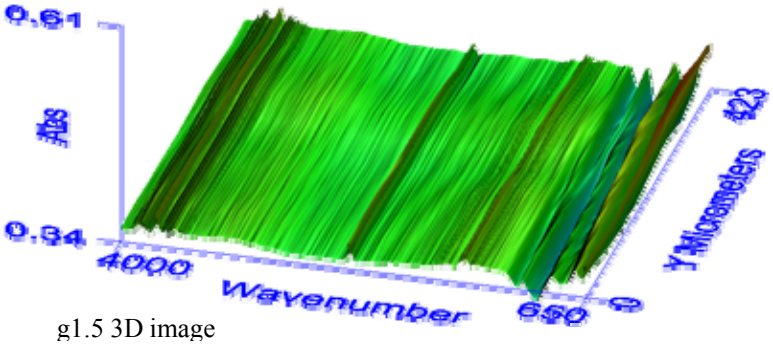

g1.5 3D image

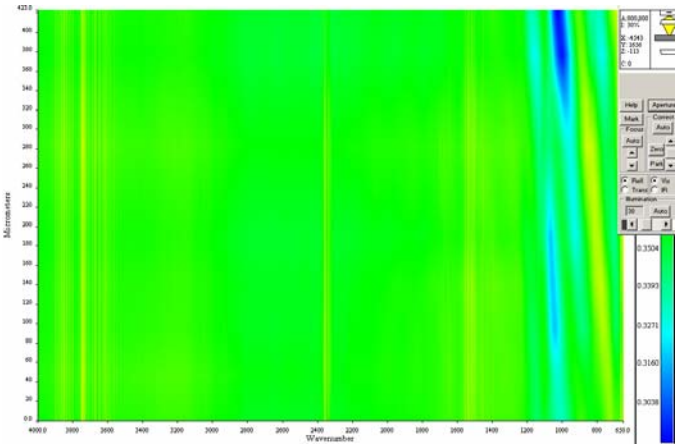

g1.5 false color map

48 hour reactions – Sample g2.0

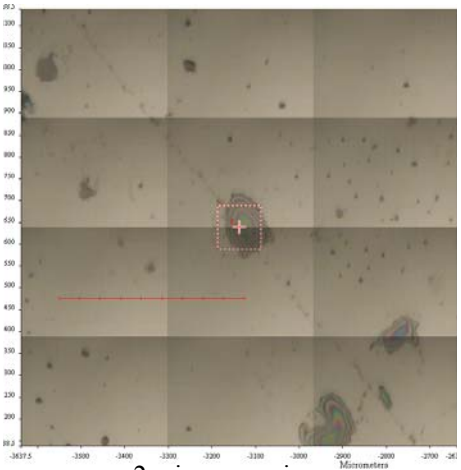

g2 microscope image

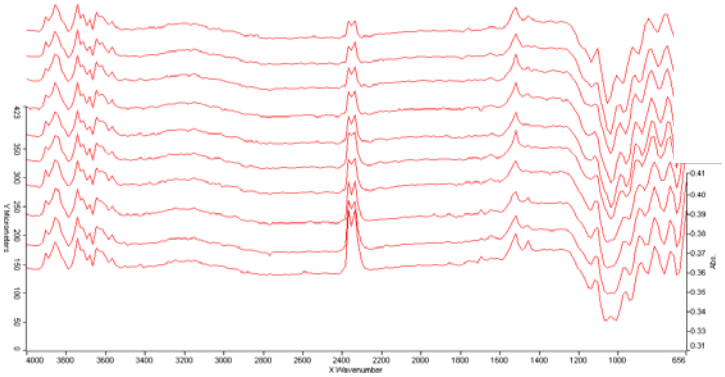

g2 wireframe spectrum – side view

This final sample shows a linear scan where the optical microscope did not capture any apparent deposition, but the spectrum is consistent with the results obtained in previous samples. The 3D image shows an almost planar surface with the characteristic peaks of the functional groups expected to be present at this generation of the PAMAM dendrimer.

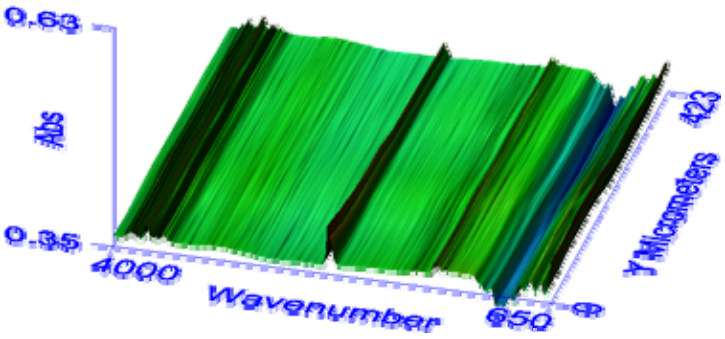

g2 3D image

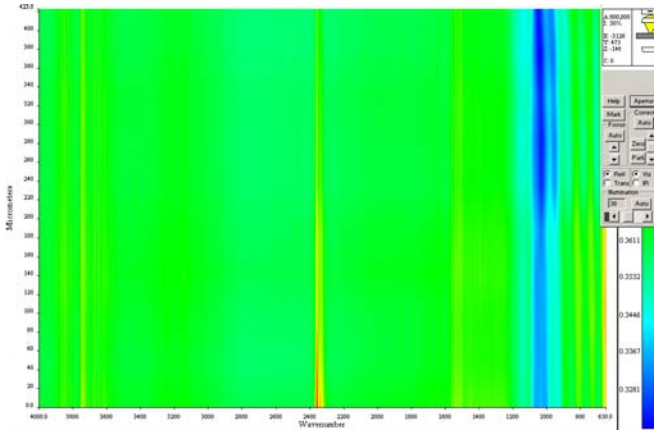

g2 false color map

13. AFM IMAGING

After the FTIR chemical characterization of the silicon surface following dendrimer deposition, an Atomic Force Microscope (AFM) was used to obtain visual confirmation of the physical topography of the samples. The AFM used in this work was provided by the Department of Physics at Tecnologico de Monterrey. Specifications for the Digital Instruments Nanoscope III Multimode ATM can be found on Appendix B.

Multiple scans of the generation 3.5 dendrimer sample were performed in air using the tapping mode with two different scanners: 100 x 100 µm and 10 x 10 µm.

According to the study mentioned in section 7.2.3 of this thesis, Piehler, Baker and Tomalia[27], reported that dendrimers of generations smaller than 5 could not be imaged as single molecules using atomic force microscopy due to their extremely small diameters, which range around 4.5 nm according to the theoretical values given in Table 1.

The samples used at this stage of the investigation were PAMAM dendrimers at generation 3.5, which would make it difficult to distinguish them as individual molecules, but would rather be perceived as densely packed areas. The aforementioned study reports that low-generation dendrimers (<G5) exist as structures with low rigidity with smaller number of functional groups in which the dendrimer branches can relatively easily interpenetrate each other and establish intermolecular interactions[27].

The following pages show several images of the G3.5 PAMAM dendrimer at different sections of the sample, which measured approximately 5mm^2. Also, it is important to note that the first set of images were obtained with a 100 x 100 µm scanner and the second set with a 10 x 10 µm scanner.

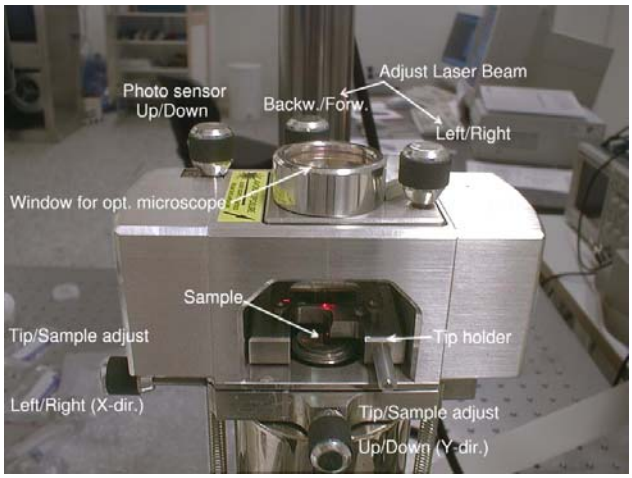

Pure silicon

For comparison purposes, as performed in the FTIR characterization, pure silicon was imaged using contact mode in order to obtain the topography of the wafers before any deposition of organic material.

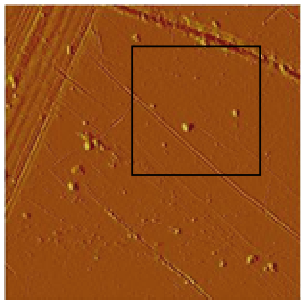

0
Data Type
Z range

10.0 µm
Deflection
5.000 nm

The image shown on the left displays a 10 x 10 µm section of the silicon sample. It can be observed that the surface is scratched and contains some dust particles, but overall, the image shows a rather smooth and uniform surface. It is important to note that the sample was not properly handled and that the silicon piece was obtained from a batch of pieces like the ones shown in Figure 21on section 9 of this report, which were in contact with one another, producing the scratches shown in the picture.

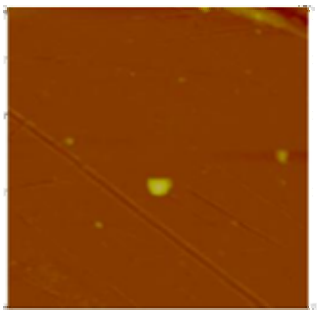

0
Data type
Z range

3.92
Height
200 µm

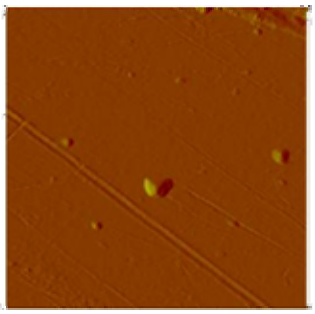

0
Data type
Z range

3.92
Deflection
5.000 nm

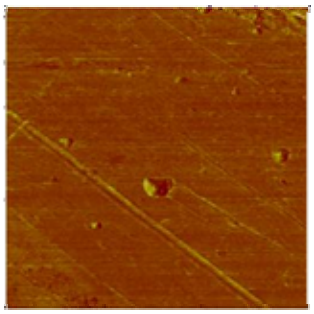

0
Data type
Z range

3.92
Friction
0.500 V

The image shown above displays a zoom of an area approximately 4 x 4 µm of the previous image. The picture displays information for height, deflection of the cantilever, and friction of the tip with the surface. Shown below, is a 3D rendering of the image showing the information for height.

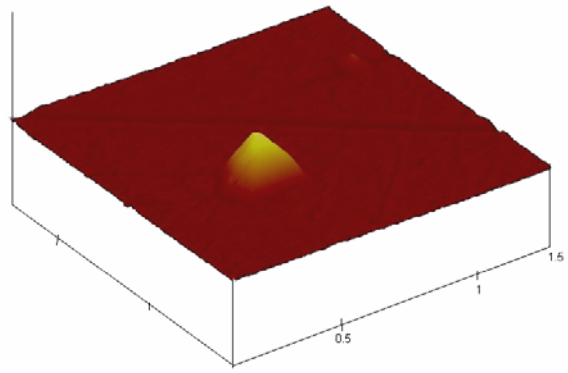

Digital Instruments Nanoscope
Scan Size: 3.922 um
Scan Rate: 1.001 Hz
# of samples: 256
Image data: Height
Data scale: 200nm

Sample G3

The first set of images was produced with a 100 x 100µm scanner in tapping mode, using areas of 20 x 20µm, 10 x 10µm, 5 x 5µm, 2 x 2µm, 1 x 1µm and 500 x 500 nm. The images shown in this page give information regarding relative "heights", cantilever oscillating "amplitude" and "phase" difference between the driving signal of the oscillating cantilever and the resulting motion of the tip. For this particular study, the image that contains the most useful information is the image containing the data for height.

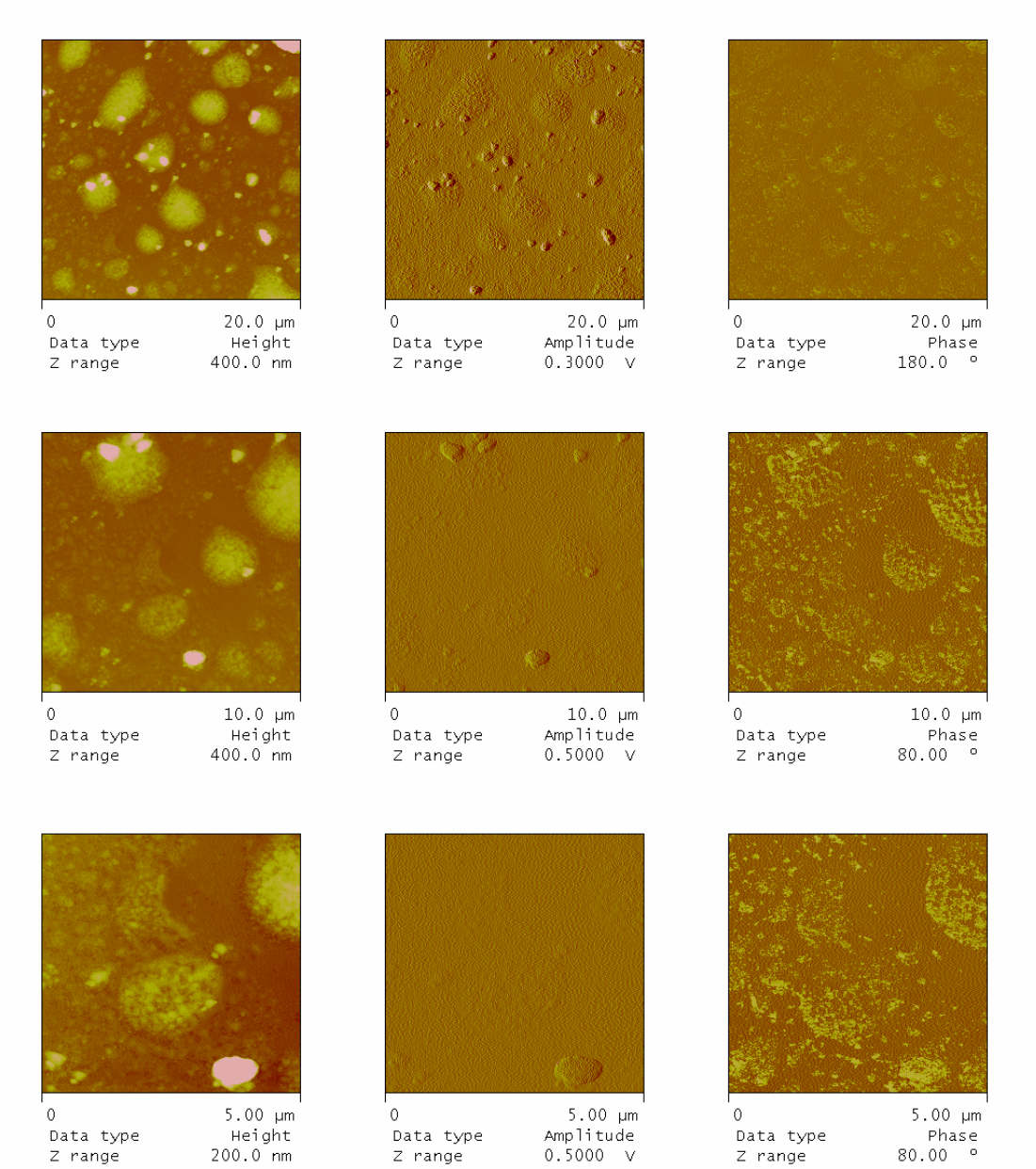

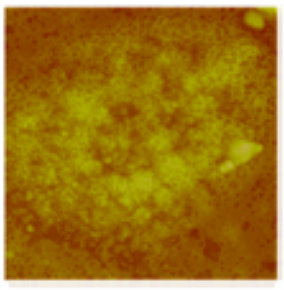
0 2.00 µm
Data type Height
Z range 50.00 nm

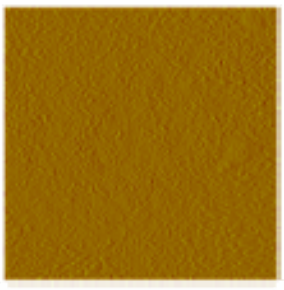
0 2.00 µm
Data type Amplitude
Z range 0.5000 V

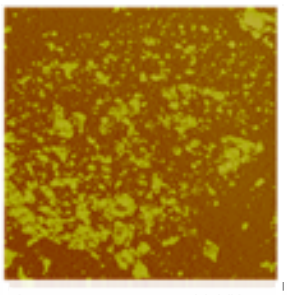
0 2.00 µm
Data type Phase
Z range 60.00 °

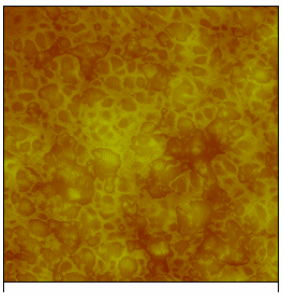
0 1.00 µm
Data type Height
Z range 200.0 nm

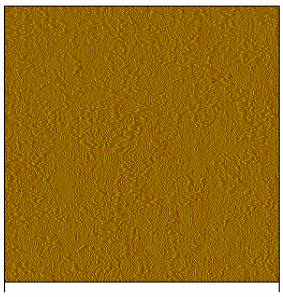
0 1.00 µm
Data type Amplitude
Z range 0.3000 V

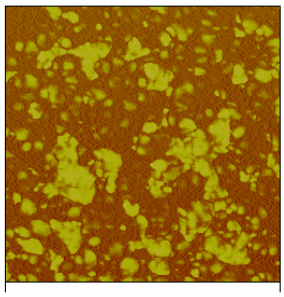
0 1.00 µm
Data type Phase
Z range 80.00 °

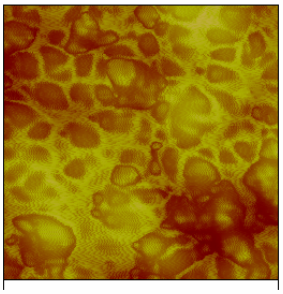
0 500 nm
Data type Height
Z range 100.0 nm

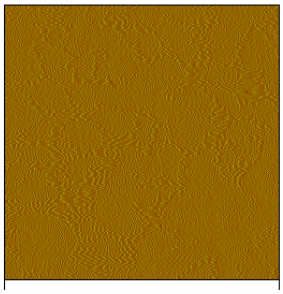
0 500 nm
Data type Amplitude
Z range 0.5000 V

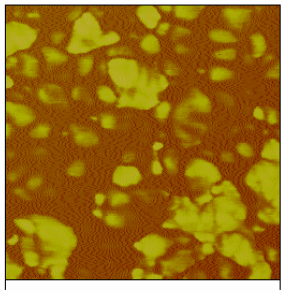
0 500 nm
Data type Phase
Z range 80.00 °

Below is a 3D rendering of the image containing the data for height of the 500x500nm sample. This image shows a rather interesting topography with multiple holes, displaying a very rugged surface.

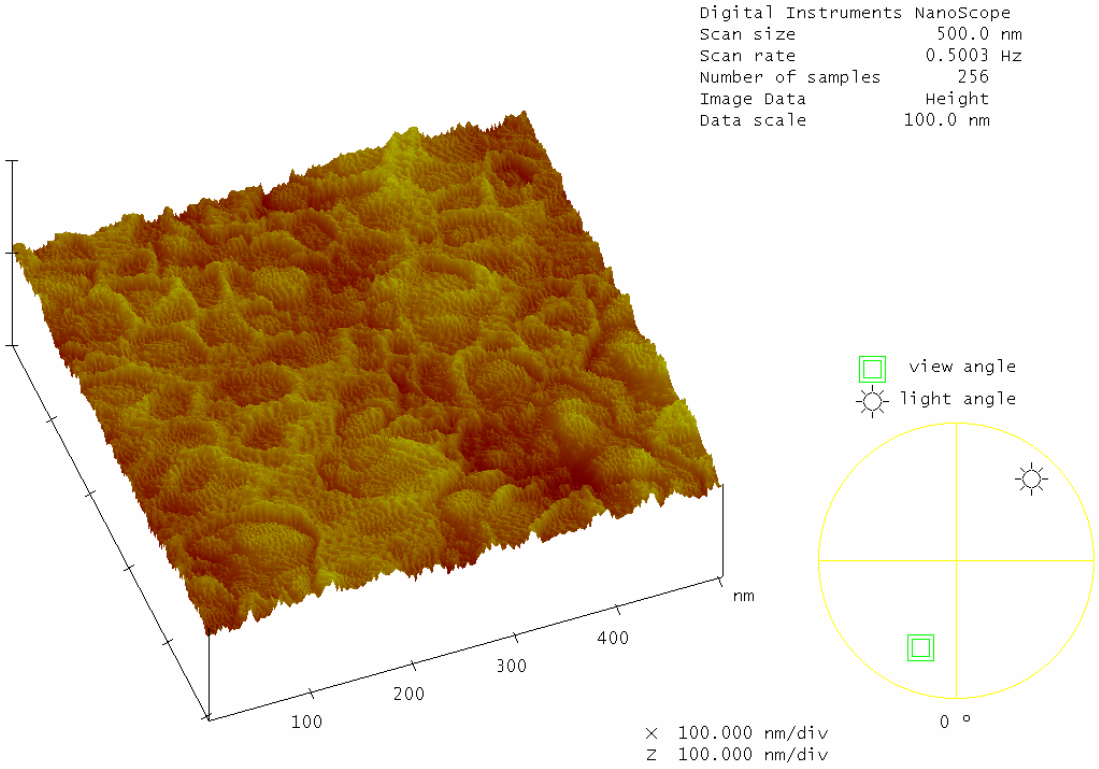

The scanner used to obtain these images was for areas up to 100 x 100 µm. It was observed that the images with areas smaller than 2µm displayed some interesting features. The images smaller than 2µm suggest that the jagged lines that can be observed could be noise caused by the underused scanner. Therefore, the scanner was switched with a 10 x 10 µm scanner, with hopes of improving the image quality and to verify if the topography given by the previous scanner could be repeatable.

The following images are also from the same G3.5 PAMAM sample using a smaller scanner. It can be observed form the 2µm, 1µm and 500nm images shown below that the AFM produced cleaner images of different areas of the sample than with the 100µm scanner.

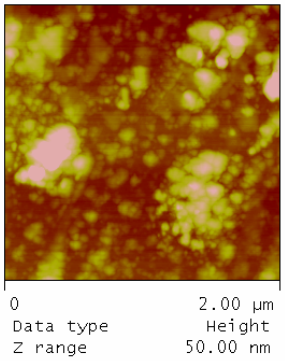

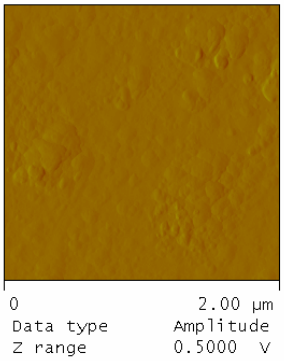

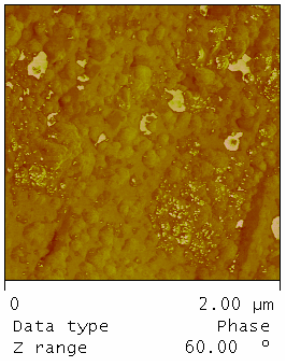

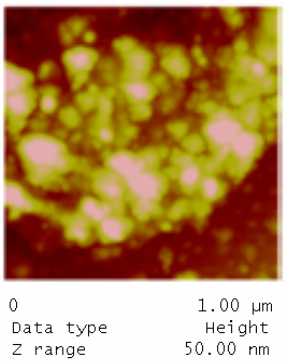

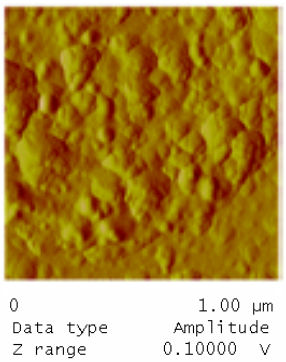

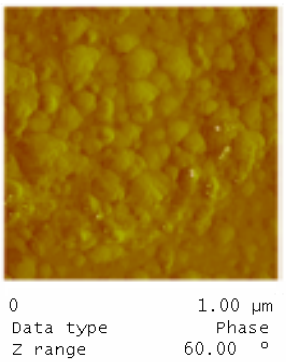

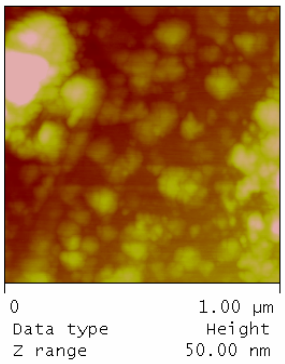

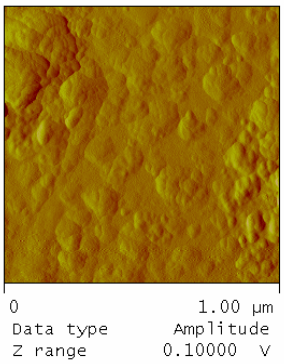

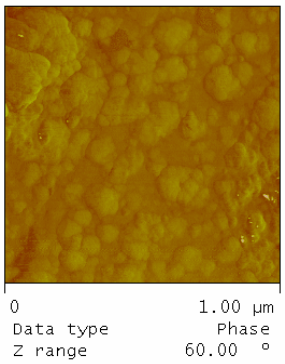

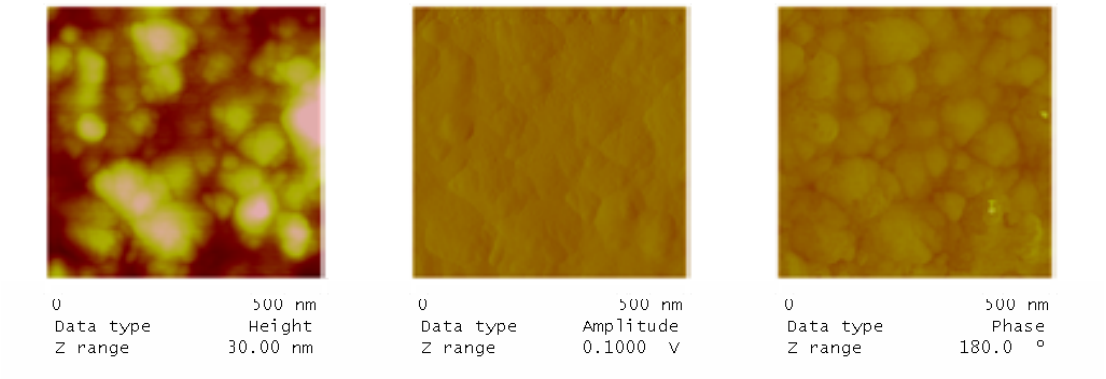

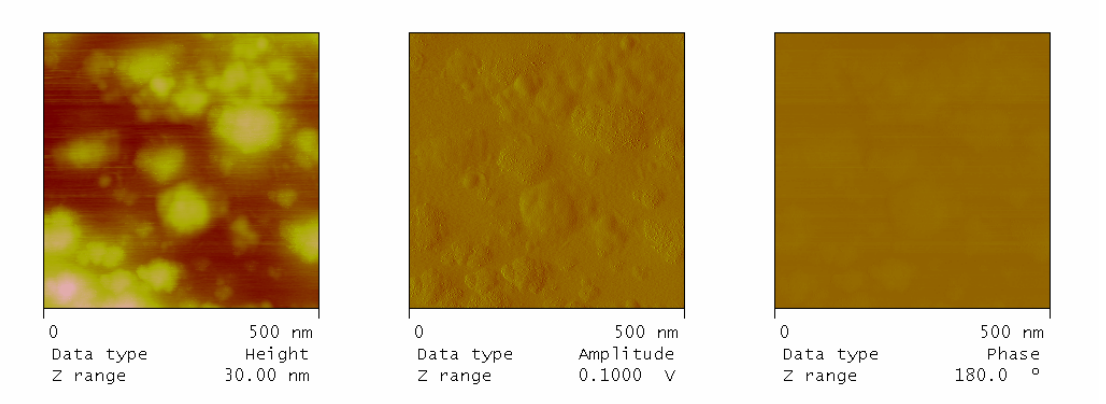

Observing the quality of images obtained from the 10 µm scanner, it can be concluded that the jagged lines shown with the previous scanner were in fact noise produced by the scanner. At this magnification, it can be seen that the dendrimers adsorbed to the surface in an irregular pattern, forming nanometric "mountains" and "valleys".

Aided with the 10X optical microscope equipped on the AFM, the surfaces chosen to be scanned were the areas with the least amount of visible material at that magnification. This was done in order to minimize the noise introduced by larger chunks of material. The following images show 3D renderings of the 1µm and 500nm samples.

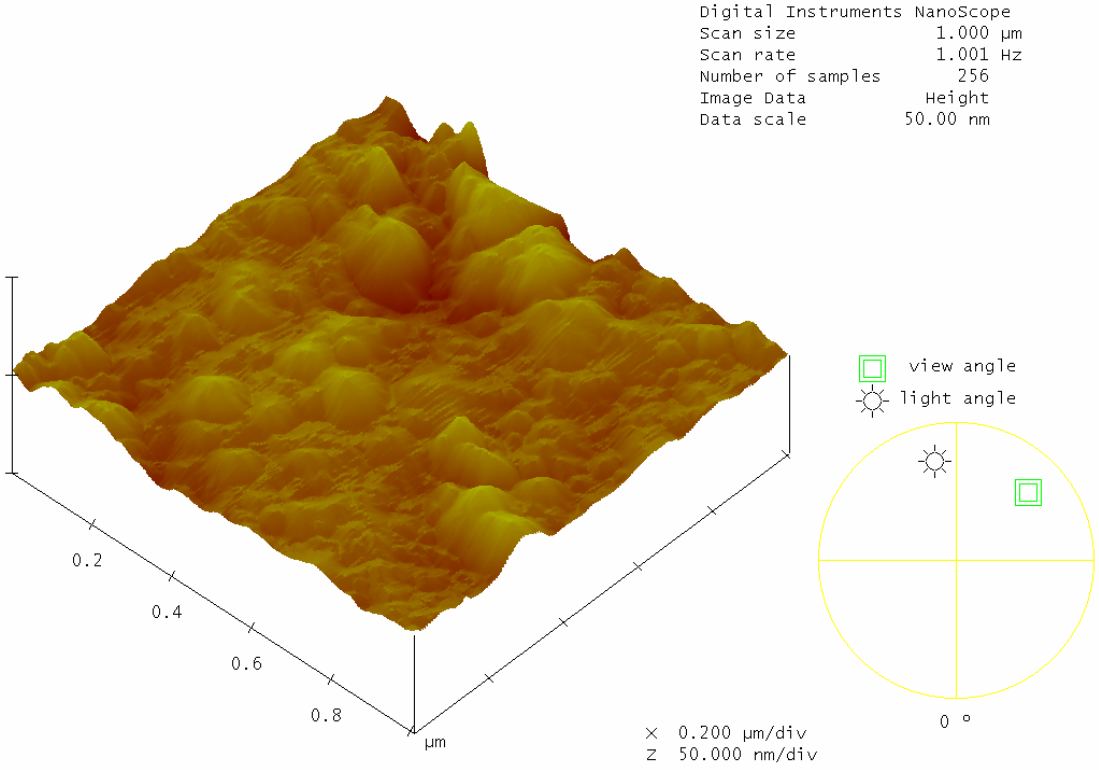
Digital Instruments NanoScope
Scan size 1.000 µm
Scan rate 1.001 Hz
Number of samples 256
Image Data Height
Data scale 50.00 nm
0.2
0.4
0.6
0.8
µm
view angle
light angle
0 °
X 0.200 µm/div
Z 50.000 nm/div

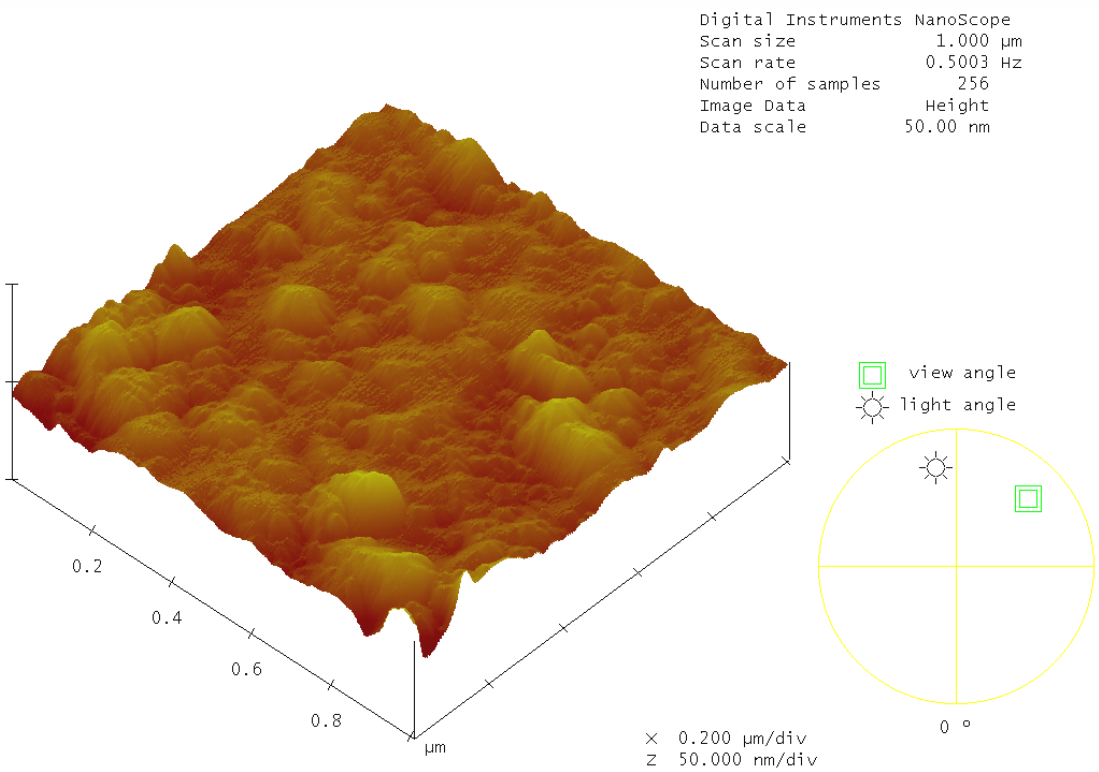
Digital Instruments NanoScope
Scan size 1.000 µm
Scan rate 0.5003 Hz
Number of samples 256
Image Data Height
Data scale 50.00 nm
0.2
0.4
0.6
0.8
µm
view angle
light angle
0 °
X 0.200 µm/div
Z 50.000 nm/div

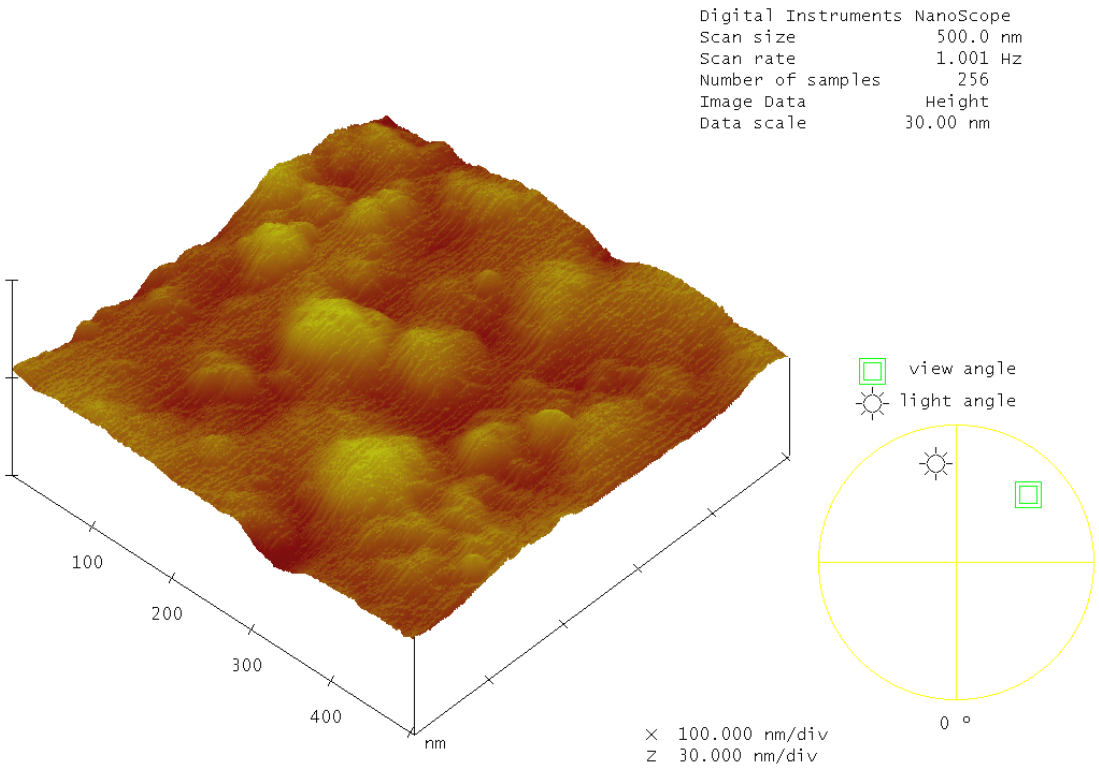

The 3D images above show a more realistic panorama of the surface topography on areas where the dendrimers adsorbed more evenly onto the surface. This is somewhat an expected result, which is in accordance with the conclusions reported on the aforementioned study by Piehler, Baker and Tomalia[27]. Since this is a low-generation dendrimer, individual molecules are too small to be detected by the AFM, but the images certainly show aggregation of organic material on the silicon surface.

In order to obtain some data on the surface topography, the following section analyses were performed. The figures displayed in the next of couple pages show cross-sectional measurements of some representative topographies found throughout the sample. These measurements were performed in order to obtain data on the relative heights. Results revealed that the surfaces have aspect features with vertical distances of up to 20 nm from the lowest point to the highest.

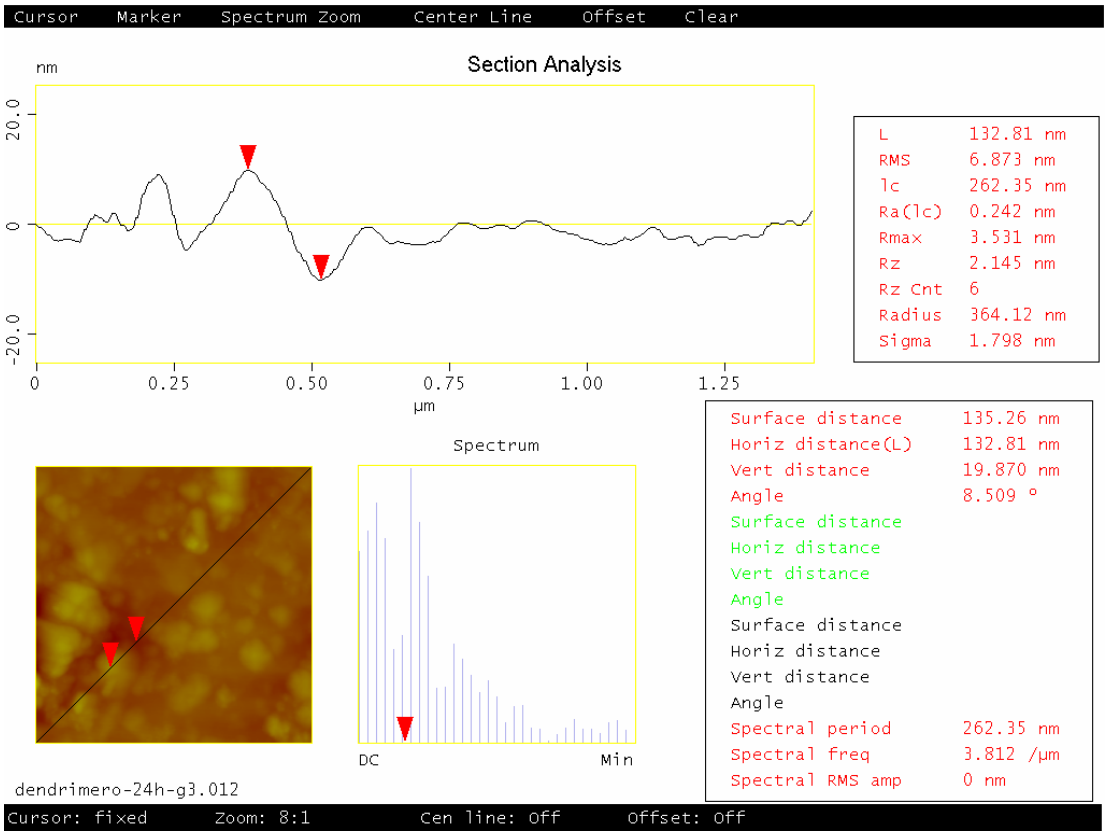
Cursor Marker Spectrum Zoom Center Line Offset Clear
Section Analysis
nm
20.0
0
-20.0
0
0.25
0.50
0.75
1.00
1.25
µm
L 132.81 nm
RMS 6.873 nm
lc 262.35 nm
Ra(lc) 0.242 nm
Rmax 3.531 nm
Rz 2.145 nm
Rz Cnt 6
Radius 364.12 nm
Sigma 1.798 nm
Spectrum
DC
Min
Surface distance 135.26 nm
Horiz distance(L) 132.81 nm
Vert distance 19.870 nm
Angle 8.509 °
Surface distance
Horiz distance
Vert distance
Angle
Surface distance
Horiz distance
Vert distance
Angle
Spectral period 262.35 nm
Spectral freq 3.812 /µm
Spectral RMS amp 0 nm
dendrimero-24h-g3.012
Cursor: fixed Zoom: 8:1 Cen line: Off Offset: Off

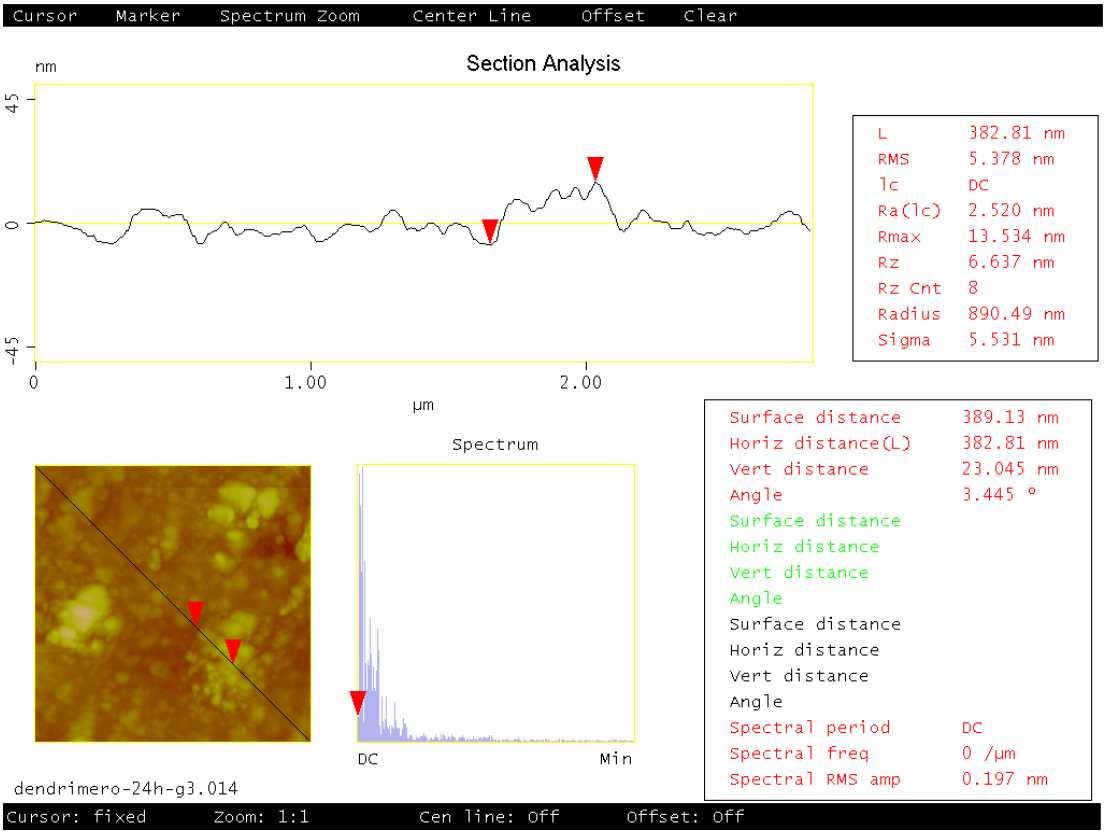
Cursor Marker Spectrum Zoom Center Line Offset Clear
Section Analysis
nm
45
0
-45
0
1.00
2.00
µm
L 382.81 nm
RMS 5.378 nm
lc DC
Ra(lc) 2.520 nm
Rmax 13.534 nm
Rz 6.637 nm
Rz Cnt 8
Radius 890.49 nm
Sigma 5.531 nm
Spectrum
DC
Min
Surface distance 389.13 nm
Horiz distance(L) 382.81 nm
Vert distance 23.045 nm
Angle 3.445 °
Surface distance
Horiz distance
Vert distance
Angle
Surface distance
Horiz distance
Vert distance
Angle
Spectral period DC
Spectral freq 0 /µm
Spectral RMS amp 0.197 nm
dendrimero-24h-g3.014
Cursor: fixed Zoom: 1:1 Cen line: Off Offset: Off

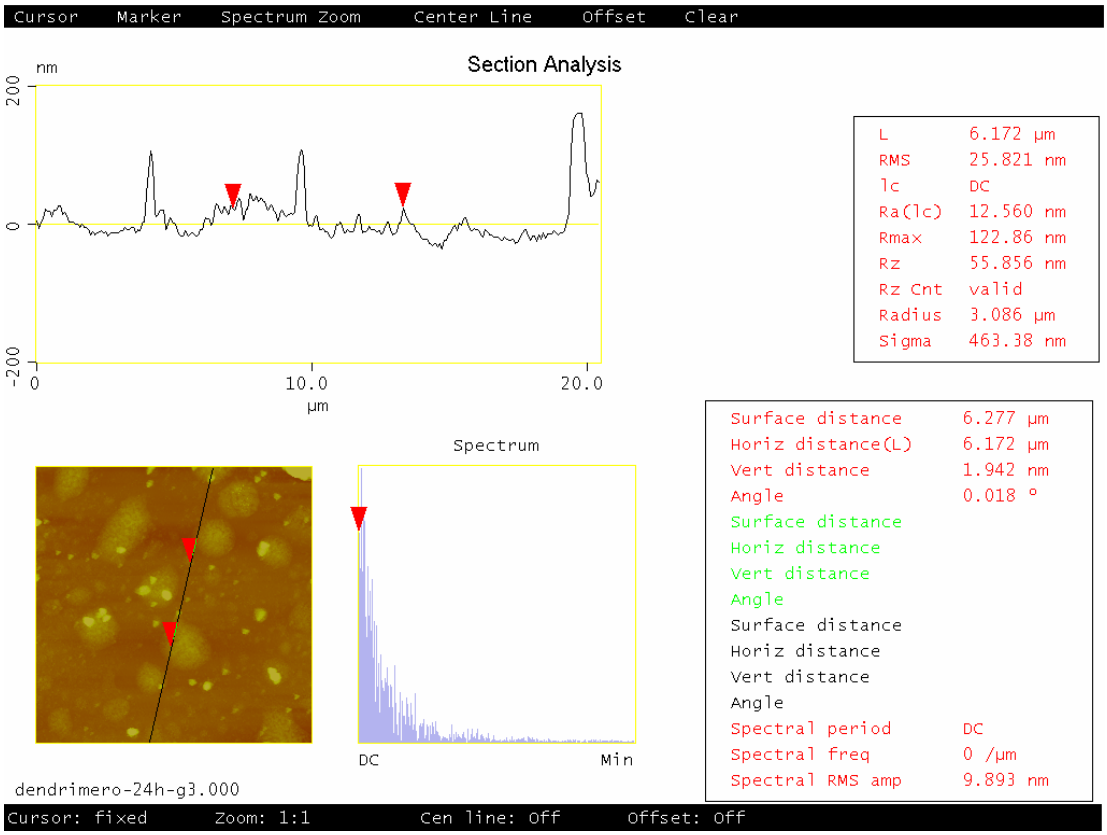
Cursor Marker Spectrum Zoom Center Line Offset Clear
Section Analysis
nm
200
0
-200
0
10.0
20.0
µm
L 6.172 µm
RMS 25.821 nm
lc DC
Ra(lc) 12.560 nm
Rmax 122.86 nm
Rz 55.856 nm
Rz Cnt valid
Radius 3.086 µm
Sigma 463.38 nm
Spectrum
DC
Min
Surface distance 6.277 µm
Horiz distance(L) 6.172 µm
Vert distance 1.942 nm
Angle 0.018 °
Surface distance
Horiz distance
Vert distance
Angle
Surface distance
Horiz distance
Vert distance
Angle
Spectral period DC
Spectral freq 0 /µm
Spectral RMS amp 9.893 nm
dendrimero-24h-g3.000
Cursor: fixed Zoom: 1:1 Cen line: Off Offset: Off

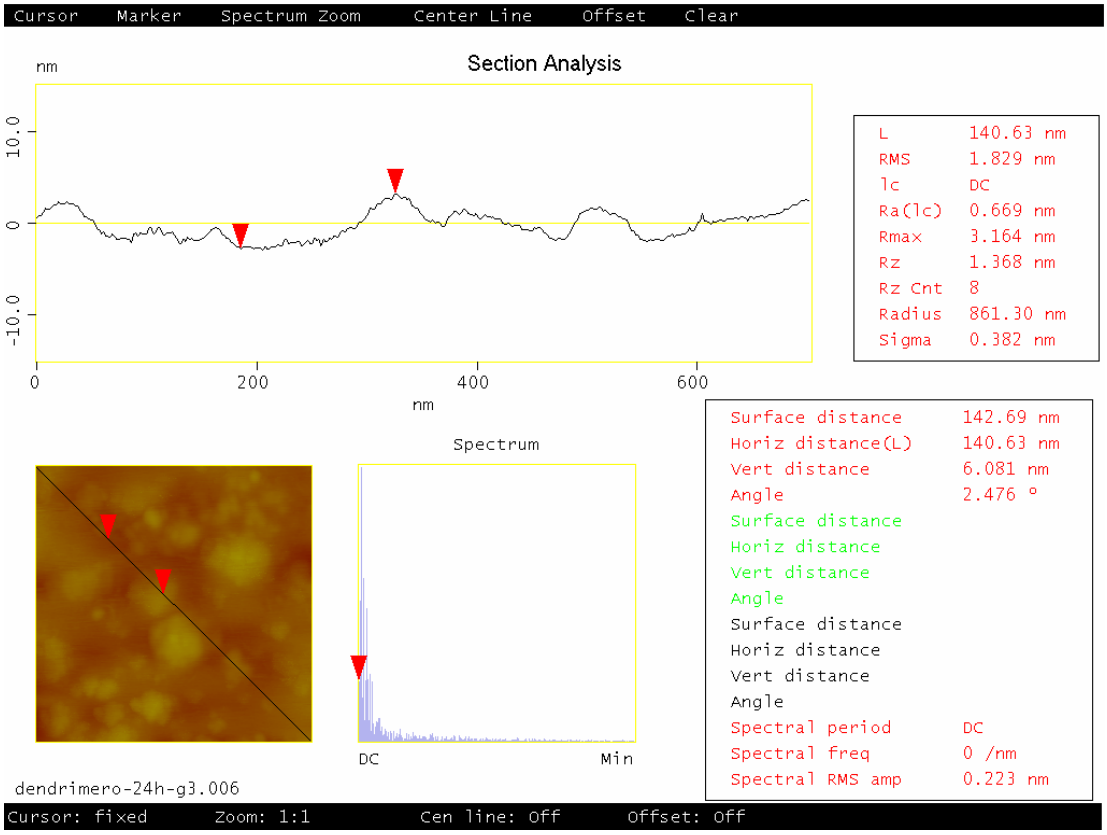
Cursor Marker Spectrum Zoom Center Line Offset Clear
Section Analysis
nm
10.0
0
-10.0
0
200
400
600
nm
L 140.63 nm
RMS 1.829 nm
lc DC
Ra(lc) 0.669 nm
Rmax 3.164 nm
Rz 1.368 nm
Rz Cnt 8
Radius 861.30 nm
Sigma 0.382 nm
Spectrum
DC
Min
Surface distance 142.69 nm
Horiz distance(L) 140.63 nm
Vert distance 6.081 nm
Angle 2.476 °
Surface distance
Horiz distance
Vert distance
Angle
Surface distance
Horiz distance
Vert distance
Angle
Spectral period DC
Spectral freq 0 /nm
Spectral RMS amp 0.223 nm
dendrimero-24h-g3.006
Cursor: fixed Zoom: 1:1 Cen line: Off Offset: Off

IV. RESULTS

14. DISCUSSION

As mentioned in the introduction, the motivation for this research came upon by the need to minimize the number of bone marrow biopsies that are performed periodically after a patient has been treated for Leukemia and to reduce the costs associated with the monitoring phase. The proposed solution is to develop an implantable enzymatic biosensor that can monitor the concentrations of the Angiotensin Converting Enzyme (ACE) inside the bone marrow and transmit data wirelessly outside the body. The work presented in this thesis gives the first step towards the development of a biosensor that takes advantage of highly selective biochemical reactions such as receptor-ligand, antibody-antigen or enzyme-substrate reactions. The contribution of this work provides a feasible support structure onto which any of the previously mentioned molecules can be attached to "trap" their molecular counterpart over a microcantilever based biosensor.

This work was started with an extensive research through academic literature and journal publications to tackle specific problems such as the sensing mechanism, the coating layer, a good coupling agent and a possible leukemia indicator. Section 9 gives a short conclusion of the results obtained from this literature review and lists the choices for design to be studied in the experimental section.

In order to implement the selected choices, an experimental phase was designed and conducted to evaluate their usefulness towards achieving the primary goal of developing an enzymatic biosensor. The first step was to study the gamma-APS as a potential coupling agent between organic and inorganic materials. Next, the divergent approach was followed in order to synthesize the PAMAM dendrimer over the functionalized silicon substrate, parting from the primary amines made available after silane adhesion. Afterwards, spectroscopic and microscopic techniques were used to characterize the chemical and physical uniformity over the samples.

The results obtained from the experimental procedures give important insight on the interactions at the molecular level of the PAMAM dendrimer used as a coating layer in biosensors. The FT-IR characterization with the microscope accessory reveals that there exists chemical uniformity throughout the samples. In the other hand, the AFM characterization revealed that physical uniformity had not been achieved. These results suggest that a better deposition technique should be followed in order to obtain a uniform deposition and presents an important result, showing that deposition was achieved all over the sample but with different thicknesses or concentrations.

In the following section, specific conclusions and recommendations for improvement and future work are given. The next section can serve as a starting point for subsequent studies in the topic, in view of the fact that it gives an overview of what worked and what failed, as well as comments on how to improve the results and take the next steps.

15. CONCLUSIONS AND RECOMMENDATIONS

Looking back at the experimental procedures, there are some improvements that can be made to optimize the obtained results. As part of the silicon wafer functionalization phase in section 10, a pre-oxidation technique can be performed in order to increase the OH groups at the silicon surface. As shown by the AFM images in section 13, the PAMAM dendrimer did not grow with a uniform thickness throughout the samples, but the infrared spectra of the samples confirm that there is chemical uniformity. This result leads to the conclusion that the adhesion of the γ-APS silane in the functionalization step, failed to attach uniformly to the surface due to the low amount of available OH groups at the silicon surface. By implementing an oxidation step prior to the silane functionalization, the OH groups can form evenly on the surface, facilitating the silane attachment. A proposed mechanism for this oxidation process is commonly known as thermal oxidation, which can be a "dry oxidation" (oxygen gas) or "wet oxidation" (water vapor). This process exposes the silicon wafer to an oxygen-rich environment at extremely high temperatures to promote the rapid formation of SiO_2 at the silicon-air interface.

One improvement that can be suggested for the divergent approach in the construction of the PAMAM dendrimer is to leave the reactions run longer than 48 hours. Although the experiments performed in this thesis did not show a significant difference between the 24 Hr reactions and the 48 Hr reactions, it has been repeatedly documented that the iterative process of the Michael addition and Amidation has reactions with long time durations that are reported to exceed 60 hours each.

Regarding the characterization technique used for this work, it was determined that the microscope accessory of the FTIR spectrometer does not have the proper sensitivity to measure certain functional groups. This is the case with the carboxyl groups that should appear as a sharp peak at 1700cm^{-1}, which due to the low resolution of the method it did not appear in the infrared spectra. A better technique might be FTIR with an Attenuated Total Reflectance (ATR) accessory, which gave promising results when a clean silicon wafer was analyzed, followed by a functionalized wafer with the γ-APS silane. Figure 28 show the comparison of these two stages in the reaction, showing the presence of functional groups that were not there before functionalization.

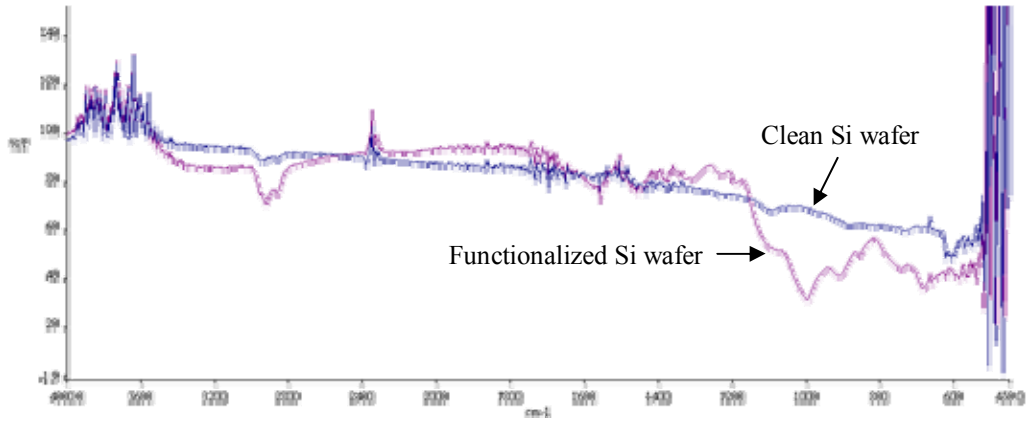

Figure 28: FTIR ATR spectrum

The spectrum in figure 28 was obtained using a Perkin-Elmer SpectrumOne from the Physics department at Tecnológico de Monterrey. Weeks after this sample was taken, the equipment suffered technical problems and was unavailable for future analysis. It is recommended to conduct the experiments once more and analyzing the samples with the FTIR-ATR using a zinc selenium crystal.

16. FUTURE WORK

Recalling the motivation stated in section 1 of this report, the main purpose was to sense a possible leukemia relapse indicator. This possible indicator was selected in section 2.2.4. as the Angiotensin Converting Enzyme (ACE), which elevated concentrations have been correlated with leukemia. In order to accomplish the goal of sensing ACE concentrations in a biological medium, a molecular sensor needs to be attached to the dendrimeric structure. This molecular sensor achieves the task of trapping the desired enzyme on top of the sensor's surface. Several molecules can be recommended to be used as a trapping structure for ACE, which range from inhibitors, antibodies, receptors and ligands. The following section proposes the attachment of Captopril, a well known enzyme inhibitor for ACE.

16.1 MECHANISM FOR ACE INHIBITOR ATTACHMENT

The structure of ACE adopts an overall ellipsoid shape (dimensions approximately 72 x 57 x 48 Å) with a central groove that extends for about 30 Å into the molecule (Figure 29). The center of this molecule contains the active site where an inhibitor can act as a lock-and-key mechanism to trap the molecule.

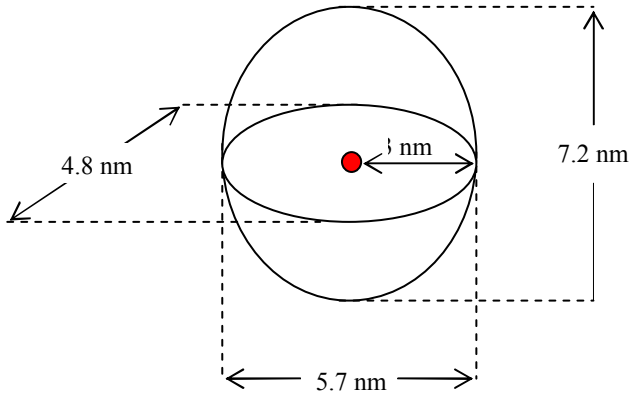

Figure 29: Dimensions of the ACE molecule

Captopril is among a group of angiotensin converting enzyme inhibitors which is commonly prescribed to patient with hypertension. This inhibitor acts on the active site of the ACE molecule and deactivates the enzyme, preventing it from converting Angiotensin I into Angiotensin II, hence reducing the effects of vasoconstriction that lead to hypertension. Captopril can be used as shown in Figure 30 to serve as the molecular sensor to trap ACE on top of the biosensor's surface.

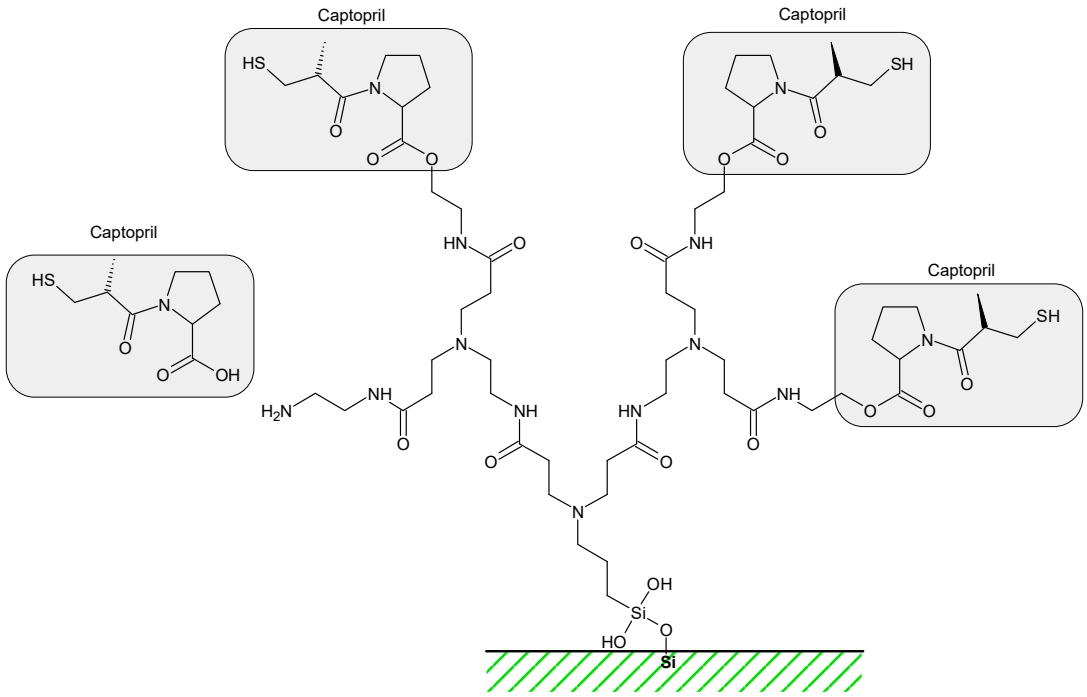

Figure 30: Attachment of Captopril to dendrimer

Captopril is just one of the many possibilities that can be used to trap the enzyme. Other ACE inhibitors could be: Benazepril, Enalapril, Fosinopril, Lisinopril, Perindopril, Quinapril, Ramipril, Spirapril and Trandolapril. Also, instead of sensing ACE directly, one can measure its product: angiotensin II. Some of the Angiotensin II receptor antagonists could be the following: Candesartan, Eprosartan, Irbesartan, Losartan, Olmesartan, Tasosartan, Telmisartan and Valsartan.

16.2 ACE CONCENTRATION MEASUREMENTS

Once the biosensor platform has been set up, several tests can be conducted to prove the validity of the model. Even before using a MEMS microcantilever structure, some experiments can be conducted to verify if the ACE is actually being trapped. The following paragraphs suggest some ideas that can be explored in order to validate the model.

Fluorescent Markers:

ACE antibodies marked with fluorescent dyes can be used to prepare solutions with photochemically-active angiotensin converting enzyme. These solutions, at various concentrations, can be used to place the silicon wafers with the active coating (dendrimer + inhibitor) in contact with the marked ACE. After some time in solution, the silicon pieces can be removed and rinsed to be analyzed under a microscope with ultraviolet light. Image analysis software can be applied to count the bright spots and compare them with samples at various concentrations and with the control (inactive PAMAM coating i.e. without the Captoril inhibitor).

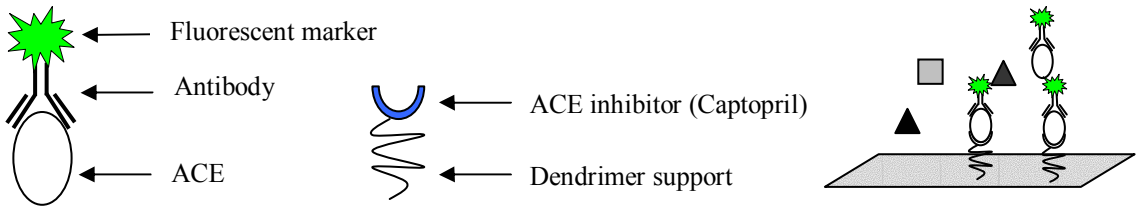

Radioligands:

If instead of using inhibitors as the molecular sensor, one can opt for immobilizing a receptor on top of the dendrimer structure. In the case of sensing components of the rennin-angiotensin system, the AT1 or AT2 receptor can be attached to the dendrimer structure to trap the Angiotensin II molecule. Using radioligands specific to the AT1 or AT2 receptor, the same procedure can be followed as with the fluorescent marker. The samples can be analyzed with positron emission tomography (PET) to quantify the amount of radiation emitted from the samples.

Residue quantification:

A less sophisticated way, but still a valid method for quantifying ACE attachment to the active coating can be by means of analyzing the residues after reacting with the silicon pieces. The silicon with the active coating can be placed in a solution with a known concentration of ACE molecules; after time in solution, the pieces can be removed and the remaining solution can be analyzed to quantify the amounts of ACE molecules present. The difference between the known initial concentration and the final concentration will be the amount of ACE attached to the silicon pieces with the active biolayer.

V. APPENDICES

17. APPENDIX A: MATERIALS SPECIFICATIONS

Silicon wafers:

Supplier: Wafer World, Inc.
1100 Technology Place, suite 104
West Palm Bach. FL 33407
www.waferworld.com

Diameter:	50.8 ± 0.5 mm
Type:	P / BORON
Orientation:	(100) ± 0.5°
Resistivity:	1 – 20 ohm-cm
Thickness:	250-300 μm
Surface:	Single side polished
Grade:	Test

Coupling agent:

Product Name:	Gamma-aminopropyltriethoxysilane
Trade Name:	A-1100 (the United Carbide Corporation)
Molecular Formula:	$NH_2CH_2CH_2CH_2Si(OC_2H_5)_3$
Formula Weight:	221.3
CAS No:	919-30-2
Descriptions:	It is a colorless or yellowish transparent liquid, flash point: 96°, boiling point: 217°, soluble in benzene, acetic acetate and water (with reaction) completely and immediately.

Specifications:

- Appearance: Colorless liquid
- Purity, % (neutralization): 99.0 min.
- Refraction Index (n25D): 1.4175-1.4200
- Specific Density(d204): 0.939-0.946 g/cm3
- Boiling point: 217°/10mmHg

18. APPENDIX B: INSTRUMENT SPECIFICATIONS

FTIR specifications

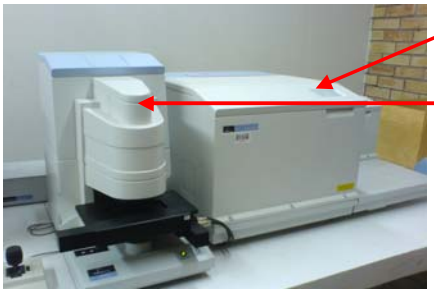

Instrument: Spectrum GX
Manufacturer: Perkin-Elmer
Accessory: AutoIMAGE FTIR microscope system

FTIR Spectrometer – Spectrum GX: Specifications

Sources
Mid/Far IR (10000 - 30 cm-1), Near-IR (15000 - 1200 cm-1) and dual (15000 - 30 cm-1) internal sources. An additional port is available for external sources, emission measurements and Raman spectroscopy.

Beamsplitters
- Quartz Near-IR (15000 - 2700 cm-1)
- CaF2 Near-IR (14000 - 1200 cm-1)
- Raman (12000 - 5000 cm-1)
- Wide-range KBr (10000 - 370 cm-1)
- Optimized KBr (7000 - 370 cm-1)
- Mid-IR Csl (6500 - 220 cm-1)
- Far-IR grid (720 - 30 cm-1)
- 6 micrometer Mylar film Far-IR (500 - 50 cm-1)
- 12 micrometer Mylar film Far-IR (250 - 30 cm-1)

Detectors
- Narrow band InSb Near-IR (15000 - 3500 cm-1)
- InSb Near-IR (15000 - 1800 cm-1)
- FR-DTGS Near-IR (15000 - 2000 cm-1)
- FR-DTGS Mid-IR (KBr) (15000 - 370 cm-1)
- FR-DTGS Mid-IR (Csl) (15000 - 220 cm-1)
- FR-DTGS Far-IR (Poly) (720 - 30 cm-1)
- Narrow band MCT Mid-IR (10000 - 750 cm-1)
- Medium band MCT Mid-IR (10000 - 700 cm-1)
- Wide band MCT Mid-IR (10000 - 450 cm-1)

Image control system
Fixed or software-controlled iris apertures available at B-stop and J-stop images.
- B-stop controls attenuation, keeping detector image size constant.
- J-stop controls beam divergence through the interferometer, allowing optimization of throughput for any resolution and range combination. Software controlled apertures may be adjusted in steps of 0.1 mm.

Resolution
Better than 0.3 cm-1 standard, better than 0.15 cm-1 optional. The resolution is continuously variable up to 64 cm-1.

Scan velocities
Continuously variable between 0.05 and 5.0 cm/sec.

Accessory –AutoIMAGE FTIR Microscope System: Specifications

- A high performance cassegrain mirror system; This has a wide collection angle and is highly efficient in collecting infrared radiation for microspectoscopy.
- Spectra can be collected in either reflectance, transmittance or ATR modes
- The same cassegrain is used to send both infrared radiation and visible light to the remote aperture. This means that the location of the image cannot change when AutoIMAGE automatically switches from viewing to infrared mode.
- A small target (0.25 mm) MCT detector. This is very well matched to the infrared image from the cassegrains, giving low noise and high signal-to-noise ratio.
- The lower cassegrain can be removed. This provides space for thick samples to be studied in reflectance mode.
- Internal coaxial illumination, with variable intensity.
- Fully purgeable infrared beam and sample stage. This eliminates the effects of water vapour and carbon dioxide from your spectra. It also provides a dust-free environment for the optics .
- An automatic infrared aperture that closes to the size and rotation selected when you choose a scan or monitor command.
- A motorised stage, controlled by a joystick and the AutoIMAGE software, enables you to find points on your sample and focus the microscope.
- AutoIMAGE software controls the operation of the microscope: focus, illumination, stage position, adjusting the correction, changing to reflectance or transmittance, and automatic changing from viewing to infrared mode.
- AutoIMAGE software also enables you to view samples, collect spectra and map samples.
- The AutoImage is also fitted with a Ge ATR crystal which enables you to take ATR measurements of small spot sizes.

AFM specifications

Instrument: Nanoscope III Multimode
Manufacturer: Digital Instruments
Scaners used: 100 x 100µm and 10 x 10µm
Mode: Tapping

MultiMode Specifications		
	Microscope:	– MultiMode SPM head; choice of scanners (see Table 1)
	Noise:	– <0.3Å RMS in vertical (Z) dimension w/ vibration isolation
	Sample size:	– ≤15mm diameter; ≤5mm thick
	Tip/cantilever holders:	– tapping mode/contact mode in air (std);
	Vibration and Acoustic Isolation:	– silicone vibration pad provided and acoustic cover (std);
		– vibration isolation tripod (optional); vibration isolation table (optional);
		– integrated vibration isolation table and acoustic enclosure (optional);

Scanner	Lateral (X-Y) Range	Vertical (Z) Range
AS-12, AS-12MF, AS-12NM ("E") • AS-12V, AS-12VMF ("EV")	10µm x 10µm	2.5µm
AS-130, AS-130MF, AS-130NM ("J") • AS-130V, AS-130VMF ("JV")	125µm x 125µm	5.0µm

Table 1 MF= Magnet Free, NM= Non-Magnetic, V= Vertical engage

19. **APPENDIX C:** IR SPECTRUM OF REAGENTS

Ethylenediamine

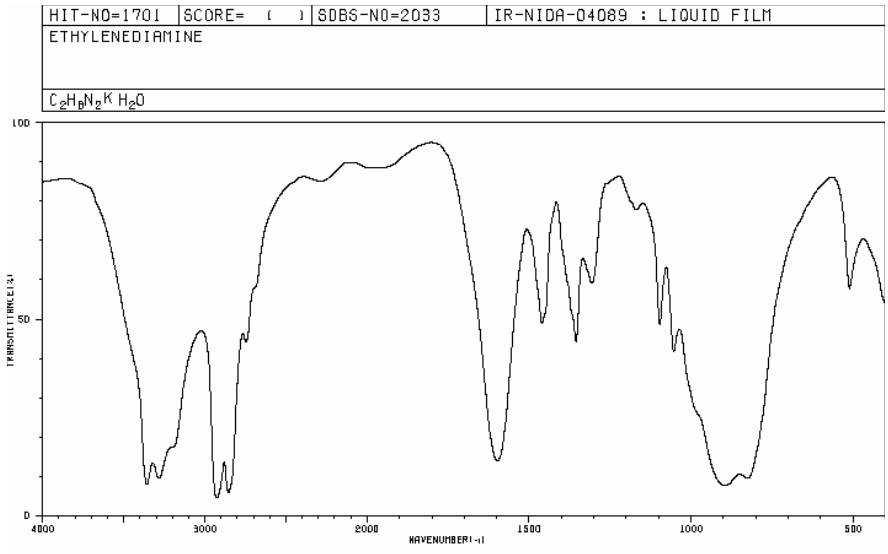

Methyl Acrylate

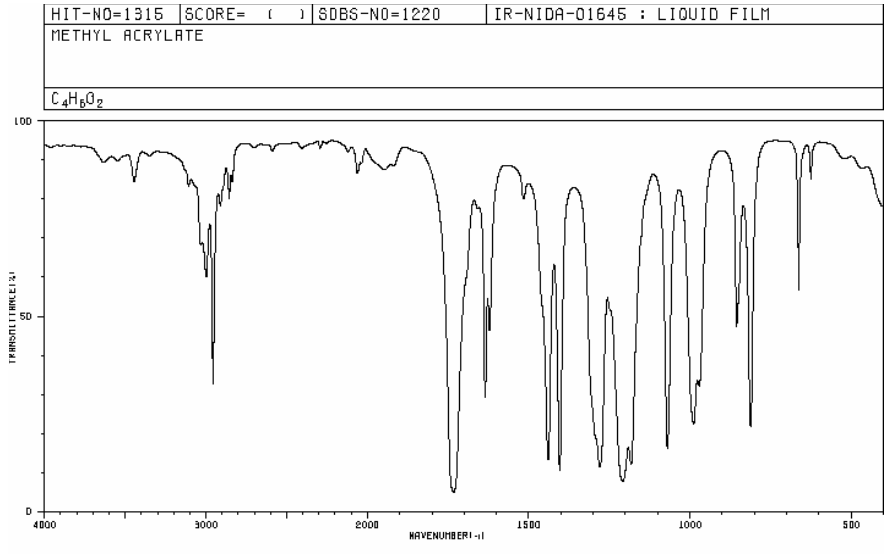

Tetrahydrofuran

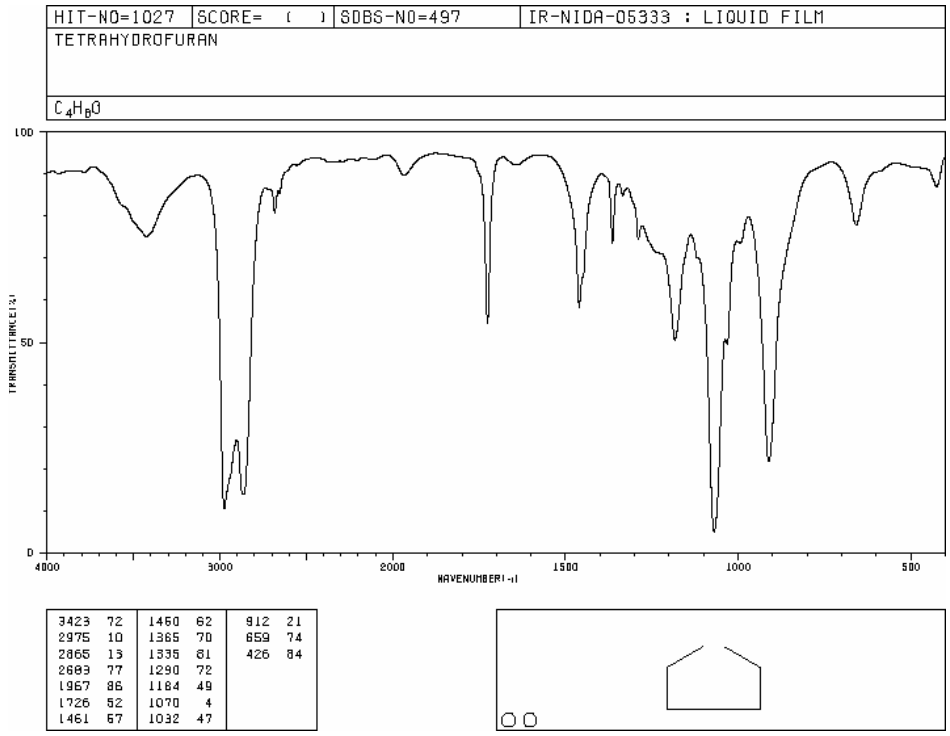

Ethyl alcohol

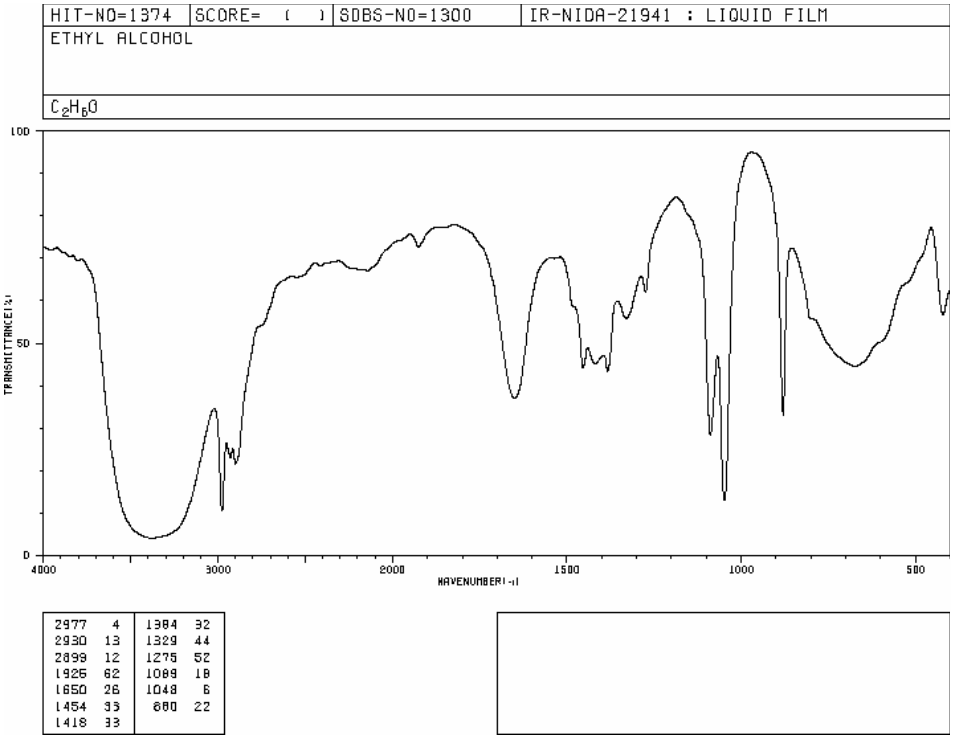

VI. REFERENCES

[1] Leukemia facts and statistics. *The Leukemia and Lymphoma Society.* 2006

[2] Hazenedaroglu I. C., et al. A local renin-angiotensin system in the bone marrow. *Medical hypothesis.* 1996: vol. 46, pp. 507-510

[3] Abali H., Hazenedaroglu I. C., et al. Circulating and local bone marrow renin-angiotensin system in leukemic hematopoiesis: preliminary evidences. *Hematology*. 2002: Vol. 7, No. 2, pp. 75-82.

[4] Rodgers K.E., et al**.** Effect of Angiotensin II on Hematopoietic Progenitor Cell Proliferation. *Stem Cells*. 2000:Vol. 18, No. 4, pp. 287-294.

[5] Gomez M. T., et al. Renin Expression in Hematological Malignancies and its Role in the Regulation of Hematopoiesis. *Leukemia and Lymphoma*. 2002: Vol. 43, No. 12, pp. 2377-2381.

[6] Chen G. Y., Thundat T., et al. Adsorption induced surface stress and its effects on resonance frequency of microcantilevers. *J. Appl. Phys*. 1995: Vol 77, pp. 3618-3622.

[7] Nuzzo R. G., Allara D. L. Adsorption of organic disulfides on gold surfaces. *J. Am. Chem. Soc.* 1983: Vol 105, 4481-4483.

[8] Bain C. D., Troughton E. B. Et al. Formation of monolayer films by the spontaneous assembly of organic thiols from solution onto gold. *J. Am. Chem. Soc.* 1989*:* Vol 111, 321-335.

[9] U. Srinivasan, et al. Alkyltrichlorosilane-based self-assembled monolayer films for stiction reduction in silicon micromachines," *J. Microelectromech. Syst*. 1998: vol. 7, p. 252,

[10] Peppas N.A.. Hydrogels. In: B. D. Ratner, ed. Biomaterials Science. San Diego, CA: Academic Press; 1996: 60-64.

[11] Byrne M.E., et al. Molecular imprinting with hydrogels. *Adv. Drug Deliv. Revs*. 2002. vol 54, 149-161

[12] Hilt J. Z., Gupta A. K., et al. Ultrasensitive biomems sensors based on microcantilevers patterned with environmentally responsive hydrogels. *Biomed. Microdev*. 2003. Issue5, vol 3. 177-184.

[13] Molecular Modeling of Dendrimers for Nanoscale Applications. By Tahir Cagin*, Guofeng Wang, Ryan Martin, and William A. Goddard III http://www.foresight.org/Conferences/MNT7/Papers/Cagin3/index.html

[14] Tully D. C., Wilder K., et al. Dendrimer-Based Self-Assembled Monolayers as Resists for Scanning Probe Lithography. *Adv. Mater.* 1999. Issue 11, No. 4. pp. 314-318.

[15] Witucki G.L.. A Silane Primer: Chemistry and Applications of Alkoxy Silanes. Chicago, IL. 57th Annual Meeting of the Federation of Societies for Coatings Technology; 1992.

[16] Tomalia D. A.; et al. 1st SPSJ Int. Polym. Conf., Soc. Polym. Sci. Jpn. (Kyoto) 1984, 65.

[17] Vögtle F.; et al. Cascade and Nonskid-Chain-like Syntheses of Molecular Cavity Topologies. *Synthesis.* 1978, pp.155-158.

[18] Newkome G. R., et al. Cascade molecules: a new approach to micelles. A [27]-arborol. *J. Org. Chem.* 1985. Issue *50*, pp. 2003-2004.

[19] Fréchet J. M. J.; Jiang, Y.; Hawker, C. J.; Philippides, A. E. *Proc. IUPAC Int. Symp., Macromol. (Seoul)* 1989, 19-20.

[20] Hawker, C. J.; Fréchet, J. M. J. Preparation of polymers with controlled molecular architecture. A new convergent approach to dendritic macromolecules. *J. Am. Chem. Soc.* 1990. vol 112. Issue 7638-7647.

[21] Hawker, C.; Fréchet, J. M. J. A new convergent approach to monodisperse dendritic macromolecules. *J. Chem. Soc., Chem. Commun.* 1990, 1010-1013.

[22] Hoagland, D.A. and Muthukumar, M. Evidence for entropic barrier transport of linear, star, and ring macromolecules in electrophoresis gels. *Macromolecules.* 1992. vol 25, pp. 6693-6695.

[23] Chen, J.-L. and Morawetz, H. Determination of molecular weight distribution of synthetic flexible-chain polyelectrolytes by polyacrylamide gel electrophoresis. *Macromolecules,* 1982. vol. 15, p.p. 1180-1185.

[24] Brothers, H.M., Piehler, L.T., Tomalia, D.A. Slab-gel and capillary electrophoretic characterization of polyamidoamine dendrimers. *J. Chromat. A.* 1998*,* Volume 814, No. 1, p.p. 233-246.

[25] Choi, J.S., et al. Poly(ethylene glycol)-*block*-poly(L-lysine) Dendrimer: Novel Linear Polymer/Dendrimer Block Copolymer Forming a Spherical Water-Soluble Polyionic Complex with DNA. *Bioconjugate Chem.,* 1999 vol. 10, No. 1, p.p. 62 - 65.

[26] Baselt, D. "How AFM Works." Atomic Force Microscopy. 1993. California Institute of Technology. 15 June 2007 <http://stm2.nrl.navy.mil/how-afm/how-afm.html>.

[27] Li, J., Piehler, L.T., Qin, D., Tomalia, D.A. and Meier, D.J. Visualization and Characterization of Poly(amidoamine) Dendrimers by Atomic Force Microscopy . *Langmuir.* 2000, vol. 16, No. 13, p.p. 5613 – 5616.

[28] Regen S.L.; Watanabe, S. Dendrimers as building blocks for multilayer construction. *J. Am. Chem. Soc.* 1994: Vol 116, pp. 8855-8856.

[29] Varahramyan, K.; Lvov, Y. Nanomanufacturing by Layer-by-Layer Assembly. *Proceedings of the I MECH E Part N Journal of Nanoengineering and Nanosystems.* 2006: Vol 220, No 1, pp. 29-37.

[30] J. Anzai, Y. Kobayashi, N. Nakamura, M. Nishimura and T. Hoshi. Layer-by-Layer Construction of Multilayer Thin Films Composed of Avidin and Biotin-Labeled Poly(amine)s. *Langmuir*. 1999, vol. 15, No. 1, p.p. 221- 226.